Published for SISSA by Springer

Received: June 28, 2025
Revised: January 13, 2026
Accepted: February 28, 2026
Published: May 15, 2026

Search for the nonresonant and resonant production of a Higgs boson in association with an additional scalar boson in the $\gamma\gamma\tau\tau$ final state in proton-proton collisions at $\sqrt{s} = 13$ TeV

The CMS collaboration

Full author list at the end of the paper

E-mail: cms-publication-committee-chair@cern.ch

Abstract: The results of a search for the production of two scalar bosons in final states with two photons and two tau leptons are presented. The search considers both nonresonant production of a Higgs boson pair, HH, and resonant production via a new boson X which decays either to HH or to H and a new scalar Y. The analysis uses up to 138 fb^{-1} of proton-proton collision data, recorded between 2016 and 2018 by the CMS experiment at the LHC at a center-of-mass energy of 13 TeV. No evidence for signal is found in the data. For the nonresonant production, the observed (expected) upper limit at 95% confidence level (CL) on the HH production cross section is set at 930 (740) fb, corresponding to 33 (26) times the standard model prediction. At 95% CL, HH production is observed (expected) to be excluded for values of κ_λ outside the range between -12 (-9.4) and 17 (15). Observed (expected) upper limits at 95% CL for the X $\to$ HH cross section are found to be within 160 to 2200 (200 to 1800) fb, depending on the mass of X. In the X $\to$ Y($\tau\tau$)H($\gamma\gamma$) search, the observed (expected) upper limits on the product of the production cross section and decay branching fractions vary between 0.059–1.2 fb (0.087–0.68 fb). For the X $\to$ Y($\gamma\gamma$)H($\tau\tau$) search the observed (expected) upper limits on the product of the production cross section and Y $\to \gamma\gamma$ branching fraction vary between 0.69–15 fb (0.73–8.3 fb) in the low Y mass search, tightening constraints on the next-to-minimal supersymmetric standard model, and between 0.64–10 fb (0.70–7.6 fb) in the high Y mass search.

Keywords: Beyond Standard Model, Hadron-Hadron Scattering, Higgs Physics

ArXiv ePrint: 2506.23012

https://doi.org/10.1007/JHEP05(2026)186

JHEP05(2026)186

Contents

JHEP05(2026)186

1 Introduction

The Higgs boson (H) holds a unique position in the standard model (SM) of particle physics as the only fundamental scalar boson. Since its discovery in 2012 at the CERN LHC by the ATLAS and CMS Collaborations [1–3], there has been an extensive research program to characterize its properties. So far, the properties have been measured to be consistent with SM predictions [4, 5]. Nevertheless, the measurements of several Higgs boson properties are extremely challenging at the LHC, leading to relatively weak constraints. One of the least constrained properties is the strength of the Higgs trilinear self-interaction, λ_{HHH}. Within the SM, the value of λ_{HHH} and subsequently the structure of the Higgs field potential are completely determined, given the Higgs boson mass, m_{H}, and the vacuum expectation value of the Higgs field. Measurements of λ_{HHH} thus provide a unique consistency test of the SM and impose constraints on the shape of the scalar potential.

At the LHC, λ_{HHH} is directly constrained through measurements of Higgs boson pair (HH) production. The primary production mechanism is via gluon-gluon fusion (ggF), with representative leading order (LO) diagrams shown in figure 1 (upper row). The destructive

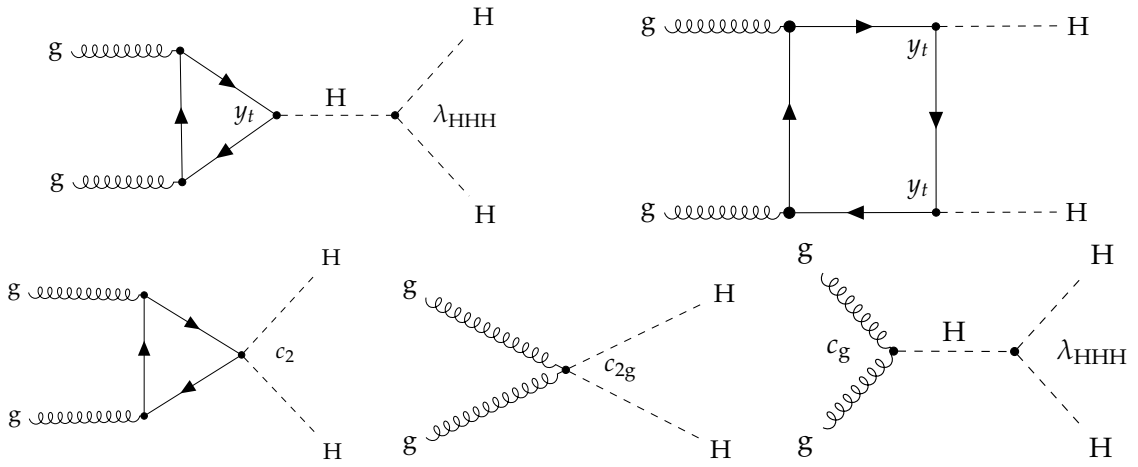

Figure 1. Leading order Feynman diagrams of the nonresonant HH production via ggF. The two diagrams in the upper row correspond to SM processes, involving the top Yukawa coupling y_t, and the trilinear Higgs boson self-coupling λ_{HHH}. The diagrams in the lower row correspond to BSM processes involving contact interactions introduced in the effective field theory, namely c_2, c_{2g} and c_g.

interference between diagrams leads to a small SM cross section at $\sqrt{s} = 13\,\text{TeV}$ of $31.1^{+2.1}_{-7.2}\,\text{fb}$, calculated for $m_H = 125\,\text{GeV}$ at next-to-next-to-leading order (NNLO), with resummation at next-to-next-to-leading-logarithm accuracy, and scale and top quark mass effects at next-to-leading order (NLO) [6–13]. This value is three orders of magnitude smaller than the single H production cross section, explaining why HH production is yet to be observed experimentally. The ultimate sensitivity is achieved via the combined analysis of final states, where CMS and ATLAS have recently reported upper limits on the HH cross section of 3.4 and 2.4 times the SM prediction at 95% confidence level (CL), respectively [4, 14].

The cross section and kinematical distributions of HH production can be significantly affected in many theories of physics beyond-the-SM (BSM). If the new particles introduced in these theories have sufficiently high masses, they will not be produced at current LHC energies. This motivates the use of an effective field theory (EFT) framework to parameterize the contributions of new physics in terms of higher-dimensional operators, suppressed by a large mass scale Λ. In this analysis, BSM contributions to nonresonant ggF HH production are parameterized through an effective Lagrangian that extends that of the SM with dimension-6 operators [15, 16]. This effective Lagrangian parameterizes BSM effects in terms of five couplings involving the Higgs boson. Two are present in the SM and are expressed as ratios to their SM values: the trilinear self-coupling ($\kappa_\lambda = \lambda_{HHH}/\lambda^{SM}_{HHH}$) and the top quark Yukawa coupling ($\kappa_t = y_t/y_t^{SM}$), while three are contact interactions not present in the SM: between two Higgs bosons and two top quarks (c_2), between two Higgs bosons and two gluons (c_{2g}), and between one Higgs boson and two gluons (c_g). Diagrams involving each of these five couplings are shown in figure 1 (lower row).

Moreover, many BSM theories predict the existence of additional scalar particles whose production can lead to the same final states studied in HH production. For example, the Randall-Sundrum (RS) bulk model [17–19], which predicts the existence of a spin-0 resonance referred to as the radion, and a spin-2 first Kaluza-Klein excitation of the graviton. Both

JHEP05(2026)186

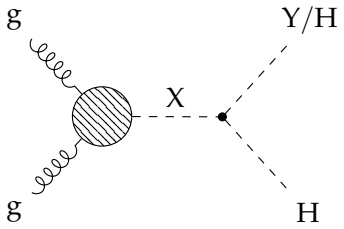

Figure 2. Feynman diagram of the resonant production of a pair of SM Higgs bosons ($X \to HH$), or of a SM Higgs boson and a new scalar particle ($X \to YH$).

resonances can decay to HH with a sizeable branching fraction, thus motivating the search for the resonant production of a Higgs boson pair.

Another example of a BSM theory is supersymmetry (SUSY), which extends upon the SM by introducing a fermionic (bosonic) partner for each boson (fermion) in the SM. One such theory, known as the next-to-minimal supersymmetric SM (NMSSM) [20], introduces an additional complex Higgs doublet and a complex singlet field. This scenario amounts to five neutral Higgs bosons, one of which being associated with the 125 GeV Higgs boson, H. Within the NMSSM, the heavier Higgs boson X may decay to lighter Higgs bosons (H or Y), inspiring the search for the $X \to YH$ process at the LHC. A Feynman diagram for the resonant production of two scalar bosons is shown in figure 2.

Recent results from the CMS experiment using data collected between 2016 and 2018 have yielded excesses in specific final states. An excess with a local (global) significance of 3.8 (2.8) standard deviations was observed in the $X \to Y(bb)H(\gamma\gamma)$ search at $m_X = 650\,\text{GeV}$ and $m_Y = 90\,\text{GeV}$ [21]. The search for a scalar particle decaying to a tau lepton pair yielded excesses at scalar masses of around 0.1 and 1.2 TeV with local (global) significances of 3.1 (2.7) and 2.8 (2.2) standard deviations respectively [22]. In addition, using data collected between 2016 and 2018, a search for a light Higgs boson decaying to a photon pair observed an excess with a local (global) significance of 2.9 (1.3) standard deviations at 95.4 GeV [23]. The compatibility in mass across these channels motivates searching for new scalar particles in different final states, complementing previous searches involving photons and tau leptons.

This paper presents a number of searches for the production of two scalar bosons in the $\gamma\gamma\tau\tau$ final state using proton-proton (pp) collision data collected by the CMS experiment between 2016 and 2018 at $\sqrt{s} = 13\,\text{TeV}$, corresponding to an integrated luminosity of 138 or $132\,\text{fb}^{-1}$, depending on the trigger path. Despite the small SM $HH \to \gamma\gamma\tau\tau$ branching fraction, the diphoton pair offers a clean experimental signature to trigger on with a good mass resolution, whilst the additional tau leptons in the event help further isolate signal from background. In total, there are five searches:

1. Nonresonant HH production via ggF.

2. Resonant HH production via a spin-0 particle, $X^{(0)} \to HH$.

3. Resonant HH production via a spin-2 particle, $X^{(2)} \to HH$.

JHEP05(2026)186

4. Resonant $X \to YH$ production, in the $X \to Y(\tau\tau)H(\gamma\gamma)$ decay channel.

5. Resonant $X \to YH$ production, in the $X \to Y(\gamma\gamma)H(\tau\tau)$ decay channel.

In addition to a search for HH production, the nonresonant search is used to place direct constraints on κ_λ, under the assumption that all other couplings of the Higgs boson have values as predicted by the SM. This search is also used to constrain EFT parameters by placing limits on the cross section of ggF HH production for thirteen non-SM benchmark scenarios involving the five couplings: κ_λ, κ_t, c_{2g}, c_g, and c_2. The benchmark scenarios are those proposed in refs. [24, 25].

In the resonant searches, no assumptions are made regarding the specific BSM theory to which new particles X and Y belong other than that they have a narrow width, are spin-0 except for $X^{(2)}$ which is spin-2, and that Y can decay to two photons or two tau leptons. The $X^{(0)} \to HH$ and $X^{(2)} \to HH$ searches consider the mass of X to be in the range from 260 to 1000 GeV. The $X \to Y(\tau\tau)H(\gamma\gamma)$ search considers a range in m_X from 300 to 1000 GeV and a range in m_Y from 50 to 800 GeV, whilst the $X \to Y(\gamma\gamma)H(\tau\tau)$ search considers the same m_X range, with a slightly reduced range in m_Y, from 70 to 800 GeV, which is imposed by a triggering requirement of $m_{\gamma\gamma} > 65$ GeV. Since X is the mother particle and Y is a decay product, m_X is required to be greater than $m_Y + m_H$.

In this analysis, results are extracted by performing fits to the diphoton invariant mass distribution, $m_{\gamma\gamma}$, in event categories designed to be enriched in signal events from one of the five searches. The first four searches amount to fitting a peak at m_H since the diphoton system is produced via the decay of a SM Higgs boson, $H \to \gamma\gamma$. In the $X \to Y(\gamma\gamma)H(\tau\tau)$ search, the strategy is different as the peak formed by $Y \to \gamma\gamma$ events must be fit over the wide range of considered m_Y values. To account for variations in the trigger efficiencies and event kinematics for different mass regimes, the $X \to Y(\gamma\gamma)H(\tau\tau)$ search is effectively split into two searches.

1. Low-mass $X \to Y(\gamma\gamma)H(\tau\tau)$ search considers m_Y in the range from 70 to 125 GeV.

2. High-mass $X \to Y(\gamma\gamma)H(\tau\tau)$ search considers m_Y in the range from 125 to 800 GeV.

This paper is organized as follows: Section 2 gives a description of the CMS detector and of the event reconstruction. The data and simulations used are detailed in section 3. An overview of the analysis strategy is provided in section 4, then the event selection is described in section 5, followed by sections 6 and 7, which explain the event categorization procedure for the nonresonant and resonant search, respectively. The signal and background modeling is described in section 8, and the treatment of systematic uncertainties is detailed in section 9. The results for each search are presented in section 10, and a summary of the paper is provided in section 11. Tabulated results are provided in the HEPData record for this analysis [26].

2 The CMS detector and event reconstruction

The central feature of the CMS apparatus is a superconducting solenoid of 6 m internal diameter, providing a magnetic field of 3.8 T. Within the solenoid volume are a silicon pixel and strip tracker, a lead tungstate crystal electromagnetic calorimeter (ECAL), and a brass and scintillator hadron calorimeter (HCAL), each composed of a barrel and two

JHEP05(2026)186

endcap sections. Forward calorimeters extend the pseudorapidity (η) coverage provided by the barrel and endcap detectors. Muons are measured in gas-ionization detectors embedded in the steel flux-return yoke outside the solenoid. A more detailed description of the CMS detector, together with a definition of the coordinate system used and the relevant kinematical variables, can be found in ref. [27].

Events of interest are selected using a two-tiered trigger system. The first level (L1), composed of custom hardware processors, uses information from the calorimeters and muon detectors to select events at a rate of around 100 kHz within a fixed latency of 4 μs [28]. The second level, known as the high-level trigger (HLT), consists of a farm of processors running a version of the full event reconstruction software optimized for fast processing, and reduces the event rate to around 1 kHz before data storage [29, 30].

A particle-flow (PF) algorithm [31] aims to reconstruct and identify each individual particle in an event, with an optimized combination of information from the various elements of the CMS detector. Photons and electrons are reconstructed, at least in part, from energy deposits in the ECAL. Reconstruction begins with a clustering algorithm that groups ECAL crystals with energies exceeding a given threshold. Then, clusters within a certain geometric area are merged into "superclusters" to include photon conversions and bremsstrahlung losses. Photon candidates are identified by clusters in the ECAL not linked to any charged-particle trajectories seeded in the pixel detector. The energy of the photon is then estimated by summing the energy of each crystal in the supercluster, calibrated and corrected for response variations in time. The direction of the photon is determined by the positions of the primary vertex (PV) and the supercluster. The PV is taken to be the vertex corresponding to the hardest scattering in the event, evaluated using tracking information alone, as described in section 9.4.1 of ref. [32]. An electron is identified by an ECAL cluster that is linked to a charged-particle trajectory, and its energy is estimated from a combination of the energy of the ECAL supercluster, and the momentum of the electron at the PV as determined by the tracker. Further detail about these reconstruction algorithms can be found in ref. [33].

The energy scale and resolution of photons and electrons are corrected in two stages. First, a multivariate regression technique based on simulation alone is employed to account for energy not being entirely deposited inside operational ECAL crystals. Then, a further set of corrections is derived using $\mathrm{Z} \to \mathrm{ee}$ events, such that simulation matches data. Both of these procedures are described in ref. [33].

The energy of muons is obtained from the curvature of the corresponding track. The energy of charged hadrons is determined from a combination of their momentum measured in the tracker and the matching ECAL and HCAL energy deposits, corrected for the response function of the calorimeters to hadronic showers. Finally, the energy of neutral hadrons is obtained from the corresponding corrected ECAL and HCAL energy deposits.

In the barrel section of the ECAL, an energy resolution of about 1% is achieved for unconverted or late-converting photons in the tens of GeV energy range. The energy resolution of the remaining barrel photons is about 1.3% up to $|\eta| = 1$, changing to about 2.5% at $|\eta| = 1.4$. In the endcaps, the energy resolution is about 2.5% for unconverted or late-converting photons, and between 3 and 4% for the other ones [34]. The diphoton mass resolution, as measured in $\mathrm{H} \to \gamma\gamma$ decays, is typically in the 1–2% range, depending on

JHEP05(2026)186

the measurement of the photon energies in the ECAL and the topology of the photons in the event [35].

The electron momentum is estimated by combining the energy measurement in the ECAL with the momentum measurement in the tracker. The momentum resolution for electrons with transverse momentum (p_T) equal to about 45 GeV from $Z \to ee$ decays ranges from 1.6 to 5%. It is generally better in the barrel region than in the endcaps, and also depends on the bremsstrahlung energy emitted by the electron as it traverses the material in front of the ECAL [33, 36].

Muons are measured in the pseudorapidity range $|\eta| < 2.4$, with detection planes made using three technologies: drift tubes, cathode strip chambers, and resistive plate chambers. The single muon trigger efficiency exceeds 90% over the full η range, and the efficiency to reconstruct and identify muons is greater than 96%. Matching muons to tracks measured in the silicon tracker results in a relative transverse momentum resolution, for muons with p_T up to 100 GeV, of 1% in the barrel and 3% in the endcaps. The p_T resolution in the barrel is better than 7% for muons with p_T up to 1 TeV [37].

For each event, hadronic jets are clustered from these reconstructed particles using the infrared- and collinear-safe anti-k_T algorithm [38, 39] with a distance parameter of 0.4. Jet momentum is determined as the vectorial sum of all particle momenta in the jet, and is found from simulation to be, on average, within 5 to 10% of the true momentum over the whole p_T spectrum and detector acceptance. Additional pp interactions within the same or nearby bunch crossings (pileup) can contribute additional tracks and calorimetric energy depositions, increasing the apparent jet momentum. To mitigate this effect, tracks identified to be originating from pileup vertices are discarded and an offset correction is applied to correct for remaining contributions [40]. Jet energy corrections are derived from simulation studies so that the average measured energy of jets becomes identical to that of particle level jets. In situ measurements of the momentum balance in dijet, photon + jet, Z + jet, and multijet events are used to determine any residual differences between the jet energy scale in data and in simulation, and appropriate corrections are made [41]. Additional selection criteria are applied to each jet to remove jets potentially dominated by instrumental effects or reconstruction failures [40]. Jets originating from b quarks are identified using the DEEPJET algorithm [42–44] at the medium working point defined by a light-quark or gluon jet misidentification rate of 1%, and a b jet identification efficiency of 75%.

Hadronic τ lepton decays (τ_h) are reconstructed from jets, using the hadrons-plus-strips algorithm [45], which combines 1 or 3 tracks with energy deposits in the calorimeters, to identify the tau decay modes. Neutral pions are reconstructed as strips with dynamic size in η-ϕ from reconstructed electrons and photons, where the strip size varies as a function of the p_T of the electron or photon candidate. A correction to the τ_h energy scale in simulation is derived by comparing simulation and data in Z/γ^* events [45].

To distinguish genuine τ_h decays from jets originating from the hadronization of quarks or gluons, and from electrons, or muons, the DeepTau algorithm is used [46]. Information from all individual reconstructed particles near the τ_h axis is combined with properties of the τ_h candidate and the event. The algorithm provides three discriminants, D_e, D_μ, and D_{jet}, which are designed to distinguish τ_h candidates from electrons, muons, and jets, respectively.

JHEP05(2026)186

The efficiency for identifying a genuine τ_h candidate using these discriminants is measured in data with $Z \to \tau\tau \to \tau_h\mu$ events for taus with $p_T < 140\,\text{GeV}$ and $W^* \to \tau\nu_\tau$ events for $p_T > 140\,\text{GeV}$. Corrections are applied to simulated events, such that the efficiencies measured in simulation match those measured in data.

The rate of a jet to be misidentified as τ_h by the DeepTau algorithm depends on the p_T and quark flavor of the jet. In simulated events from W boson production in association with jets, it has been estimated to be 0.43% for a genuine τ_h identification efficiency of 70%. The misidentification rate for electrons (muons) is 2.60 (0.03)% for a genuine τ_h identification efficiency of 80 (>99)%.

The missing transverse momentum vector $\vec{p}_T^{\,\text{miss}}$ is computed as the negative vector sum of the transverse momenta of all the PF candidates in an event, and its magnitude is denoted as p_T^{miss} [47]. The $\vec{p}_T^{\,\text{miss}}$ is modified to account for corrections to the energy scale of the reconstructed jets in the event.

3 Data and simulated samples

This analysis uses data collected by the CMS detector during LHC pp collisions corresponding to a total integrated luminosity of $138\,\text{fb}^{-1}$, in which 36.3, 41.5, and $59.8\,\text{fb}^{-1}$ were collected during 2016, 2017, and 2018, respectively [48–50]. In 2018, the trigger used in the low-mass $X \to Y(\gamma\gamma)H(\tau\tau)$ search was not introduced until after the start of that year's data taking, resulting in a lower integrated luminosity of $54.4\,\text{fb}^{-1}$.

The Monte Carlo (MC) simulation of the ggF HH signal is generated with powheg 2.0 using the full top quark mass dependence [25] and with NLO accuracy in perturbative quantum chromodynamics (QCD) [51–58]. Both SM ($\kappa_\lambda = 1$) and BSM ($\kappa_\lambda = 0, 2.45, 5$) scenarios are studied. The dependence of the ggF HH cross section on κ_λ and κ_t can be expressed, to any order in QCD, by three terms, corresponding to diagrams involving κ_λ, κ_t, and their interference [53]. Therefore, any linear superposition of three samples involving unique κ_λ values can be used to obtain the signal sample corresponding to an arbitrary point in the $(\kappa_\lambda, \kappa_t)$ parameter space.

Following the recommendations from refs. [24, 25], a reweighting of the NLO κ_λ samples is applied to produce 13 EFT benchmark hypotheses, each corresponding to a different point in the 5D parameter space defined by the couplings: κ_λ, κ_t, c_2, c_g, and c_{2g}. The list of benchmark hypotheses generated is provided in table 1. The reweighting procedure operates at the event level by using a parameterization of the differential cross section in the true invariant mass of the HH system and the angular distance between the two Higgs bosons in the azimuthal plane, which completely characterizes the hard scattering because it only has two degrees of freedom [59, 60].

In the resonant searches, we consider the production of X via ggF. The signal simulation samples for these searches are generated using MadGraph5_aMC@NLO (version 2.6.5) at LO accuracy [61]. Within the search ranges of m_X and m_Y, 17, 17, 91 and 83 simulation samples are generated for the $X^{(0)} \to HH$, $X^{(2)} \to HH$, $X \to Y(\tau\tau)H(\gamma\gamma)$ and $X \to Y(\gamma\gamma)H(\tau\tau)$ processes respectively.

The dominant irreducible background for this analysis arises from prompt diphoton production ($\gamma\gamma$ + jets), while a dominant reducible background comes from γ + jets events,

JHEP05(2026)186

	SM	1	2	3	4	5	6	7	8	8*a*	9	10	11	12
κ_λ	1.0	7.5	1.0	1.0	-3.5	1.0	2.4	5.0	15.0	1.0	1.0	10.0	2.4	15.0
κ_t	1.0	1.0	1.0	1.0	1.5	1.0	1.0	1.0	1.0	1.0	1.0	1.5	1.0	1.0
c_2	0.0	-1.0	0.5	-1.5	-3.0	0.0	0.0	0.0	0.0	0.5	1.0	-1.0	0.0	1.0
c_g	0.0	0.0	-0.8	0.0	0.0	0.8	0.2	0.2	-1.0	4/15	-0.6	0.0	1.0	0.0
c_{2g}	0.0	0.0	0.6	-0.8	0.0	-1.0	-0.2	-0.2	1.0	0.0	0.6	0.0	-1.0	0.0

Table 1. Parameter values of nonresonant BSM benchmark hypotheses. The first column corresponds to the SM sample, while the next 13 correspond to the benchmark hypotheses identified using the method from refs. [24, 25].

where jets can be misidentified as photons or tau leptons. The $\gamma\gamma$ + jets process is modeled at LO with SHERPA v.2.2.1 [62], which includes tree-level processes with up to three additional jets, as well as box processes at LO accuracy. The γ + jets process is instead modeled at LO with MADGRAPH5_aMC@NLO v2.6.5 [61, 63].

Other nonresonant backgrounds include V + γ, $t\bar{t}$, $t\bar{t}$ + γ, and $t\bar{t}$ + $\gamma\gamma$ where $t\bar{t}$ is a top quark-antiquark pair and the vector bosons (either from direct production or decays of the top quark) can decay into τ leptons and associated jets can be misidentified as photons. These processes are simulated at NLO in QCD using MADGRAPH5_aMC@NLO v2.6.5 [61, 63, 64] for all except $t\bar{t}$ which uses MADGRAPH5_aMC@NLO v2.6.1.

Single Higgs boson production in the SM, where the Higgs boson decays to a pair of photons, is considered a resonant background. We include the following production modes: ggF, vector-boson fusion (VBF), vector boson associated production (VH), and production associated with a $t\bar{t}$ pair ($t\bar{t}$H). These processes are simulated using MADGRAPH5_aMC@NLO v2.4.2, with cross sections and decay branching ratios taken from ref. [15]. No other processes with a single Higgs boson are considered, as their contributions are negligible.

All simulated samples are interfaced using PYTHIA 8.240 with the CP5 tune [65, 66] for parton showering, fragmentation with the standard p_T-ordered parton shower scheme and the underlying event description. Parton distribution functions (PDFs) are taken from the NNLO NNPDF 3.1 set [67]. The detector response is modeled using the GEANT4 package [68]. The simulation includes a description of pileup interactions and a reweighting is applied to the simulated events such that the distribution of the number of interaction vertices matches that seen in data.

4 Analysis strategy

Proton-proton collision events deemed compatible with the $\gamma\gamma\tau\tau$ final state are selected starting from a diphoton high-level trigger with asymmetric photon p_T thresholds of 30 and 18 GeV. For all except the low-mass $X \to Y(\gamma\gamma)H(\tau\tau)$ search, the subleading photon threshold is increased to 22 GeV for 2017 and 2018. The triggers also apply loose isolation requirements. After the trigger selection, the photon candidates are required to pass a loose selection on kinematical variables, with different thresholds for the low-mass $X \to Y(\gamma\gamma)H(\tau\tau)$, and a photon identification criterion, as discussed in section 5. The invariant mass of the diphoton candidate, $m_{\gamma\gamma}$, is required to be greater than 65 GeV for the low-mass $X \to Y(\gamma\gamma)H(\tau\tau)$

JHEP05(2026)186

search, and greater than 100 GeV for all other searches. In addition, to enter the analysis events must contain a valid $\tau\tau$ candidate or have a single τ_h candidate, as detailed in section 5.

In each search, a separate machine-learning classifier is used to further isolate events with signal-like characteristics from background. The classifiers are trained independently in each search using MC simulation of signal and background events. For the nonresonant search, a boosted decision tree (BDT) discriminant is applied which uses input features related to the kinematical properties of the event constituents. Sequential boundaries are placed on the BDT output to define event categories of different signal purity, where the boundary positions are chosen to maximize signal sensitivity. Further details are provided in section 6.

In the resonant searches, we look for signal events produced over a wide range of resonance mass hypotheses. As the kinematical properties of the signal events vary dramatically over the considered mass range, it would be suboptimal to train a single classification algorithm using all mass points to identify signal from background. However, it would not be feasible to train a separate classification algorithm at each mass point due to the large number of mass points considered. A parameterized neural network (pNN) [69] is thus employed, which uses the nominal m_X (and m_Y for the $X \to YH$ searches) as additional training features. The pNN is trained with signal simulation from multiple mass hypotheses simultaneously, allowing it to implicitly learn how the kinematical distributions evolve with m_X (and m_Y) and thereby change the way it discriminates between signal and background based upon the resonance mass. In this approach, only one pNN is needed for each of the resonant searches, leading to five pNNs in total. Furthermore, provided that enough mass hypotheses within a given range are used in training, the pNN can be applied to mass hypotheses inside that range, regardless of whether they were used in training or not.

A set of analysis categories is defined by placing boundaries on the pNN output, where the pNN is evaluated at the values of m_X (and m_Y) that correspond to the mass hypothesis considered. The boundary positions are chosen to provide good signal sensitivity whilst maintaining a sufficient background yield to be able to fit the background model successfully. A new set of categories with its own boundaries is defined using the pNN output for each mass hypothesis considered.

The granularity in m_X (and m_Y) chosen to evaluate the pNN and define the analysis categories is motivated by the experimental resolution in m_X (and m_Y). Initially, a granularity of mass hypotheses corresponding to the simulation samples generated is considered, and for each hypothesis, results are obtained using categories defined for that hypothesis and also for neighbouring hypotheses in m_X (and m_Y). If the results differ by more than 10%, the event selection is considered to have changed significantly enough to justify a finer granularity. In this case, the ranges between the mass hypotheses are divided into equal-sized intervals to keep the variations of the results below 10%, under the assumption that the results vary linearly. In total, there are 27, 27, 398, 1765 and 2547 mass hypotheses considered in the $X^{(0)} \to HH$, $X^{(2)} \to HH$, $X \to Y(\tau\tau)H(\gamma\gamma)$, low-mass $X \to Y(\gamma\gamma)H(\tau\tau)$ and high-mass $X \to Y(\gamma\gamma)H(\tau\tau)$ searches, respectively. Details on the pNN training and on the interpolation between mass points are given in sections 7 and 8.

In each search, maximum likelihood fits are performed to the $m_{\gamma\gamma}$ distributions of the corresponding event categories. A likelihood function is defined for each analysis category

JHEP05(2026)186

using analytic probability density functions (pdf) of $m_{\gamma\gamma}$ for the signal and backgrounds. The smoothly falling background (continuum) is modeled directly from data. The signal and the single H production, which constitutes a resonant background, are modeled from simulation. In the $X \to Y(\gamma\gamma)H(\tau\tau)$ search, there is an additional background from Drell-Yan (DY) process where the two electrons from a Z decay are misidentified as photons. This background is modeled from data using an ABCD method [70]. The fits are used to extract 95% CL upper limits on the relevant production cross sections.

5 Event selection

Events are required to have at least two photon candidates. Photons are required to have $|\eta| < 2.5$, excluding the barrel-endcap transition region ($1.442 < |\eta| < 1.566$). Depending on their psudorapidity they are labelled as barrel photons ($|\eta| < 1.442$) or endcap photons ($1.566 < |\eta| < 2.5$). The variables used to select photon candidates include:

- Charged-hadron isolation ($\mathcal{I}_{\text{ch}}$), the p_{T} sum of charged hadrons within a cone of $R = 0.3$ centered around the photon direction.
- Photon isolation ($\mathcal{I}_{\text{ph}}$), the p_{T} sum of photons within a cone of $R = 0.3$ centered around the photon direction.
- Track isolation ($\mathcal{I}_{\text{tk}}$), the p_{T} sum of all charged-particle tracks within a cone of $R = 0.3$ centered around the photon direction.
- Hadronic over electromagnetic energy ratio (H/E), the ratio of the energy in the HCAL tower behind the photon supercluster to the energy of the photon's supercluster.
- R_9, the energy sum of the 3×3 crystals centered around the most energetic crystal in the cluster divided by the energy of the photon.
- $\sigma_{i\eta i\eta}$, the energy-weighted spread in η of the 5×5 crystals centered around the most energetic crystal in the cluster [33].

The isolation variables are corrected to mitigate the contribution from pileup [33]. Selected photons are required to have $p_{\text{T}} > 25\,\text{GeV}$, $\mathcal{I}_{\text{ch}} < 20\,\text{GeV}$, $\mathcal{I}_{\text{ch}}/p_{\text{T}}^{\gamma} < 0.3$, H/E < 0.08, and pass a "conversion-safe" electron veto criterion that rejects photons consistent with any charged particle tracks not matched to a conversion vertex [34]. Further requirements are applied separately for barrel and endcap photons in the low R_9 category. These requirements are shown in table 2 for the respective R_9 ranges. No further requirements are applied to the high R_9 category (>0.85 and >0.90 for barrel and encaps, respectively). Photon candidates are also required to satisfy a loose identification criterion based on a BDT classifier trained to separate photons from jets [33]. The BDT is trained using variables that describe the shape of the photon's electromagnetic shower and isolation.

All events are required to have at least one diphoton candidate and in the case where several candidates exist, the candidate with the highest scalar sum p_{T} of the photons is chosen. Additionally, at least one photon in the pair must have $p_{\text{T}} > 30\,\text{GeV}$. Diphoton candidates are required to have an invariant mass ($m_{\gamma\gamma}$) in the range 100–180 GeV for the searches

JHEP05(2026)186

	R_9	$\sigma_{i\eta i\eta}$	$\mathcal{I}_{\text{ph}}$ (GeV)	$\mathcal{I}_{\text{tk}}$ (GeV)
Barrel	[0.50, 0.85]	<0.015	<4.0	<6.0
Endcaps	[0.80, 0.90]	<0.035	<4.0	<6.0

Table 2. Additional photon requirements for barrel and endcap photons at different ranges of R_9, intended to mimic the HLT requirements.

targeting processes with a $\mathrm{H} \to \gamma\gamma$ decay. For the $\mathrm{Y} \to \gamma\gamma$ decay, this range is extended to 65–150 GeV and 100–1000 GeV for the low-mass and high-mass searches respectively. In all but the low-mass $\mathrm{X} \to \mathrm{Y}(\gamma\gamma)\mathrm{H}(\tau\tau)$ search, we impose mass-dependent photon p_{T} requirements of $p_{\mathrm{T}}/m_{\gamma\gamma} > 1/3$ and $>1/4$ for the highest p_{T} (leading) and second-highest p_{T} (subleading) photons, respectively.

When constructing an $\mathrm{H/Y} \to \tau\tau$ candidate, both hadronic and leptonic decay modes of the τ lepton are considered. Therefore, three primary physics objects are considered: e, μ, and τ_{h}.

Electron candidates are required to have $p_{\mathrm{T}} > 10\,\mathrm{GeV}$ and $|\eta| < 2.5$, excluding the barrel-endcap transition region ($1.442 < |\eta| < 1.566$). Furthermore, the electron's impact parameter with respect to the PV in the transverse plane (d_{xy}) is required to be less than 0.045 cm, and the distance between the vertex and electron along the beam axis (d_{z}) is required to be less than 0.2 cm.

Muon candidates are selected by demanding: $p_{\mathrm{T}} > 15\,\mathrm{GeV}$, $|\eta| < 2.4$, $d_{\mathrm{xy}} < 0.045\,\mathrm{cm}$, $d_{\mathrm{z}} < 0.2\,\mathrm{cm}$. In addition, isolation and identification requirements are imposed on both electron and muon candidates [37, 71]. Finally, an isolation requirement of $\Delta R = \sqrt{\Delta\eta^2 + \Delta\phi^2} > 0.2$ with respect to selected photons is placed.

The τ_{h} candidates are required to have $p_{\mathrm{T}} > 20\,\mathrm{GeV}$, $|\eta| < 2.3$, $d_{\mathrm{z}} < 0.2\,\mathrm{cm}$. Additionally, an isolation requirement of $\Delta R > 0.2$ with respect to the selected photons and leptons is placed. Finally, a selection is applied using the DeepTau discriminants. For genuine τ_{h} candidates with $p_{\mathrm{T}} \in [30, 70]\,\mathrm{GeV}$ from $\mathrm{H} \to \tau\tau$ events, the selections result in identification efficiencies of 99%, 99.95%, and 80% for D_{e}, D_{μ}, and D_{jet}, respectively [46].

If only one τ_{h} candidate is found in the event, with no additional electrons or muons passing the selection, further tau lepton candidates are searched for as isolated tracks. These tracks must be associated with PF candidates, originate from the PV, have $p_{\mathrm{T}} > 5\,\mathrm{GeV}$, $d_{\mathrm{xy}} < 0.2\,\mathrm{cm}$ and $d_z < 0.1$ cm. An isolation requirement of $\Delta R > 0.2$ is applied with respect to the selected photons, electrons, muons, and τ_{h}.

A $\tau\tau$ candidate can be identified from any of the following pairs of reconstructed objects: $\tau_{\mathrm{h}}\tau_{\mathrm{h}}$, $\tau_{\mathrm{h}}\mu$, $\tau_{\mathrm{h}}\mathrm{e}$, $\mu\mathrm{e}$, $\mu\mu$, ee, τ_{h} + isolated track. Any event with an opposite-sign same flavor (OSSF) ee or $\mu\mu$ pair is rejected if either: $m_{\ell\ell} \in [80, 100]\,\mathrm{GeV}$ or $m_{\ell\ell\gamma} \in [86, 96]\,\mathrm{GeV}$, where $m_{\ell\ell\gamma}$ is calculated with respect to both the leading and subleading photons, and m_Z is the nominal Z boson mass. This selection rejects events consistent with a $\mathrm{Z} \to \ell\ell$ or $\mathrm{Z} \to \ell\ell\gamma$ decay. Events are selected if they have a valid $\tau\tau$ candidate or if they have a single τ_{h} candidate.

In this analysis, information about jets in the event is used by the multivariate techniques described in sections 6 and 7 to reject backgrounds, such as $\mathrm{t\bar{t}}$ production. Selected jets

JHEP05(2026)186

are required to have $p_T > 25\,\text{GeV}$, $|\eta| < 2.4$, and to be isolated from photons, leptons, or τ_h candidates, which is attained by requiring $\Delta R > 0.4$ between the jet and those objects.

6 Nonresonant search event categorization

After the selection described in section 5 is applied, events are categorized according to a discriminant designed to separate signal from background. In the nonresonant search, this discriminant is the output of a BDT trained with the XGBOOST [72] framework on simulated samples of signal and background processes. The nonresonant background simulated samples include γ + jets, $\gamma\gamma$ + jets, $t\bar{t}$ + jets, $t\bar{t} + \gamma$, $t\bar{t} + \gamma\gamma$, and $V + \gamma$ processes, while the resonant background simulated samples include ggH, VBF, VH, and $t\bar{t}H$. The samples used for training are independent from the ones used to evaluate the categorization performance and to create the final signal and resonant background models. This is also the case in the resonant searches.

Input features of the BDT include kinematical properties of the physics objects in each event: jets, leptons, photons, jet and lepton multiplicities, p_T^{miss}, and the b tagging scores of jets from the DEEPJET algorithm [42–44]. In channels that include more than one tau lepton candidate, a likelihood-based estimate of the invariant mass $m_{\tau\tau}$ [73] is also included. This estimation combines the measurement of p_T^{miss} and measurements of the visible $\tau\tau$ decay products. A further consideration in the input feature selection is the effect the BDT selection could have on the $m_{\gamma\gamma}$ spectrum. The background modeling later described in section 8.3 requires the $m_{\gamma\gamma}$ distribution of the continuum background to be smoothly falling such that the analytical functions chosen can model it well. It is important that no peaking structure is induced in the distribution which could lead to an artificial excess. Therefore, $m_{\gamma\gamma}$ is not included as an input feature, and the p_T of the photon candidates are divided by $m_{\gamma\gamma}$ to reduce correlations between the photon's p_T and $m_{\gamma\gamma}$. The $m_{\gamma\gamma}$ distributions of the continuum background in simulation after the BDT selection are studied and no peaking structure is found.

The output score distribution from the BDT is shown in figure 3. Events are then categorized according to boundaries placed on the output score. The boundaries are set by optimizing the expected upper limit on the cross section of nonresonant HH production, where the limit is calculated with signal and background yields from simulation and without systematic uncertainties included. Events are discarded if they have a BDT score <0.974. Two categories are defined with the rest of the events. The category purest in nonresonant ggF HH production (Cat 0), with a BDT score >0.989, has a signal efficiency with respect to the inclusive phase space of 10.5%. The second category (Cat 1), with a BDT score <0.989, has a signal efficiency of 3.5%. The possibility of having a greater number of categories was investigated but the improvement to the expected upper limit was found to be negligible.

7 Resonant searches event categorization

In the resonant search, the discriminants used for event categorization are the outputs of pNNs which were first introduced in section 4. Events passing the initial selection are used to train a pNN in each resonant search. The background simulation includes the $\gamma\gamma$ + jets, $t\bar{t} + \gamma$,

JHEP05(2026)186

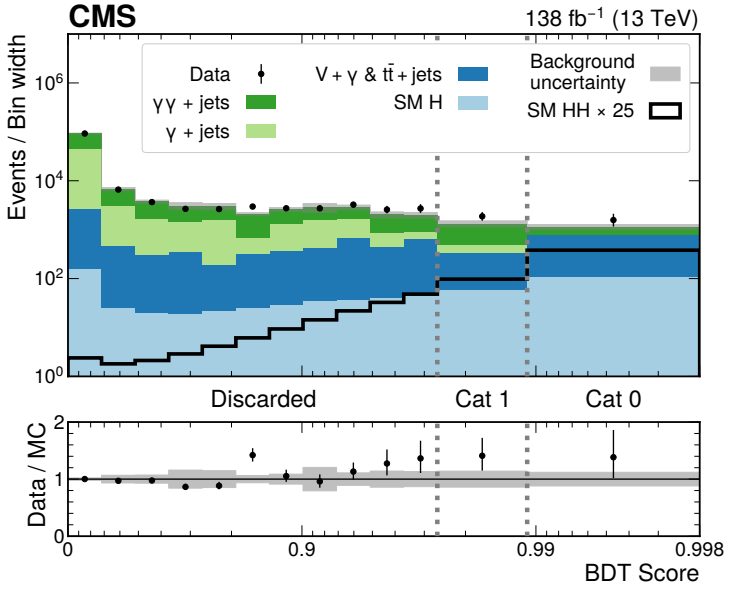

Figure 3. Distribution of the BDT scores used for the nonresonant analysis event categorization from data (black points) and predictions from MC simulation (colored histograms). The "SM H" process includes ggH, VBF, VH, and $\mathrm{t\bar{t}H}$, and the $\mathrm{t\bar{t}}$ + jets process also includes the $\mathrm{t\bar{t}} + \gamma$ and $\mathrm{t\bar{t}} + \gamma\gamma$ processes. The background histograms are stacked, while the signal distribution is shown separately. The normalization of the signal distribution is set to 25 times the SM prediction and the background MC simulation is normalized to data. The ratio of the data to the sum of the background predictions is shown in the lower panel. Statistical MC uncertainties for the background are represented by the gray shaded bands. The gray dotted lines represent the boundaries that define the two analysis categories (Cat 0 and Cat 1). The rest of the data, labeled as 'discarded' is not used in the fit to data.

$\mathrm{t\bar{t}} + \gamma\gamma$, and $\mathrm{V} + \gamma$ processes. The γ + jets and $\mathrm{t\bar{t}}$ + jets processes are not used in training because they have limited sample sizes after the initial selection and lead to overtraining.

Each signal sample (one for every mass hypothesis) is then weighted such that they all have an equal sum of weights. In each training batch, there are an equal number of signal and background events. These events are randomly sampled from the entire data set with probabilities given by their weights. Once a batch is created, the weight of every event is set to be unity so that the events are unweighted in the loss function.

A neural network that is trained to discriminate background from signal for a single mass hypothesis ($m_\mathrm{X} = m_\mathrm{i}$) has an output score that can be written as $f^i(\vec{x})$ where $\vec{x}$ is a vector of input features. In the case of a pNN, the function that we want to obtain is instead $f(\vec{x}; m_\mathrm{X})$, where $f(\vec{x}; m_\mathrm{X} = m_i) = f^i(\vec{x})$. This way we can have a single network, which adapts the way it discriminates based upon the target mass hypothesis.

To achieve the intended parameterized behavior, the pNN is trained on simulated events from background and from all the signal hypotheses simultaneously. The parameters are included as additional input features, whose distributions are identical for the signal and background processes by construction. The simulated signal events for the $\mathrm{X} \to \mathrm{HH}$ ($\mathrm{X} \to \mathrm{YH}$) processes are assigned values of m_X (and m_Y), which correspond to the simulation sample they originated from. For the sake of assigning m_X (and m_Y) to the background

JHEP05(2026)186

events, each background event in a batch is randomly paired with a signal event, and the m_X (and m_Y) values from the signal event are given to the background event. This ensures that on a batch-by-batch basis, there is no direct discrimination power provided by the parameters. Therefore, the network's dependence on the parameters is motivated purely by the correlation between the parameters and the rest of the variables.

To check whether the pNN performs well for mass hypotheses not used in training, tests are performed where the pNN is trained using samples from all nominal hypotheses except one, and the performance of that pNN for the excluded hypothesis is compared to the pNN which is trained on all hypotheses. This test is performed in every search and for all mass hypotheses which are not at the boundaries of the mass ranges. At a background efficiency of 1%, the relative changes to the signal efficiency are less than 1% for all but three of the tests, and less than 2% for all of them.

The input features for the resonant pNNs are the same as those used for the nonresonant search BDT with the addition of the invariant mass of the $\gamma\gamma\tau\tau$ system, $m_{\gamma\gamma\tau\tau}$, which includes a p_T^{miss} correction. As in the nonresonant search, the continuum background distributions of $m_{\gamma\gamma}$ are studied in simulation to look for peaking structures induced by the pNN selection. In the high-mass $X \to Y(\gamma\gamma)H(\tau\tau)$ search, which has a significantly different range in $m_{\gamma\gamma}$ compared to the other searches, the exclusion of $m_{\gamma\gamma\tau\tau}$ and $m_{\ell\ell\gamma}$ from the input features was found necessary to prevent sculpting. In all other searches, no peaking structures were found.

For each mass hypothesis, we perform a probability integral transform so that the distribution of the output score for the simulated background events is uniform. This transformation is applied to both data and simulation before defining the pNN boundaries for each category. This choice helps with the interpolation of the signal efficiency because a set of boundaries on a pNN score now corresponds to the same efficiency on the simulated background events, regardless of m_X (and m_Y). Given also that the network input distributions of the signal evolve in a continuous way with m_X (and m_Y), it is expected that the signal efficiencies for a given background efficiency, or equivalently, a set of pNN boundaries, will evolve in a predictable manner. In section 8, one finds that this is indeed the case.

The transformed pNN output score distributions evaluated at $m_X = 260\,\text{GeV}$ and 800 GeV for data and simulated signal and background events (including γ + jets and $t\bar{t}$ + jets) are shown in figure 4 for the $X^{(2)} \to HH$ search. The plots demonstrate how the discriminating power changes as a function of m_X. At the high m_X value of 800 GeV, the signal distribution has migrated towards higher scores, showing it is easier to discriminate a high m_X signal from background. In addition, the background composition in the signal-like bins changes. For example, the relative contribution to the background from single H production is larger for $m_X = 800\,\text{GeV}$, compared to $m_X = 260\,\text{GeV}$.

Examples of transformed pNN output score distributions for all resonant searches are shown in figure 5. For each search, taking into account the search results discussed in section 10, the pNN is evaluated at the mass hypothesis where the largest excess with respect to the background-only hypothesis is found in data.

Event categories are defined by placing boundaries on the transformed pNN output scores according to the expected number of simulated background events (including γ + jets and $t\bar{t}$ + jets) in each category. The events are ordered by their pNN scores and categorized

JHEP05(2026)186

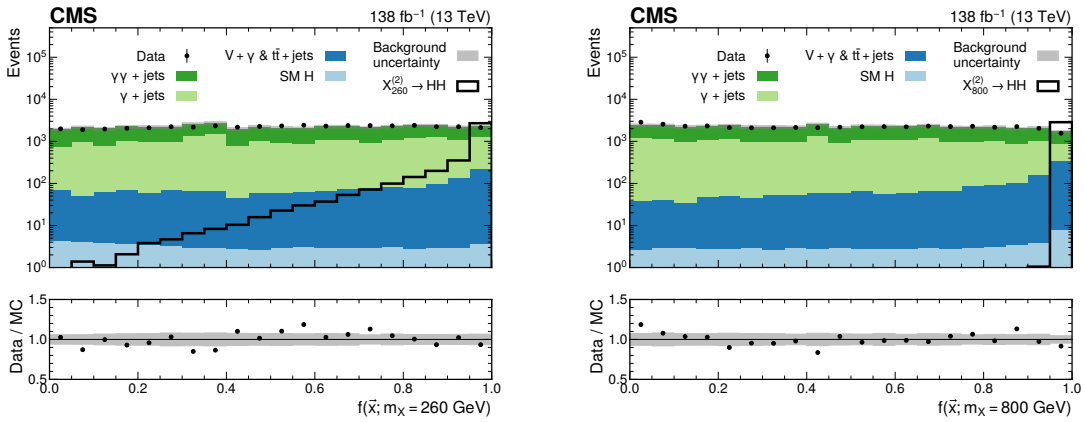

Figure 4. Transformed output of the pNN used in the $X^{(2)} \to HH$ search, evaluated at $m_X = 260\,\text{GeV}$ (left) and 800 GeV (right). The filled histograms represent the background simulation, and the data are shown by the black points. The "SM H" process includes ggH, VBF, VH, and $t\bar{t}H$, and the $t\bar{t}$ + jets process also includes the $t\bar{t} + \gamma$ and $t\bar{t} + \gamma\gamma$ processes. The targeted signal distributions for which the pNN is evaluated are shown by the black unfilled histograms. The background MC simulation is normalized to data and the signal is normalized to an arbitrary cross section for representation purposes. The ratio of the data to the sum of the background predictions is shown in the lower panel. Statistical MC uncertainties for the background are represented by the gray shaded bands.

starting from the highest pNN scores. A minimum number of expected events in a category was found needed to reduce bias originating from the choice of function used to model the background $m_{\gamma\gamma}$ distribution. This bias is reduced by using the discrete profiling method [74] but is not completely eliminated. To quantify the residual bias, a large number of pseudo-datasets are generated for a representative set of mass points and significances are calculated for each pseudo-dataset when fixing the background function to the one used to generate the datasets and when allowing the background function to float. For a given mass point, the fraction of datasets with a significance higher than X, where the range $0 < X < 3$ is considered, were compared and the maximum difference was taken to be the residual bias. A minimum number of 10 expected events was chosen since it was the lowest number (and therefore most sensitive) which still led to acceptable bias of 20%.

In each resonant search, event categories are sequentially defined, starting with 10 expected background events, and continuing to add categories with 10 events, evaluating the expected limits on $\sigma(X \to (Y/H)H \to \gamma\gamma\tau\tau)$ with every category added. This continues until none of the limits improve by more than 1%, at which point a category with twice the number of events is considered instead. This continues until the sum of events across all categories is greater than the number in data after preselection. This results in four categories of 10 events, one category of 20 events and one category of 80 events for each search, going from the most to least sensitive, and the $X \to YH$ searches have a final, extra category of 320 events.

In the $X^{(2)} \to HH$ search, the expected limits at the nominal mass hypotheses using this categorization were compared to those found using an alternative categorization strategy that was performed for each hypothesis individually, and was a grid search of category boundaries aimed at minimizing the expected limit. For $m_X > 320\,\text{GeV}$, the grid-search

JHEP05(2026)186

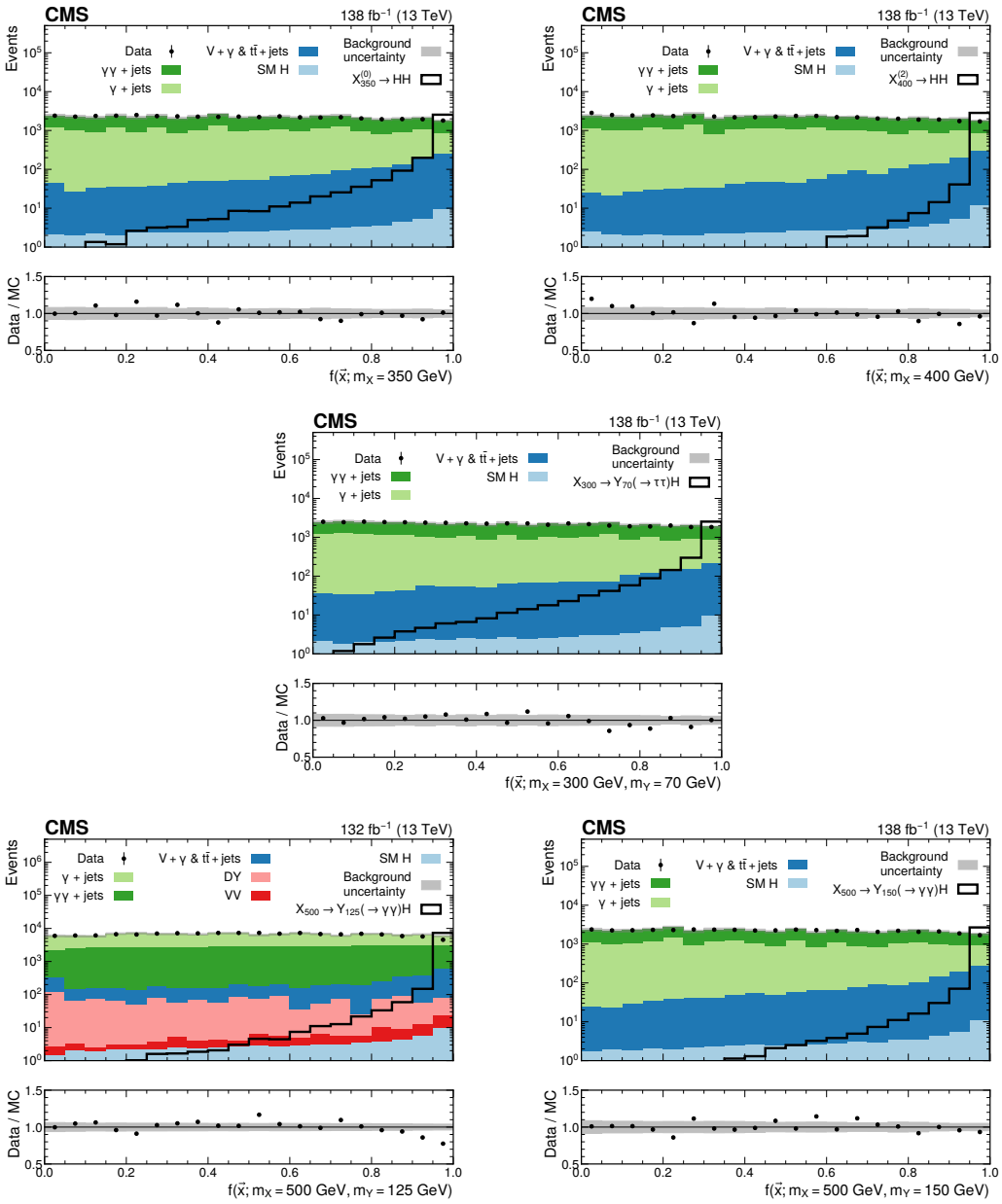

Figure 5. Transformed output of the pNNs used in the $X^{(0)} \to HH$ (upper left), $X^{(2)} \to HH$ (upper right), $X \to Y(\tau\tau)H(\gamma\gamma)$ (middle), low-mass $X \to Y(\gamma\gamma)H(\tau\tau)$ (lower left) and high-mass $X \to Y(\gamma\gamma)H(\tau\tau)$ (lower right) searches. The pNNs are evaluated at the mass points where the largest excess with respect to the background-only hypothesis is observed. If the MC simulation at this mass point is not available, then the sample produced at a mass point closest to the excess is shown. The filled histograms represent the background simulation, and the data are shown by the black points. The "SM H" process includes ggH, VBF, VH, and $t\bar{t}H$, and the $t\bar{t}$ + jets process also includes the $t\bar{t} + \gamma$ and $t\bar{t} + \gamma\gamma$ processes. The targeted signal distributions for which the pNN is evaluated are shown by the black open histograms. The background MC simulation is normalized to data and the signal is normalized to an arbitrary cross section for representation purposes. The ratio of the data to the sum of the background predictions is shown in the lower panel. Statistical MC uncertainties for the background are represented by the gray shaded bands.

JHEP05(2026)186

approach improved the limits by at most 0.2%, and for $m_X < 320\,\text{GeV}$, by at most 1.4%. The categorization strategy based upon expected background events is used despite this because it can be applied to the intermediate mass hypothesis too, which is not possible with the grid-search approach, and the losses in sensitivity at the nominal mass hypotheses are considered small.

8 Signal and background modeling

This section describes the construction of the signal and background models used in the maximum likelihood fits. For the nonresonant HH, $X^{(0)} \to HH$, $X^{(2)} \to HH$ and $X \to Y(\tau\tau)H(\gamma\gamma)$ searches, the probability density functions (pdfs) are defined over the range of $100 < m_{\gamma\gamma} < 180\,\text{GeV}$. In the high-mass $X \to Y(\gamma\gamma)H(\tau\tau)$ search, the pdfs are defined in the range of $100 < m_{\gamma\gamma} < 1000\,\text{GeV}$, whilst in the low-mass $X \to Y(\gamma\gamma)H(\tau\tau)$ search, the pdfs are defined in the range of $65 < m_{\gamma\gamma} < 150\,\text{GeV}$. These ranges ensure there is a sufficient number of background events that populate the $m_{\gamma\gamma}$ distribution in order to accurately model the continuum background component. The lower bound at 65 GeV in the low-mass $X \to Y(\gamma\gamma)H(\tau\tau)$ search is chosen to avoid the trigger efficiency turn-on curve at low $m_{\gamma\gamma}$.

The shape and normalization of the signal models are derived assuming $m_H = 125.38\,\text{GeV}$, which is the most precise measurement of the Higgs boson mass reported by CMS [35].

8.1 Signal modeling in the nonresonant search

The shape of the $m_{\gamma\gamma}$ distribution for signal events is derived using simulated events. This is done independently in each nonresonant search analysis category, for each year of data-taking. The signal pdf is constructed by fitting the $m_{\gamma\gamma}$ distribution with a double Crystal Ball (DCB) function [75, 76].

The normalization of the signal model in analysis category, i, is defined by the formula,

$$N_i = 2\,\sigma(pp \to HH)\,\mathcal{B}(H \to \gamma\gamma)\,\mathcal{B}(H \to \tau\tau)\,\epsilon_i\,\mathcal{L}\,\mathcal{C}(\vec{\theta}), \tag{8.1}$$

where $\sigma(pp \to HH)$ is the nonresonant ggF HH cross section, on which an upper limit is placed, $\mathcal{B}(H \to \gamma\gamma)$ and $\mathcal{B}(H \to \tau\tau)$ are the SM branching fractions for $H \to \gamma\gamma$ and $H \to \tau\tau$ respectively, ϵ_i is the efficiency for signal events to be reconstructed in analysis category i, which is derived directly from simulation, and $\mathcal{L}$ is the integrated luminosity. The final term, $\mathcal{C}(\vec{\theta})$, corresponds to the corrections to the signal yield estimates from nuisance parameters, $\vec{\theta}$, representing systematic uncertainties in the analysis (see section 9). Figure 6 shows the signal model for the purest analysis category in the nonresonant search, which fits well to the simulated events and has a shape that is indicative of the rest of the signal models used in this analysis, including the resonant searches. The gray shaded areas correspond to the σ_{eff}, defined as half the width of the narrowest interval containing 68.3% of the $m_{\gamma\gamma}$ distribution. For the purest and second purest categories, σ_{eff} is 1.54 GeV and 1.64 GeV respectively, and the shapes of the models are otherwise similar.

8.2 Signal modeling in the resonant searches

Extracting limits for mass hypotheses, for which a simulation was not generated, introduces additional complexity to the signal modeling for the resonant search. The signal models for

JHEP05(2026)186

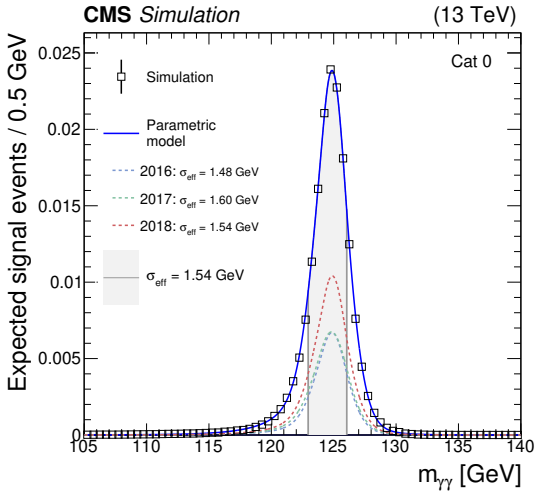

Figure 6. Signal model for the purest analysis category in the nonresonant search, shown for each year of simulated data, and for the sum of all years together. The open squares represent the weighted simulated events, whose uncertainty are smaller than the marker size, and the blue line is the corresponding model. The gray shaded areas correspond to the σ_{eff}. The contribution from each year of data taking is illustrated with the dotted lines.

these hypotheses, denoted as intermediate mass points, are derived by interpolating both the shape and normalization from the neighbouring mass points in which simulated samples were generated, denoted as nominal mass points. For the $X^{(0)} \to HH$ and $X^{(2)} \to HH$ searches, the interpolation of parameters is performed in one dimension, m_X, whilst the $X \to YH$ searches require interpolation in two dimensions, m_X and m_Y.

As in the nonresonant search, DCB functions are used to model the signal. For the nominal mass points, the DCB shape parameters are extracted in a χ^2 fit to the simulated data points. For the intermediate mass points, the mean, $\overline{m}_{\gamma\gamma}$, and width, σ, of the Gaussian core of the DCB are determined by interpolating the values at the nominal mass points with a linear spline. The rest of the shape parameters do not change significantly as a function of m_X and m_Y and therefore the values are simply taken from the closest nominal mass point.

In the $X^{(0)} \to HH$, $X^{(2)} \to HH$ and $X \to Y(\tau\tau)H(\gamma\gamma)$ searches, a set of analysis categories are defined for each considered mass hypothesis m_X (and m_Y). Signal events produced under the targeted m_X (and m_Y) hypothesis in analysis category, i, are normalized according to

$$N_i(m_X, m_Y) = \sigma(pp \to X \to (H/Y)H \to \gamma\gamma\tau\tau)\, \epsilon_i(m_X, m_Y)\, \mathcal{L}\, \mathcal{C}(\vec{\theta}), \tag{8.2}$$

where the quantity $\sigma(pp \to X \to (H/Y)H \to \gamma\gamma\tau\tau)$ is the BSM cross section on which an upper limit is placed. The key difference with respect to eq. (8.1) is that the signal efficiency, ϵ_i, becomes a function of m_X for the $X \to HH$ searches, or m_X and m_Y for the $X \to Y(\tau\tau)H(\gamma\gamma)$ search.

The signal efficiencies ϵ_i for the nominal mass points are computed directly from the simulation as the fraction of signal events that pass the selection for analysis category i. The signal efficiencies for the intermediate mass points are determined by interpolating the nominal mass point values using splines. Both linear and cubic splines are considered, where

JHEP05(2026)186

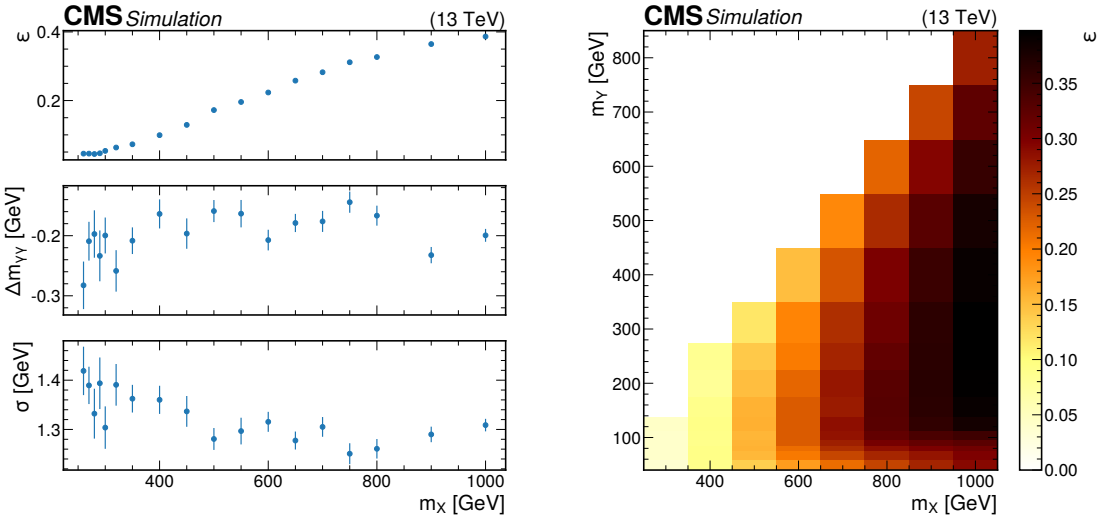

Figure 7. Signal efficiency, ϵ, and interpolated DCB shape parameters, $\Delta m_{\gamma\gamma}$ and σ, for the highest purity analysis category in the $X^{(2)} \to HH$ search, as functions of m_X (left). The first shape parameter, $\Delta m_{\gamma\gamma}$, is defined as $\overline{m}_{\gamma\gamma} - m_H$. Signal efficiency in the (m_X, m_Y) plane for the highest purity analysis category in the $X \to Y(\tau\tau)H(\gamma\gamma)$ search (right).

the type of spline used at a given mass point is the one that leads to the lowest interpolation systematic uncertainty (as discussed in section 9). These splines are implemented using the SciPy package [77] where the cubic spline in 2D uses techniques described in ref. [78]. In figure 7 (left), the DCB shape parameters and signal efficiency for the highest purity analysis category are shown as functions of m_X, for the $X^{(2)} \to HH$ search. Figure 7 (right) shows the signal efficiency in the (m_X, m_Y) plane, for the highest purity analysis category in the $X \to Y(\tau\tau)H(\gamma\gamma)$ search.

In the $X \to Y(\gamma\gamma)H(\tau\tau)$ search, the mean of the DCB's Gaussian core is instead parameterized by $\Delta m_{\gamma\gamma} = \overline{m}_{\gamma\gamma} - m_Y$ to account for the changing peak position as a function of m_Y. Additionally, the spacing in m_Y points in which a limit is calculated is driven by the experimental $m_{\gamma\gamma}$ resolution ($\approx$1.5 GeV at $m_Y = 125$ GeV). Given the large m_Y range considered in this search, it is not feasible to define optimized analysis categories at every m_Y point. It is also unnecessary since the kinematical distributions of the signal, which the pNN mainly uses to discriminate with, do not change significantly over the scale dictated by the resolution. Therefore, analysis categories are constructed for a less granular set of (m_X, m_Y) hypotheses, and when placing a limit at a particular m_Y, the closest set of analysis categories is used. This feature introduces an additional complication to the signal model, as it requires interpolating the signal model parameters for nearby values of m_Y, for which the analysis category is not optimized. These secondary interpolations are derived for the ϵ, $\Delta m_{\gamma\gamma}$, and σ parameters by propagating the neighboring nominal mass point simulated samples into the analysis categories optimized for m_Y. Compared to the primary interpolation described above, the secondary interpolation has a smaller effect in general since the changes in m_Y that it interpolates over are smaller. Averaging over all mass points and categories, the changes to ϵ, $\Delta m_{\gamma\gamma}$ and σ at the maximal change in m_Y are 0.2%, 0.3 GeV, and 0.8 GeV, respectively.

JHEP05(2026)186

8.3 Background modeling

Background events consist of two contributions: the continuum background, which forms a smoothly falling distribution in $m_{\gamma\gamma}$, and events from single H production in the diphoton final state $\mathrm{H} \to \gamma\gamma$, which form a peak around m_{H}. The $\mathrm{H} \to \gamma\gamma$ contribution is modeled using the same procedure used for signal events and is normalized according to the best available cross section and branching fraction recommendations from the LHC Higgs Working Group [15], within appropriate theoretical uncertainties. The remainder of this section details the modeling of the continuum background component. In the final maximum likelihood fit, the total background model is taken as the sum of the continuum and $\mathrm{H} \to \gamma\gamma$ components.

The continuum background model is extracted directly from data using the discrete profiling method [74]. With this technique, the systematic uncertainty associated with choosing a particular analytic function to fit the $m_{\gamma\gamma}$ distribution is accounted. This works by introducing a discrete nuisance parameter into the maximum likelihood fit, which describes the choice of background function in an analysis category.

A large set of candidate function families is considered, including exponential functions, Bernstein polynomials, Laurent series, and power law functions. For each family of functions, an $\mathcal{F}$-test [79] is performed to determine the maximum order of parameters to be used, whilst the minimum order is determined by placing a requirement on the goodness-of-fit to data. In the $\mathcal{F}$-test, each function is fit to the $m_{\gamma\gamma}$ distribution by minimizing twice the negative logarithm of the likelihood ($-2\Delta \ln L$). For the nonresonant HH, $\mathrm{X}^{(0)} \to \mathrm{HH}$, $\mathrm{X}^{(2)} \to \mathrm{HH}$, and $\mathrm{X} \to \mathrm{Y}(\tau\tau)\mathrm{H}(\gamma\gamma)$ searches, the fits are performed only in the mass sidebands, defined as $m_{\gamma\gamma} \in [100, 115] \cup [135, 180]\,\mathrm{GeV}$, to avoid introducing a bias from the signal region.

The fitting strategy for the $\mathrm{X} \to \mathrm{Y}(\gamma\gamma)\mathrm{H}(\tau\tau)$ searches is slightly different, as it involves searching for a resonance Y over a large range in $m_{\gamma\gamma}$. To account for this, the mass sidebands used to construct the continuum background model are defined by a sliding blinded region in $m_{\gamma\gamma}$,

$$m_{\mathrm{Y}} \pm 10\,\mathrm{GeV}\frac{m_{\mathrm{Y}}}{125.38\,\mathrm{GeV}}, \tag{8.3}$$

where the size of the blinded region increases as a function of m_{Y} to account for the increase in the resonance width. This formula holds for all considered m_{Y}, with the exception of $70 < m_{\mathrm{Y}} < 72\,\mathrm{GeV}$ in the low-mass $\mathrm{X} \to \mathrm{Y}(\gamma\gamma)\mathrm{H}(\tau\tau)$ search. For these m_{Y} points, data with $65 < m_{\gamma\gamma} < 68\,\mathrm{GeV}$ is kept to form a low-mass sideband; the fraction of signal events in this region from an $m_{\mathrm{Y}} = 70\,\mathrm{GeV}$ resonance is around 4%, and therefore will have a negligible impact on the construction of the background model.

In the resonant searches, the Bernstein polynomials were removed from the envelope and replaced by an exponential of a polynomial function, which was found to provide a better description of the data over the invariant mass range used in these searches. For the same reason, in the high-mass $\mathrm{X} \to \mathrm{Y}(\gamma\gamma)\mathrm{H}(\tau\tau)$ search, the so-called dijet functions [80] are also added to the continuum background model.

When extracting the results in the final maximum likelihood fits, the discrete profiling method minimizes the overall $-2\Delta \ln L$ considering all allowed functions for each analysis category. Both the normalization and the shape parameters of these functions are included

JHEP05(2026)186

as free parameters in the fit. A penalty term equal to the number of parameters of the function is added to $-2\Delta \ln L$ to take into account the number of floating parameters in each candidate function, thus penalizing functions with high complexity. Checks are performed to ensure that modeling the continuum background $m_{\gamma\gamma}$ distribution using the discrete profiling method introduces negligible bias to the final results.

8.4 Drell-Yan modeling

In the low-mass $X \to Y(\gamma\gamma)H(\tau\tau)$ search, there is an additional background from DY where two electrons from a Z boson decay can be misidentified as photons, leading to a peak in the $m_{\gamma\gamma}$ spectrum close to the Z boson mass. To model this background contribution, an "ABCD method" [70] based on control samples in data is employed. Three control regions are defined by inverting the electron veto (region B), or inverting the pNN selection (region C) or inverting both (region A). This leaves the signal region, labeled as D. By inverting the electron veto, regions A and B are enriched in DY. These regions constrain the shape of the DY distribution in $m_{\gamma\gamma}$. In regions A and C, the yields for DY are extracted, constraining the electron veto efficiency.

Since kinematical variables are input to the pNN, and the shape of the diphoton mass peak is dependent mainly on the kinematical variables of the two photons, the shape of the DY process is assumed to be the same in regions with the same pNN selection (in A and C, and in B and D). For regions A and C, the shape is modeled by a Gaussian function, except in cases where a poor goodness-of-fit is found and a DCB is used instead. When extracting the final results, the shape parameters are allowed to float. Similarly, the rates of the DY background in regions A, B and C are allowed to float. The rate of DY in region D is given by the rate in region B, multiplied by the electron veto efficiency (rate in region C divided by rate in region A).

Finally, given that there are 7 pNN regions, this method is applied 7 times, where there are 7 independent B and D regions, and the A and C regions remain the same.

9 Systematic uncertainties

As described in section 8, the systematic uncertainty associated with the nonresonant background estimation is calculated with the discrete profiling method. Systematic uncertainties affecting the signal models and/or the resonant background models are implemented in one of two ways. First, uncertainties that modify the shape of the $m_{\gamma\gamma}$ distribution are incorporated as nuisance parameters affecting the mean and width of the DCB functions that comprise the signal model. Second, uncertainties that do not affect the shape of the $m_{\gamma\gamma}$ distribution are implemented as log-normal uncertainties in the event yield. Uncertainties of the first type are typically experimental sources of uncertainty that impact the energy of individual photons, while uncertainties of the second type include both theoretical and experimental sources, which have a negligible impact on the shape of the $m_{\gamma\gamma}$ distribution.

JHEP05(2026)186

9.1 Theoretical uncertainties

Sources of theoretical uncertainties considered in this analysis are those that affect the $H \to \gamma\gamma$ branching fraction, the uncertainty, for which is currently estimated to be around 3% [15], and those that affect the inclusive cross sections of ggF HH and single H production.

Sources that affect the cross sections include the PDFs, the strong coupling constant (α_S), and variations of the renormalization (μ_R) and factorization (μ_F) scales, which account for missing higher-order terms in the perturbative calculations of the cross sections. Additionally, for the ggF HH production cross section, there is a source of uncertainty related to the scheme and scale choice of the top quark mass [13]. These sources may also affect the kinematical variables of simulated events, thereby changing signal efficiencies. However, this effect has been found to be significantly smaller than the cross section uncertainty in recent $H \to \gamma\gamma$ measurements [81] and is therefore not considered.

The magnitudes of the uncertainties in the inclusive cross sections from these sources are taken from refs. [6–12] for ggF HH production and from refs. [15, 82, 83] for single H boson production. The total effect of uncertainties on HH production is found to be $^{+6.7\%}_{-23.2\%}$ for $\kappa_\lambda = 1$, while the effect on resonant background production is between 2% and 11%, depending on the production mode.

9.2 Experimental uncertainties

As described previously, the sources of experimental uncertainty are split into two categories: those modifying the shape of the $m_{\gamma\gamma}$ distribution (incorporated as nuisance parameters) and those affecting only the normalization (incorporated as log-normal uncertainties). This includes effects that lead to a migration of a process across analysis categories. Sources of experimental uncertainty that modify the shape of the $m_{\gamma\gamma}$ distribution are related to the corrections applied to the photon energy scale and resolution in simulation. These corrections, and associated uncertainties, are computed using $Z \to ee$ events [33]. The most dominant sources of experimental uncertainty, which affect only the normalization of signal and resonant background processes are:

- *Integrated luminosity.* The integrated luminosities for the 2016, 2017, and 2018 data-taking years have individual uncertainties of 1.2–2.5% [48–50], while the overall uncertainty in the measurement for the 2016–2018 period is 1.6%. The correlations from different common sources of luminosity measurements are taken into account.

- *Trigger efficiency.* This efficiency is calculated with the "tag-and-probe" method using $Z \to ee$ events in data [84]. The size of uncertainty in the efficiency is between 0.1 and 3.5% depending on the signal process and category. An additional uncertainty is also added to include the trigger inefficiency arising from a gradual shift in the timing of the inputs of the ECAL L1 trigger for $|\eta| > 2.0$ in 2016–2017 data-taking years [28]. The size of this uncertainty is between 2 and 8%.

- *Diphoton preselection.* The efficiency after photon preselections is measured with simulated events and data, also using the "tag-and-probe" method with $Z \to ee$ events [84]. The ratio of the efficiencies from data and MC simulations is used to derive

JHEP05(2026)186

the correction factor and corresponding uncertainties. The size of the uncertainty in the efficiency is between 4 and 5%.

- *b jet tagging.* The DeepJet discriminant distributions in MC simulations are reshaped by data-to-simulation scale factors [42]. The impact of different systematic uncertainty sources on the reshaping is studied. The most important effects lead to efficiency uncertainties up to 10%.

- τ_h *identification.* Selections are made using the DeepTau algorithm to distinguish genuine τ_h from jets, muons, and electrons. Measurements of the selection efficiency are made in data (as discussed in section 2) and are used to correct simulation. Uncertainties associated with those corrections are propagated into an uncertainty in the signal efficiency, which is found to be up to 7%.

- *Signal model interpolation.* There is an uncertainty related to the interpolation required to calculate signal efficiencies for the intermediate mass points. For each spline used, an alternative spline is considered where the nominal mass point closest to the intermediate mass point is removed. The relative difference between the prediction of the nominal and alternative spline is taken as an uncertainty in the efficiency of the signal within that category.

Further sources of systematic uncertainty are included but are negligible compared to the dominant sources described above. In the final fits to data, the nuisance parameters are found to be consistent with their prefit values, and the combined impact of all systematic uncertainties is found to be less than 1% on any of the upper limits reported in section 10. Overall, the sensitivity for this search is limited mostly by the statistical uncertainty, given the low data yields in the sensitive analysis categories.

10 Results

For each search, a simultaneous maximum likelihood fit is performed to the $m_{\gamma\gamma}$ distributions in data in the corresponding analysis categories. In the resonant searches, a separate fit is performed for each considered mass hypothesis. The best fit signal-plus-background models are shown for the best analysis categories in each search in figure 8. The figures for the resonant searches show the analysis categories for the m_X and (m_X, m_Y) points where the largest excesses with respect to the background-only hypothesis are observed.

10.1 Results from the nonresonant search

In the nonresonant HH search, an upper limit at 95% CL is set on the production cross section of a pair of Higgs bosons, $\sigma(pp \to HH)$, using the CL_s modified frequentist criterion [85, 86], taking the LHC profile likelihood ratio as the test statistic [87], in the asymptotic approximation [88]. The observed (expected) 95% CL upper limit amounts to 930 (740) fb, which corresponds to 33 (26) times the SM prediction.

Limits are also derived for the nonresonant HH search as a function of κ_λ, assuming that all other couplings of the Higgs boson have values as predicted by the SM. The result is

JHEP05(2026)186

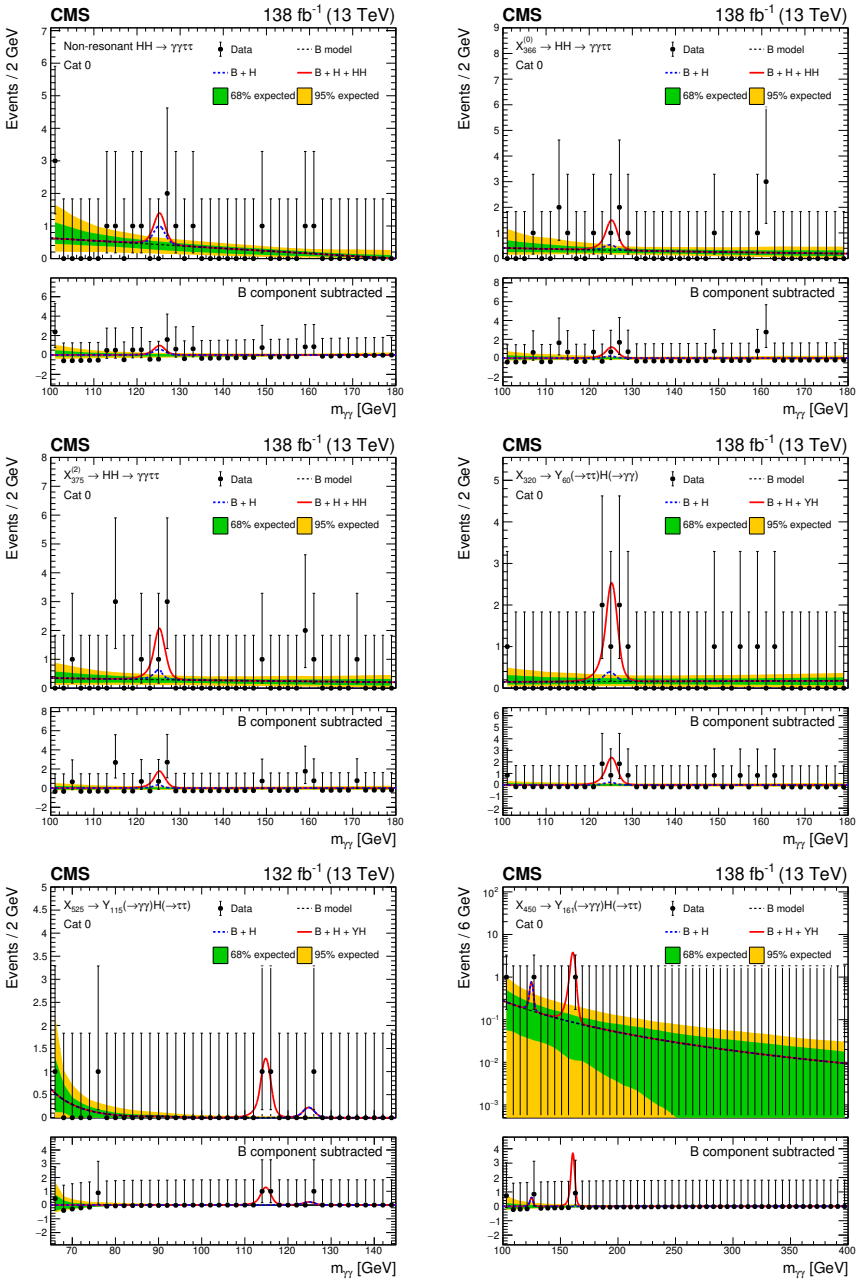

Figure 8. Data points (black) and signal-plus-background models for the most sensitive analysis category in each search are shown: nonresonant (upper left), $X^{(0)} \to HH$ (upper right), $X^{(2)} \to HH$ (middle left), $X \to Y(\tau\tau)H(\gamma\gamma)$ (middle right), low-mass $X \to Y(\gamma\gamma)H(\tau\tau)$ (lower left) and the high-mass $X \to Y(\gamma\gamma)H(\tau\tau)$ (lower right). The analysis categories for the resonant searches correspond to the mass hypotheses where the largest excesses with respect to the background-only hypothesis are observed. The one (green) standard deviation and two (yellow) standard deviation bands show the uncertainties in the background component of the fit. The solid red line shows the sum of the fitted signal and background components, the dashed blue line shows the continuum background and the background from single H production together, and the dashed black line shows only the continuum background component. The lower panel in each plot shows the residual signal yield after subtraction of the background.

JHEP05(2026)186

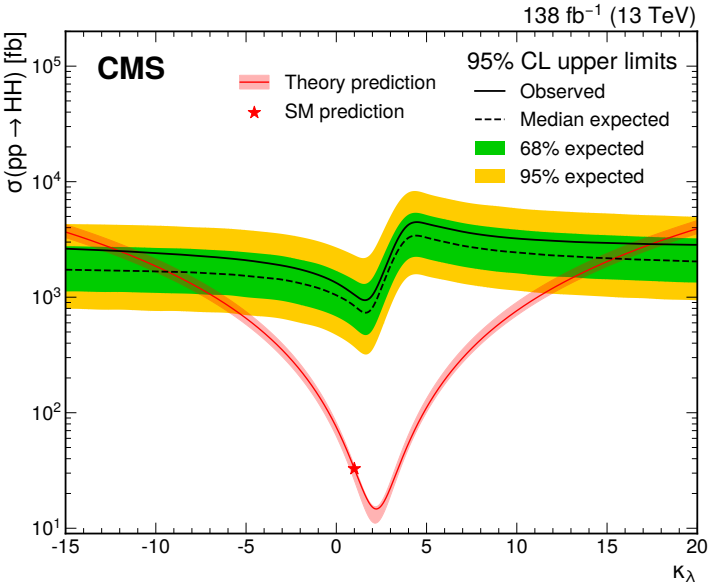

Figure 9. Expected and observed upper limits on the nonresonant HH production cross section at 95% CL, obtained for different values of κ_λ. The green and yellow bands represent the one and two standard deviations for the expected limit, respectively. The theoretical prediction with the uncertainty of the cross section as a function of κ_λ is shown by the red band.

shown in figure 9. The variation in the excluded cross section as a function of κ_λ arises due to the different kinematical properties of nonresonant HH production for different values of κ_λ. At 95% CL, HH production is observed (expected) to be excluded for values of κ_λ outside the range between -12 (-9.4) and 17 (15). The κ_λ-dependent NLO corrections in electroweak theory to single H production [89] are neglected in this result. Upper limits at 95% CL are also set for the thirteen BSM benchmark scenarios listed in table 1. These limits are shown in figure 10.

10.2 Results from the resonant searches

In the resonant searches, the limit-setting procedure is the same as in the nonresonant search except that the test statistic is not assumed to be distributed according to the asymptotic approximation. The results are extracted both in the asymptotic approximation and using pseudo-datasets. In case the results are not compatible, the ones using the pseudo-datasets are presented. This is most important in the high-mass $\mathrm{X} \to \mathrm{Y}(\gamma\gamma)\mathrm{H}(\tau\tau)$ search where there are small numbers of events in the tail of the $m_{\gamma\gamma}$ distribution. Upper limits are presented on production cross sections, factoring out the relevant branching fractions where known. The $\mathrm{X} \to \mathrm{Y}(\tau\tau)\mathrm{H}(\gamma\gamma)$ search is an exception to this rule and the $\mathrm{H} \to \gamma\gamma$ branching fraction is not factored out to allow for a more straightforward comparison to the $\mathrm{X} \to \mathrm{Y}(\mathrm{bb})\mathrm{H}(\gamma\gamma)$ search presented in ref. [21].

Upper limits on the resonant production cross section, $\sigma(\mathrm{pp} \to \mathrm{X})B(\mathrm{X} \to \mathrm{HH})$, are shown in figure 11 as a function of the resonant mass m_X, for the $\mathrm{X}^{(0)} \to \mathrm{HH}$ (upper plot) and $\mathrm{X}^{(2)} \to \mathrm{HH}$ (lower plot) searches. The expected limits are shown to decrease as a function of m_X, which follows from the improved signal vs. background discrimination for high m_X

JHEP05(2026)186

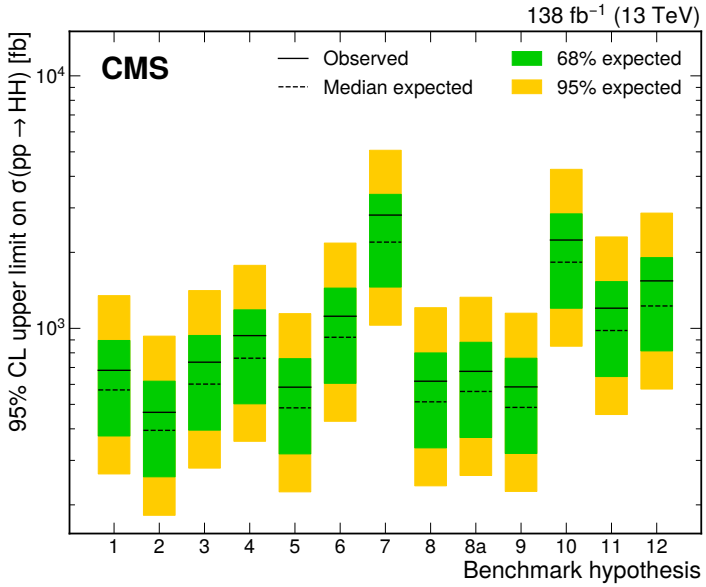

Figure 10. Expected and observed upper limits on the nonresonant HH production cross section at 95% CL, for different thirteen BSM benchmark scenarios which consider different values of the couplings, κ_λ, κ_t, c_{2g}, c_g, and c_2 (defined in table 1). The green and yellow bands represent the one and two standard deviations for the expected limits, respectively.

values. The observed (expected) upper limits vary between 160–2200 fb (240–1800 fb) and 180–1900 fb (200–1800 fb) for the $X^{(0)} \to HH$ and $X^{(2)} \to HH$ searches, respectively. In the context of the RS bulk model, these results exclude m_X values between 260 and 360 GeV, between 380 and 410 GeV, and between 500 and 550 GeV for the spin-0 radion resonance with decay constant $\Lambda_R = 3$ TeV, and up to 950 GeV at $\Lambda_R = 2$ TeV. For the spin-2 KK graviton resonance with coupling factor $\kappa/\overline{M_{pl}} = 1$, masses between 310 and 750 GeV are excluded.

The upper limits on the product of the production cross section and the decay branching fraction $\sigma(pp \to X)B(X \to YH \to \gamma\gamma\tau\tau)$ for the $X \to Y(\tau\tau)H(\gamma\gamma)$ search are shown in figures 12, 13, and 14. The limits are shown as a function of m_Y for different m_X hypotheses (figure 12) or as a function of m_X for different m_Y hypotheses (figure 13). The observed upper limits in the 2D (m_X, m_Y) plane are also shown in figure 14. Analogously, the upper limits on the product of the production cross section and the decay branching fraction $\sigma(pp \to X \to YH)B(Y \to \gamma\gamma)$ for the $X \to Y(\gamma\gamma)H(\tau\tau)$ searches are shown in figures 15, 16, and 17 for the low-mass search, which considers m_Y in the range from 70 to 125 GeV, and in figures 18, 19, and 20 for the high-mass search, which considers m_Y in the range from 125 to 800 GeV. The limits are shown as a function of m_Y for different m_X hypotheses (figures 15 and 18), as a function of m_X for different m_Y hypotheses (figures 16 and 19), and in the 2D (m_X, m_Y) plane (figures 17 and 20).

For the $X \to Y(\tau\tau)H(\gamma\gamma)$ search, the observed (expected) upper limits vary between 0.059–1.2 fb (0.087–0.68 fb), depending on the m_X and m_Y values. In the low-mass $X \to Y(\gamma\gamma)H(\tau\tau)$ search, the observed (expected) upper limits vary between 0.69–15 fb (0.73–8.3 fb), depending on the m_X and m_Y values. These limits can be compared to a set of maximally allowed cross sections in the NMSSM taken from ref. [91], which are calculated using the NMSSMTools

JHEP05(2026)186

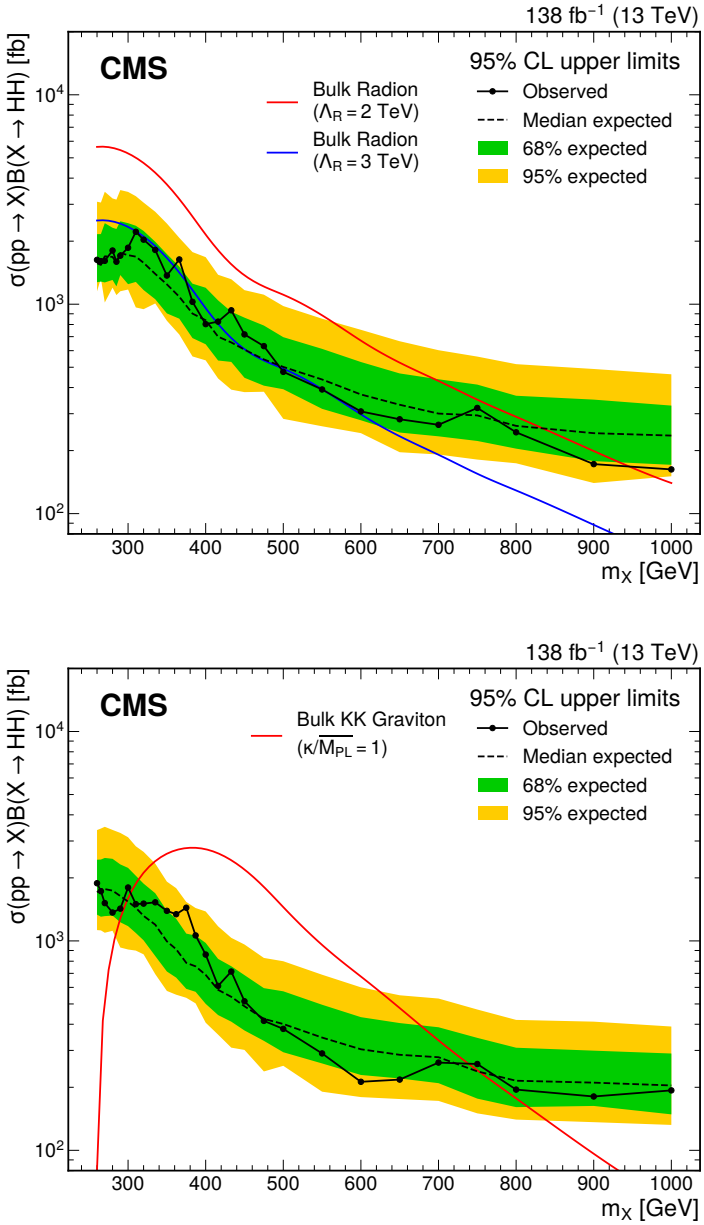

Figure 11. Expected and observed 95% CL upper limits on the resonant production cross section, $\sigma(\mathrm{pp} \to \mathrm{X})B(\mathrm{X} \to \mathrm{HH})$ for the spin-0 $\mathrm{X}^{(0)} \to \mathrm{HH}$ search (upper plot) and spin-2 $\mathrm{X}^{(2)} \to \mathrm{HH}$ search (lower plot). The dashed and solid black lines represent the expected and observed limits, respectively. The green and yellow bands represent the one and two standard deviations for the expected limit, respectively. The red and blue lines show the theoretical predictions with different energy scales and couplings [90].

JHEP05(2026)186

v5.6.2 package [92–94]. Owing to the allowance of a high $\mathrm{Y} \to \gamma\gamma$ branching fraction, a region in (m_{X}, m_{Y}) parameter space is found where the observed limits are below the maximally allowed limits, implying that these results can be used to provide tighter constraints on the NMSSM. This region is shown by the red dashed area in figure 17. For the high-mass $\mathrm{X} \to \mathrm{Y}(\gamma\gamma)\mathrm{H}(\tau\tau)$ search, the observed (expected) upper limits vary between 0.64–10 fb (0.70–7.6 fb), depending on the m_{X} and m_{Y} values.

In the $\mathrm{X} \to \mathrm{HH}$ searches, no excesses with local significances above 1.7 standard deviations are found. In the $\mathrm{X} \to \mathrm{Y}(\tau\tau)\mathrm{H}(\gamma\gamma)$ search, the highest local significance seen is 2.6 standard deviations at (m_{X}, m_{Y}) = (320, 60) GeV. In the low-mass and high-mass $\mathrm{X} \to \mathrm{Y}(\gamma\gamma)\mathrm{H}(\tau\tau)$ searches, the highest local significances found are 3.2 standard deviations at (m_{X}, m_{Y}) = (525, 115) GeV, and 3.2 standard deviations at (m_{X}, m_{Y}) = (450, 161) GeV respectively. Due to the recent CMS excesses discussed in section 1 which are consistent with resonances of masses 650 GeV and 90–100 GeV, excesses at similar masses are also worth reporting. No significant excess is seen in the $\mathrm{X} \to \mathrm{Y}(\tau\tau)\mathrm{H}(\gamma\gamma)$ search at these masses, but in the $\mathrm{X} \to \mathrm{Y}(\gamma\gamma)\mathrm{H}(\tau\tau)$ search, local significances of 2.2 and 2.3 standard deviations are seen at (m_{X}, m_{Y}) = (600,94.5) GeV and (m_{X}, m_{Y}) = (650,95) GeV respectively. The significance values have been determined for a finer granularity of mass points than that used for the presentation of upper limits. The largest excesses are therefore not necessarily clearly visible in the figures presented.

Due to the large range in mass hypotheses considered and the narrow resolution of the signal peak, there is a large look-elsewhere effect. The global significance, determined as the probability to observe an excess at any of the mass points considered in the scans that is at least as large as the largest one observed in data, is computed by running multiple pseudo-experiments. The global significances for the $\mathrm{X} \to \mathrm{Y}(\tau\tau)\mathrm{H}(\gamma\gamma)$, low-mass $\mathrm{X} \to \mathrm{Y}(\gamma\gamma)\mathrm{H}(\tau\tau)$, and high-mass $\mathrm{X} \to \mathrm{Y}(\gamma\gamma)\mathrm{H}(\tau\tau)$ searches are 2.2, 0.1, and 0.3 standard deviations, respectively. Therefore, as a standalone analysis, these searches do not show significant deviation from the SM. However, the excesses at $m_{\mathrm{Y}} = 95$ GeV are interesting since they are consistent with other excesses reported by CMS, and they provide further motivation to perform measurements at these mass points in the future.

JHEP05(2026)186

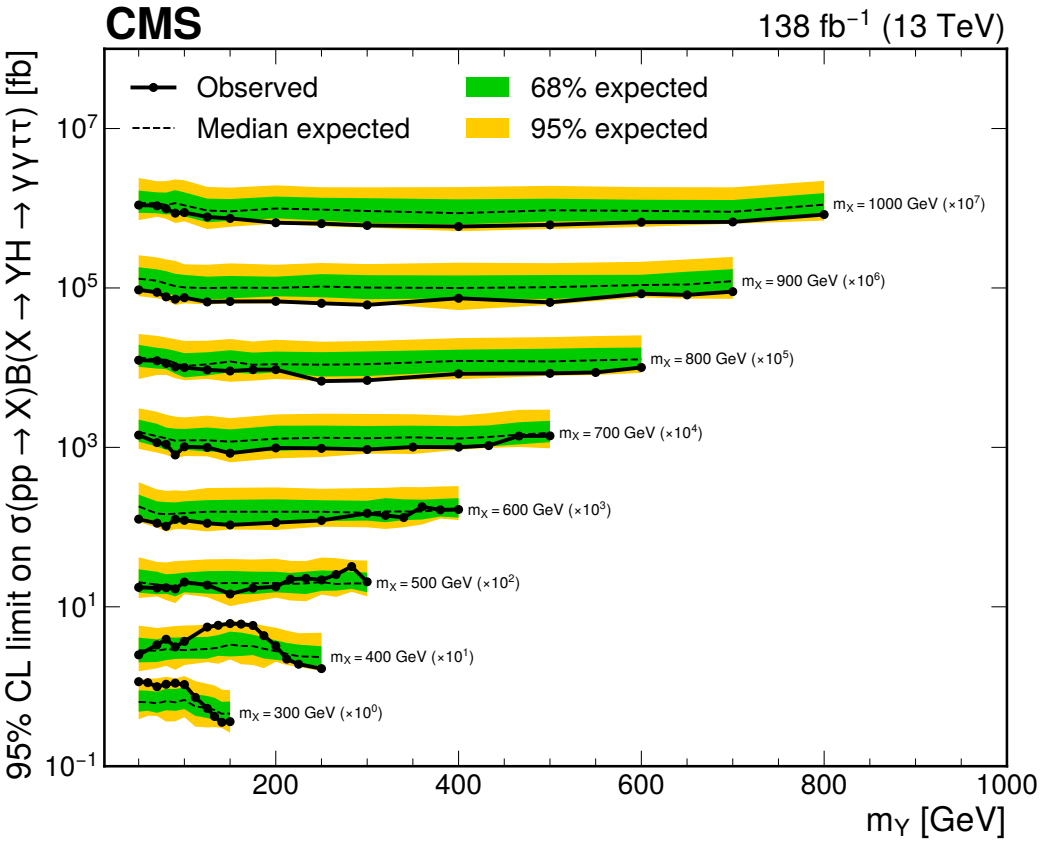

Figure 12. Expected and observed 95% CL upper limits on $\sigma(\mathrm{pp} \to \mathrm{X})B(\mathrm{X} \to \mathrm{YH} \to \gamma\gamma\tau\tau)$ for the $\mathrm{X} \to \mathrm{Y}(\tau\tau)\mathrm{H}(\gamma\gamma)$ search as a function as a function of m_Y for different m_X hypotheses. The dashed and solid black lines represent the expected and observed limits, respectively. The green and yellow bands represent the one and two standard deviations for the expected limit, respectively. Limits are scaled by orders of 10, labeled in the plot.

JHEP05(2026)186

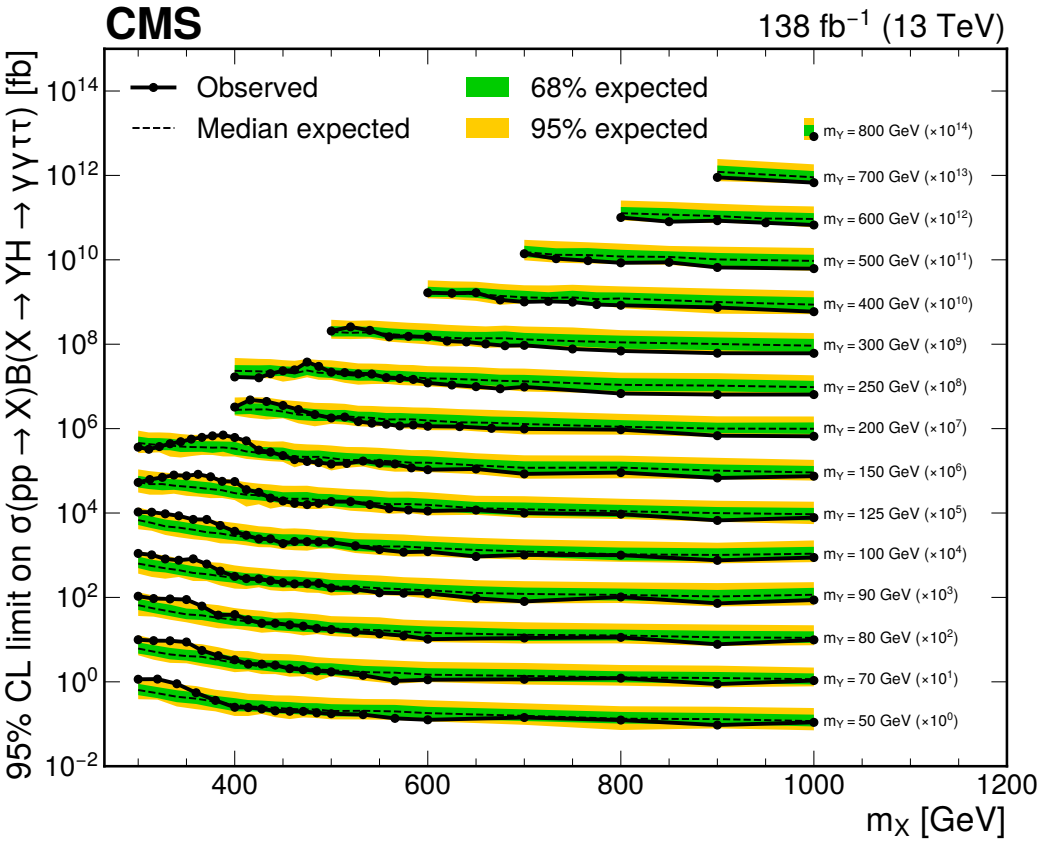

Figure 13. Expected and observed 95% CL upper limits on $\sigma(\mathrm{pp} \to \mathrm{X})B(\mathrm{X} \to \mathrm{YH} \to \gamma\gamma\tau\tau)$ for the $\mathrm{X} \to \mathrm{Y}(\tau\tau)\mathrm{H}(\gamma\gamma)$ search as a function of m_X for different m_Y hypotheses. The dashed and solid black lines represent the expected and observed limits, respectively. The green and yellow bands represent the one and two standard deviations for the expected limit, respectively. Limits are scaled by orders of 10, labeled in the plot.

JHEP05(2026)186

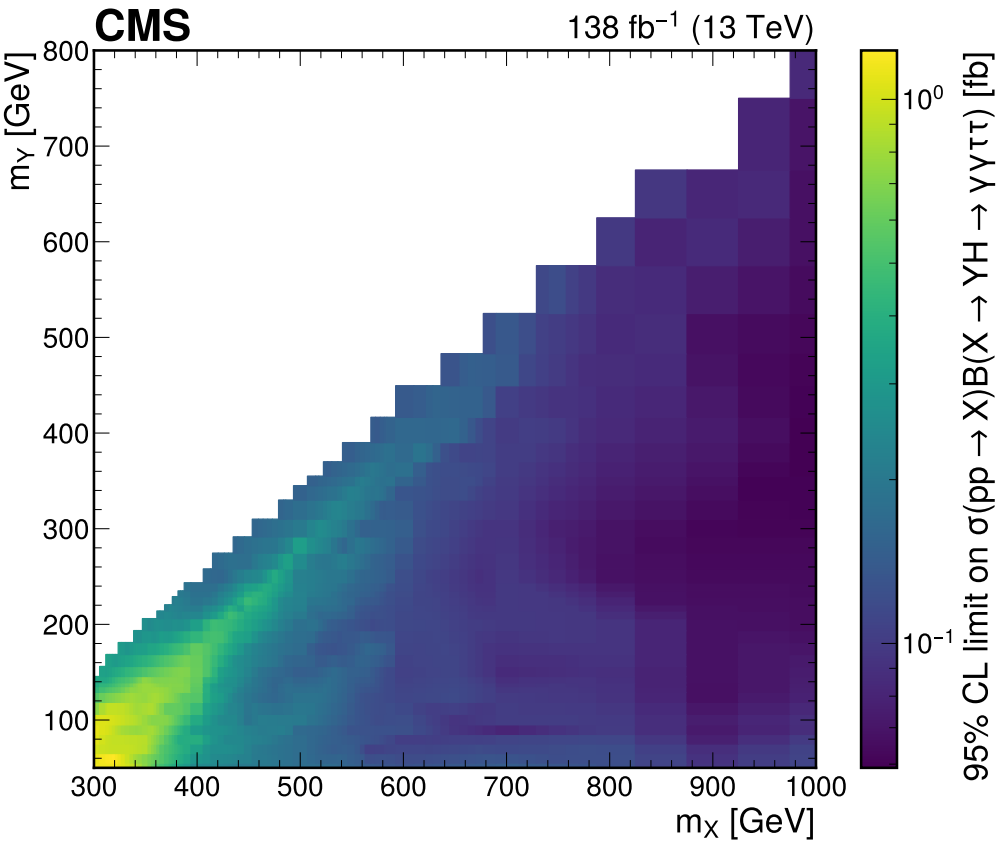

Figure 14. Observed upper limits in the 2D (m_X, m_Y) plane for the X → Y(ττ)H(γγ) search. The values of the limits are shown by the color scale.

JHEP05(2026)186

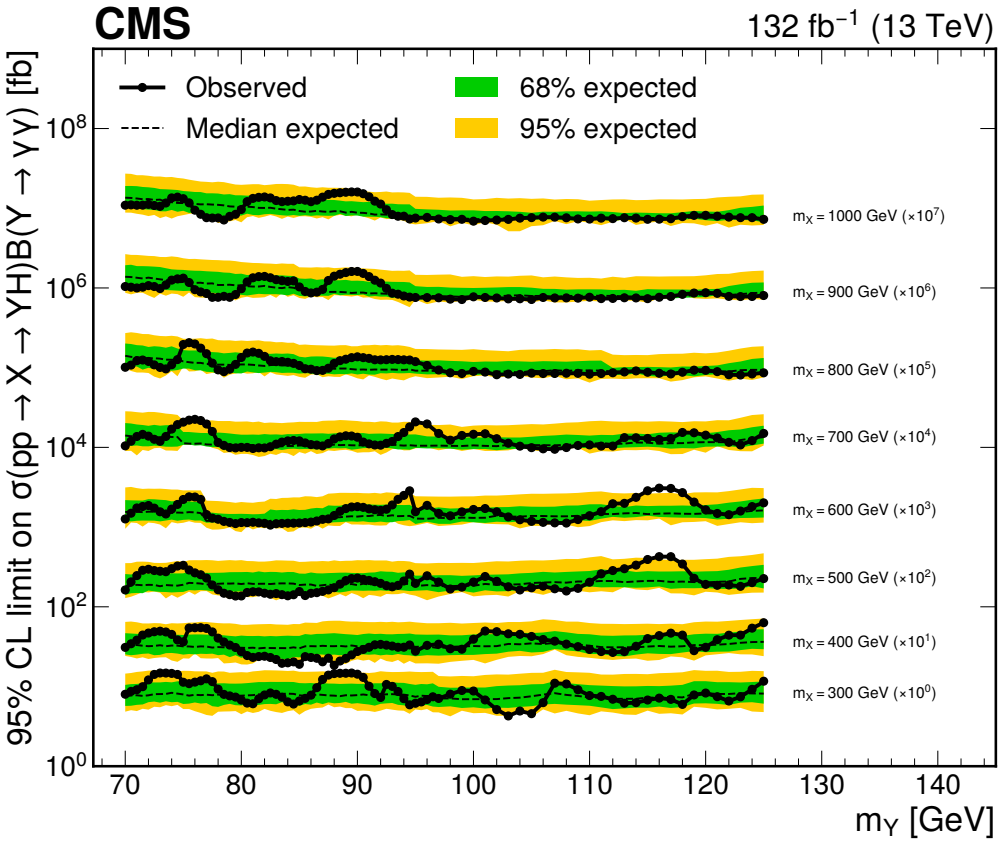

Figure 15. Expected and observed 95% CL upper limits on $\sigma(\mathrm{pp} \to \mathrm{X} \to \mathrm{YH})B(\mathrm{Y} \to \gamma\gamma)$ for the low-mass $\mathrm{X} \to \mathrm{Y}(\gamma\gamma)\mathrm{H}(\tau\tau)$ search as a function of m_Y for different m_X hypotheses. The dashed and solid black lines represent the expected and observed limits, respectively. The green and yellow bands represent the one and two standard deviations for the expected limit, respectively. Limits are scaled by orders of 10, labeled in the plot.

JHEP05(2026)186

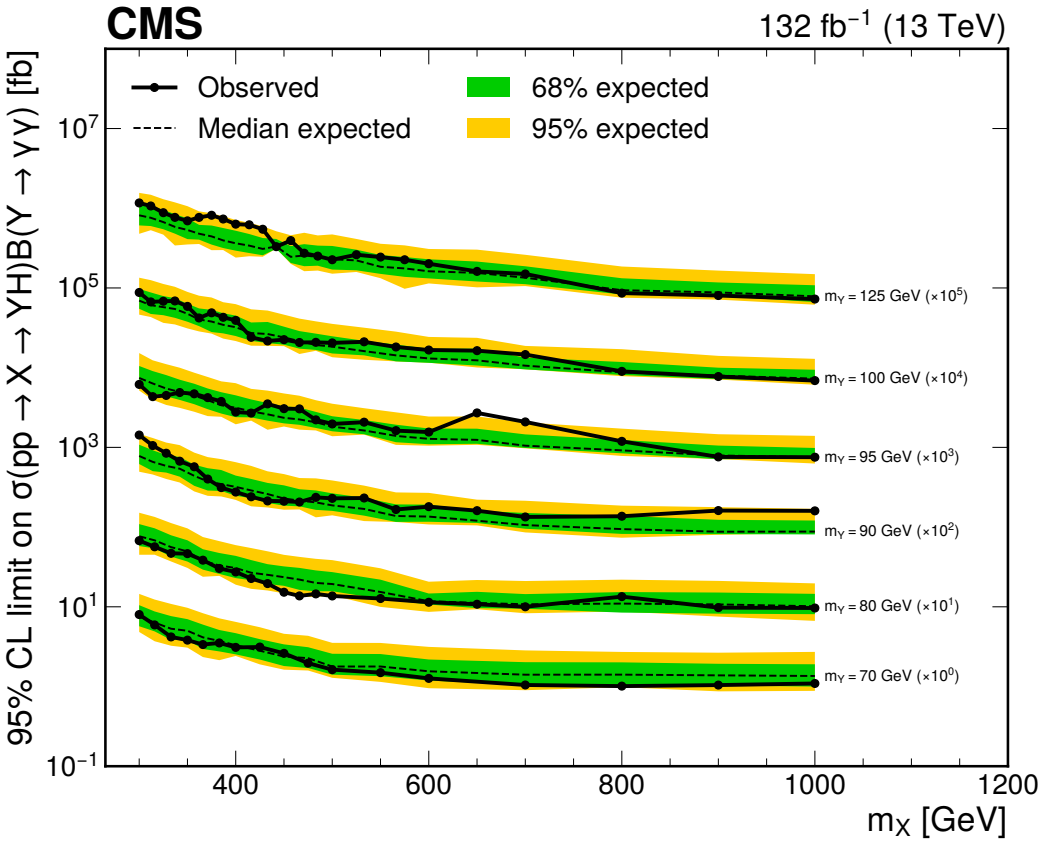

Figure 16. Expected and observed 95% CL upper limits on $\sigma(\mathrm{pp} \to \mathrm{X} \to \mathrm{YH})B(\mathrm{Y} \to \gamma\gamma)$ for the low-mass $\mathrm{X} \to \mathrm{Y}(\gamma\gamma)\mathrm{H}(\tau\tau)$ search as a function of m_X for different m_Y hypotheses. The dashed and solid black lines represent the expected and observed limits, respectively. The green and yellow bands represent the one and two standard deviations for the expected limit, respectively. Limits are scaled by orders of 10, labeled in the plot.

JHEP05(2026)186

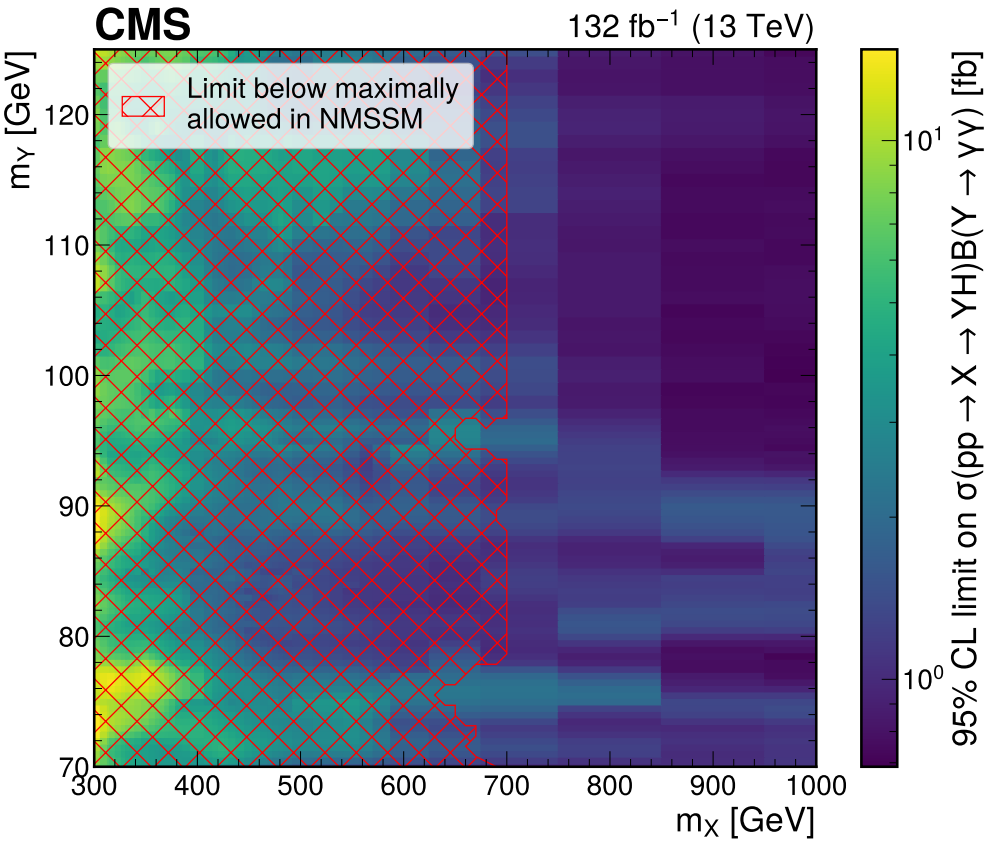

Figure 17. Observed upper limits in the 2D (m_{X}, m_{Y}) plane for the low-mass $\mathrm{X} \to \mathrm{Y}(\gamma\gamma)\mathrm{H}(\tau\tau)$ search. The values of the limits are shown by the color scale. The red hatched region indicates masses for which the observed limits exclude largest possible cross-section in the NMSSM from previous constraints, taken from ref. [91].

JHEP05(2026)186

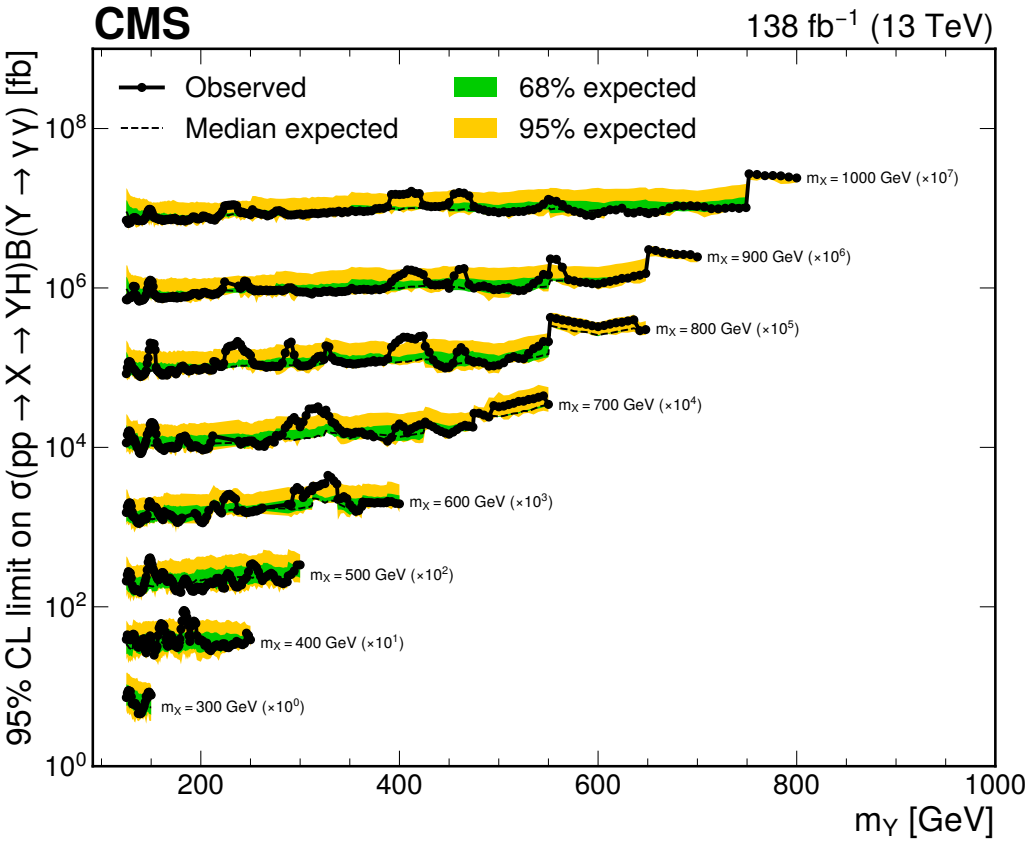

Figure 18. Expected and observed 95% CL upper limits on $\sigma(\mathrm{pp} \to \mathrm{X} \to \mathrm{YH})B(\mathrm{Y} \to \gamma\gamma)$ for the high-mass $\mathrm{X} \to \mathrm{Y}(\gamma\gamma)\mathrm{H}(\tau\tau)$ search as a function of m_Y for different m_X hypotheses. The dashed and solid black lines represent the expected and observed limits, respectively. The green and yellow bands represent the one and two standard deviations for the expected limit, respectively. Limits are scaled by orders of 100, labeled in the plot.

JHEP05(2026)186

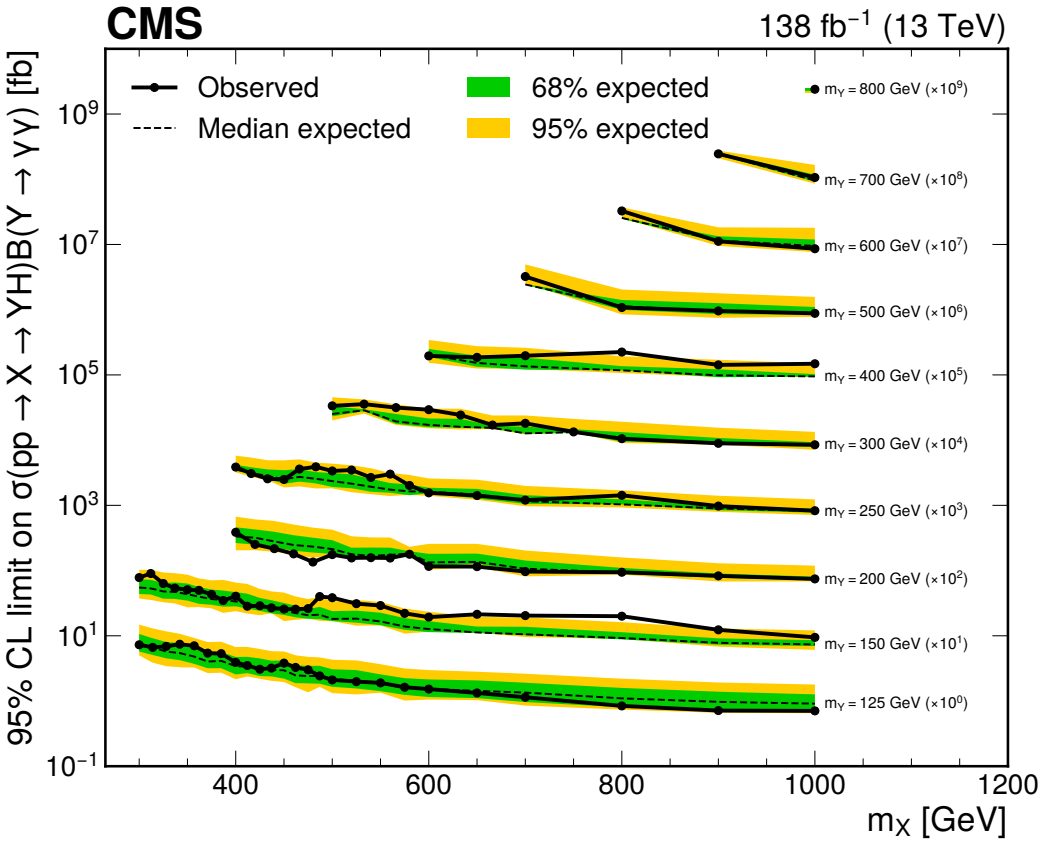

Figure 19. Expected and observed 95% CL upper limits on $\sigma(\mathrm{pp} \to \mathrm{X} \to \mathrm{YH})B(\mathrm{Y} \to \gamma\gamma)$ for the high-mass $\mathrm{X} \to \mathrm{Y}(\gamma\gamma)\mathrm{H}(\tau\tau)$ search as a function of m_X for different m_Y hypotheses. The dashed and solid black lines represent the expected and observed limits, respectively. The green and yellow bands represent the one and two standard deviations for the expected limit, respectively. Limits are scaled by orders of 10, labeled in the plot.

JHEP05(2026)186

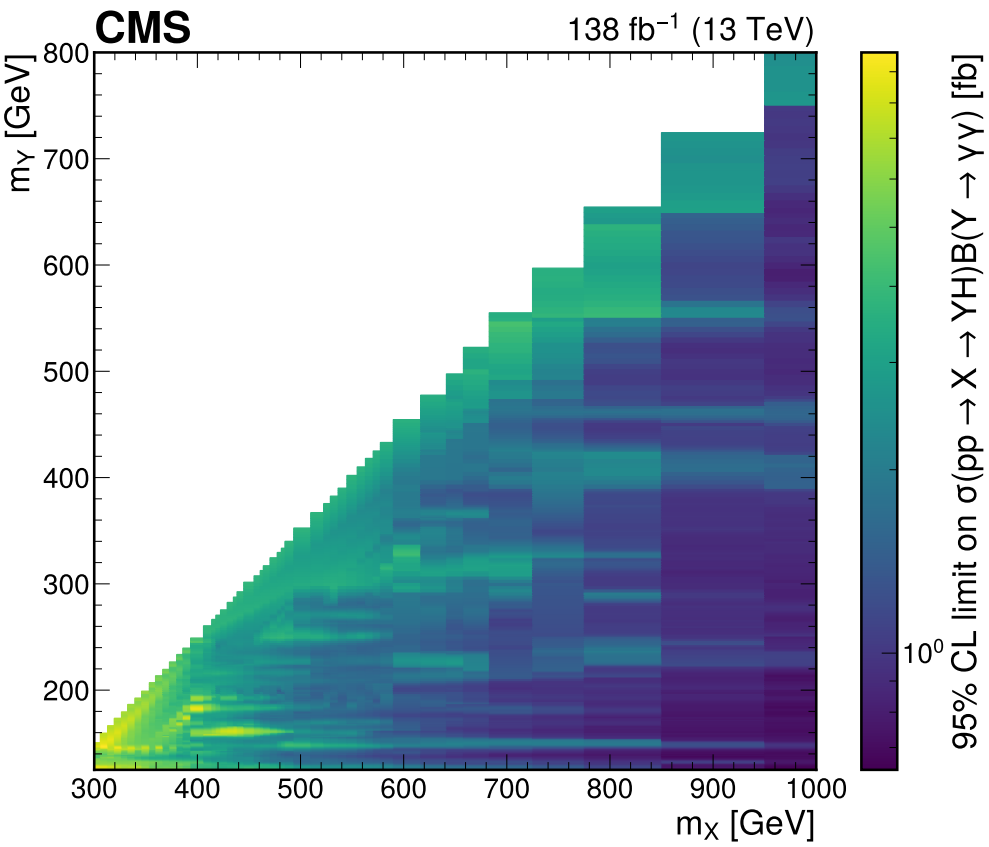

Figure 20. Observed upper limits in the 2D (m_X, m_Y) plane for the high-mass X → Y(γγ)H(ττ) search. The values of the limits are shown by the color scale.

JHEP05(2026)186

11 Summary

A search for the production of two scalar bosons in the $\gamma\gamma\tau\tau$ final state is presented. The search uses data from proton-proton collisions collected by the CMS experiment at the LHC in 2016–2018 at a center-of-mass energy of 13 TeV, corresponding to 138 or 132 fb^{-1} of integrated luminosity, depending on the trigger path. In total, five searches are performed. One search targets the nonresonant production of a Higgs boson pair, HH, via gluon-gluon fusion, where no significant deviation from the background-only hypothesis is observed. Upper limits at 95% confidence level (CL) on the HH production cross section are extracted for production in the standard model (SM) and in several beyond-the-SM scenarios. The observed (expected) upper limit for the SM production is found to be 930 (740) fb, corresponding to 33 (26) times the SM prediction. The limit is also derived as a function of the Higgs boson self-coupling modifier, κ_λ, assuming all other Higgs boson couplings are as predicted in the SM, and HH production is observed (expected) to be excluded at 95% CL outside the range between -12 (-9.4) and 17 (15). In addition, the limit is extracted for numerous beyond-the-SM benchmark scenarios and the results are consistent with the SM predictions.

This analysis also targets the resonant production of two scalar bosons. Two searches are constructed to search for a resonance X decaying to a SM Higgs boson pair, $\text{X} \to \text{HH}$, for both the spin-0 resonance and spin-2 resonance scenarios. Furthermore, the analysis targets the $\text{X} \to \text{YH}$ process, where Y is an additional, lighter (than X) scalar particle. Three searches are constructed, namely the $\text{X} \to \text{Y}(\tau\tau)\text{H}(\gamma\gamma)$, low-mass $\text{X} \to \text{Y}(\gamma\gamma)\text{H}(\tau\tau)$ and high-mass $\text{X} \to \text{Y}(\gamma\gamma)\text{H}(\tau\tau)$, which target the different decay chains in different mass regimes. The global significances of each search indicate that no significant deviation from the background-only hypothesis is observed, but some local excesses in the $\text{X} \to \text{Y}(\gamma\gamma)\text{H}(\tau\tau)$ search that are consistent with other CMS results warrant further measurements.

In the $\text{X} \to \text{HH}$ search, upper limits at the 95% CL on the $\text{X} \to \text{HH}$ production cross section are observed (expected) to be within 160 to 2200 (200 to 1800) fb, depending on the mass of X. In the $\text{X} \to \text{Y}(\tau\tau)\text{H}(\gamma\gamma)$ search, upper limits at the 95% CL on the product of the production cross section and the decay branching fractions are observed (expected) to vary between 0.059–1.2 fb (0.087–0.68 fb), depending on the mass of X and Y. In the $\text{X} \to \text{Y}(\gamma\gamma)\text{H}(\tau\tau)$ search, the observed (expected) upper limits on the product of the production cross section and $\text{Y} \to \gamma\gamma$ branching fraction vary between 0.69–15 fb (0.73–8.3 fb) in the low Y mass search and between 0.64–10 fb (0.70–7.6 fb) in the high Y mass search. In the low Y mass search, these limits are compared to a set of maximally allowed cross sections in the next-to-minimal supersymmetric SM taken from ref. [91]. A region in the (m_X, m_Y) parameter space where the observed limits are lower than the maximum allowed is found, meaning that these results can be used to provide tighter constraints on the next-to-minimal supersymmetric SM.

JHEP05(2026)186

Acknowledgments

We congratulate our colleagues in the CERN accelerator departments for the excellent performance of the LHC and thank the technical and administrative staffs at CERN and at other CMS institutes for their contributions to the success of the CMS effort. In addition, we gratefully acknowledge the computing centers and personnel of the Worldwide LHC Computing Grid and other centers for delivering so effectively the computing infrastructure essential to our analyses. Finally, we acknowledge the enduring support for the construction and operation of the LHC, the CMS detector, and the supporting computing infrastructure provided by the following funding agencies: SC (Armenia), BMBWF and FWF (Austria); FNRS and FWO (Belgium); CNPq, CAPES, FAPERJ, FAPERGS, and FAPESP (Brazil); MES and BNSF (Bulgaria); CERN; CAS, MoST, and NSFC (China); MINCIENCIAS (Colombia); MSES and CSF (Croatia); RIF (Cyprus); SENESCYT (Ecuador); ERC PRG, RVTT3 and MoER TK202 (Estonia); Academy of Finland, MEC, and HIP (Finland); CEA and CNRS/IN2P3 (France); SRNSF (Georgia); BMBF, DFG, and HGF (Germany); GSRI (Greece); NKFIH (Hungary); DAE and DST (India); IPM (Iran); SFI (Ireland); INFN (Italy); MSIT and NRF (Republic of Korea); MES (Latvia); LMTLT (Lithuania); MOE and UM (Malaysia); BUAP, CINVESTAV, CONACYT, LNS, SEP, and UASLP-FAI (Mexico); MOS (Montenegro); MBIE (New Zealand); PAEC (Pakistan); MES and NSC (Poland); FCT (Portugal); MESTD (Serbia); MICIU/AEI and PCTI (Spain); MOSTR (Sri Lanka); Swiss Funding Agencies (Switzerland); MST (Taipei); MHESI and NSTDA (Thailand); TUBITAK and TENMAK (Türkiye); NASU (Ukraine); STFC (United Kingdom); DOE and NSF (U.S.A.).

Individuals have received support from the Marie-Curie program and the European Research Council and Horizon 2020 Grant, contract Nos. 675440, 724704, 752730, 758316, 765710, 824093, 101115353, 101002207, 101001205, and COST Action CA16108 (European Union); the Leventis Foundation; the Alfred P. Sloan Foundation; the Alexander von Humboldt Foundation; the Science Committee, project no. 22rl-037 (Armenia); the Fonds pour la Formation à la Recherche dans l'Industrie et dans l'Agriculture (FRIA-Belgium); the Beijing Municipal Science & Technology Commission, No. Z191100007219010, the Fundamental Research Funds for the Central Universities, the Ministry of Science and Technology of China under Grant No. 2023YFA1605804, and the Natural Science Foundation of China under Grant No. 12061141002 (China); the Ministry of Education, Youth and Sports (MEYS) of the Czech Republic; the Shota Rustaveli National Science Foundation, grant FR-22-985 (Georgia); the Deutsche Forschungsgemeinschaft (DFG), among others, under Germany's Excellence Strategy – EXC 2121 "Quantum Universe" – 390833306, and under project number 400140256 – GRK2497; the Hellenic Foundation for Research and Innovation (HFRI), Project Number 2288 (Greece); the Hungarian Academy of Sciences, the New National Excellence Program – ÚNKP, the NKFIH research grants K 131991, K 133046, K 138136, K 143460, K 143477, K 146913, K 146914, K 147048, 2020-2.2.1-ED-2021-00181, TKP2021-NKTA-64, and 2021-4.1.2-NEMZ_KI-2024-00036 (Hungary); the Council of Science and Industrial Research, India; ICSC – National Research Center for High Performance Computing, Big Data and Quantum Computing, FAIR – Future Artificial Intelligence Research, and CUP I53D23001070006 (Mission 4 Component 1), funded by the NextGenerationEU program (Italy); the Latvian Council of Science; the Ministry of Education and Science, project

JHEP05(2026)186

no. 2022/WK/14, and the National Science Center, contracts Opus 2021/41/B/ST2/01369 and 2021/43/B/ST2/01552 (Poland); the Fundação para a Ciência e a Tecnologia, grant CEECIND/01334/2018 (Portugal); the National Priorities Research Program by Qatar National Research Fund; MICIU/AEI/10.13039/501100011033, ERDF/EU, "European Union NextGenerationEU/PRTR", and Programa Severo Ochoa del Principado de Asturias (Spain); the Chulalongkorn Academic into Its 2nd Century Project Advancement Project, and the National Science, Research and Innovation Fund via the Program Management Unit for Human Resources & Institutional Development, Research and Innovation, grant B39G680009 (Thailand); the Kavli Foundation; the Nvidia Corporation; the SuperMicro Corporation; the Welch Foundation, contract C-1845; and the Weston Havens Foundation (U.S.A.).

Data Availability Statement. Release and preservation of data used by the CMS Collaboration as the basis for publications is guided by the CMS data preservation, re-use and open access policy.

Code Availability Statement. The CMS core software is publicly available on GitHub.

References

[1] ATLAS collaboration, *Observation of a new particle in the search for the Standard Model Higgs boson with the ATLAS detector at the LHC*, *Phys. Lett. B* **716** (2012) 1 [arXiv:1207.7214] [INSPIRE].

[2] CMS collaboration, *Observation of a New Boson at a Mass of 125 GeV with the CMS Experiment at the LHC*, *Phys. Lett. B* **716** (2012) 30 [arXiv:1207.7235] [INSPIRE].

[3] CMS collaboration, *Observation of a New Boson with Mass Near 125 GeV in pp Collisions at* $\sqrt{s} = 7$ *and* 8 *TeV*, *JHEP* **06** (2013) 081 [arXiv:1303.4571] [INSPIRE].

[4] CMS collaboration, *A portrait of the Higgs boson by the CMS experiment ten years after the discovery*, *Nature* **607** (2022) 60 [arXiv:2207.00043] [INSPIRE].

[5] ATLAS collaboration, *A detailed map of Higgs boson interactions by the ATLAS experiment ten years after the discovery*, *Nature* **607** (2022) 52 [*Erratum ibid.* **612** (2022) E24] [arXiv:2207.00092] [INSPIRE].

[6] M. Grazzini et al., *Higgs boson pair production at NNLO with top quark mass effects*, *JHEP* **05** (2018) 059 [arXiv:1803.02463] [INSPIRE].

[7] S. Dawson, S. Dittmaier and M. Spira, *Neutral Higgs boson pair production at hadron colliders: QCD corrections*, *Phys. Rev. D* **58** (1998) 115012 [hep-ph/9805244] [INSPIRE].

[8] S. Borowka et al., *Higgs Boson Pair Production in Gluon Fusion at Next-to-Leading Order with Full Top-Quark Mass Dependence*, *Phys. Rev. Lett.* **117** (2016) 012001 [*Erratum ibid.* **117** (2016) 079901] [arXiv:1604.06447] [INSPIRE].

[9] J. Baglio et al., *Gluon fusion into Higgs pairs at NLO QCD and the top mass scheme*, *Eur. Phys. J. C* **79** (2019) 459 [arXiv:1811.05692] [INSPIRE].

JHEP05(2026)186

[10] D. de Florian and J. Mazzitelli, *Higgs Boson Pair Production at Next-to-Next-to-Leading Order in QCD*, *Phys. Rev. Lett.* **111** (2013) 201801 [arXiv:1309.6594] [INSPIRE].

[11] D.Y. Shao, C.S. Li, H.T. Li and J. Wang, *Threshold resummation effects in Higgs boson pair production at the LHC*, *JHEP* **07** (2013) 169 [arXiv:1301.1245] [INSPIRE].

[12] D. de Florian and J. Mazzitelli, *Higgs pair production at next-to-next-to-leading logarithmic accuracy at the LHC*, *JHEP* **09** (2015) 053 [arXiv:1505.07122] [INSPIRE].

[13] J. Baglio et al., $gg \to HH$*: Combined uncertainties*, *Phys. Rev. D* **103** (2021) 056002 [arXiv:2008.11626] [INSPIRE].

[14] ATLAS collaboration, *Constraints on the Higgs boson self-coupling from single- and double-Higgs production with the ATLAS detector using pp collisions at* $\sqrt{s} = 13$ *TeV*, *Phys. Lett. B* **843** (2023) 137745 [arXiv:2211.01216] [INSPIRE].

[15] LHC Higgs Cross Section Working Group collaboration, *Handbook of LHC Higgs Cross Sections: 4. Deciphering the Nature of the Higgs Sector*, *CERN Yellow Rep. Monogr.* **2** (2017) 1 [arXiv:1610.07922] [INSPIRE].

[16] F. Goertz, A. Papaefstathiou, L.L. Yang and J. Zurita, *Higgs boson pair production in the* $D = 6$ *extension of the SM*, *JHEP* **04** (2015) 167 [arXiv:1410.3471] [INSPIRE].

[17] L. Randall and R. Sundrum, *A large mass hierarchy from a small extra dimension*, *Phys. Rev. Lett.* **83** (1999) 3370 [hep-ph/9905221] [INSPIRE].

[18] W.D. Goldberger and M.B. Wise, *Modulus stabilization with bulk fields*, *Phys. Rev. Lett.* **83** (1999) 4922 [hep-ph/9907447] [INSPIRE].

[19] H. Davoudiasl, J.L. Hewett and T.G. Rizzo, *Phenomenology of the Randall-Sundrum Gauge Hierarchy Model*, *Phys. Rev. Lett.* **84** (2000) 2080 [hep-ph/9909255] [INSPIRE].

[20] A. Djouadi, *The anatomy of electro-weak symmetry breaking. II. The Higgs bosons in the minimal supersymmetric model*, *Phys. Rept.* **459** (2008) 1 [hep-ph/0503173] [INSPIRE].

[21] CMS collaboration, *Search for a new resonance decaying into two spin-0 bosons in a final state with two photons and two bottom quarks in proton-proton collisions at* $\sqrt{s} = 13$ *TeV*, *JHEP* **05** (2024) 316 [arXiv:2310.01643] [INSPIRE].

[22] CMS collaboration, *Searches for additional Higgs bosons and for vector leptoquarks in* $\tau\tau$ *final states in proton-proton collisions at* $\sqrt{s} = 13$ *TeV*, *JHEP* **07** (2023) 073 [arXiv:2208.02717] [INSPIRE].

[23] CMS collaboration, *Search for a standard model-like Higgs boson in the mass range between 70 and 110 GeV in the diphoton final state in proton-proton collisions at* $\sqrt{s} = 13$ *TeV*, *Phys. Lett. B* **860** (2025) 139067 [arXiv:2405.18149] [INSPIRE].

[24] A. Carvalho et al., *Higgs Pair Production: Choosing Benchmarks With Cluster Analysis*, *JHEP* **04** (2016) 126 [arXiv:1507.02245] [INSPIRE].

[25] G. Buchalla et al., *Higgs boson pair production in non-linear Effective Field Theory with full* m_t*-dependence at NLO QCD*, *JHEP* **09** (2018) 057 [*Erratum ibid.* **06** (2025) 094] [arXiv:1806.05162] [INSPIRE].

[26] *HEPData record for this analysis*, (2025), DOI:10.17182/hepdata.158371.

[27] CMS collaboration, *The CMS Experiment at the CERN LHC*, 2008 *JINST* **3** S08004 [INSPIRE].

[28] CMS collaboration, *Performance of the CMS Level-1 trigger in proton-proton collisions at* $\sqrt{s} = 13$ *TeV*, 2020 *JINST* **15** P10017 [arXiv:2006.10165] [INSPIRE].

JHEP05(2026)186

[29] CMS collaboration, *The CMS trigger system*, 2017 *JINST* **12** P01020 [arXiv:1609.02366] [INSPIRE].

[30] CMS collaboration, *Performance of the CMS high-level trigger during LHC Run 2*, 2024 *JINST* **19** P11021 [arXiv:2410.17038] [INSPIRE].

[31] CMS collaboration, *Particle-flow reconstruction and global event description with the CMS detector*, 2017 *JINST* **12** P10003 [arXiv:1706.04965] [INSPIRE].

[32] D. Contardo et al., *Technical Proposal for the Phase-II Upgrade of the CMS Detector*, CERN-LHCC-2015-010 (2015) [DOI:10.17181/CERN.VU8I.D59J] [INSPIRE].

[33] CMS collaboration, *Electron and photon reconstruction and identification with the CMS experiment at the CERN LHC*, 2021 *JINST* **16** P05014 [arXiv:2012.06888] [INSPIRE].

[34] CMS collaboration, *Performance of Photon Reconstruction and Identification with the CMS Detector in Proton-Proton Collisions at* $\sqrt{s} = 8$ *TeV*, 2015 *JINST* **10** P08010 [arXiv:1502.02702] [INSPIRE].

[35] CMS collaboration, *A measurement of the Higgs boson mass in the diphoton decay channel*, *Phys. Lett. B* **805** (2020) 135425 [arXiv:2002.06398] [INSPIRE].

[36] CMS Collaboration, *ECAL 2016 refined calibration and Run2 summary plots*, CMS Detector Performance Summary CMS-DP-2020-021 (2020).

[37] CMS collaboration, *Performance of the CMS muon detector and muon reconstruction with proton-proton collisions at* $\sqrt{s} = 13$ *TeV*, 2018 *JINST* **13** P06015 [arXiv:1804.04528] [INSPIRE].

[38] M. Cacciari, G.P. Salam and G. Soyez, *The anti-*k_t *jet clustering algorithm*, *JHEP* **04** (2008) 063 [arXiv:0802.1189] [INSPIRE].

[39] M. Cacciari, G.P. Salam and G. Soyez, *FastJet User Manual*, *Eur. Phys. J. C* **72** (2012) 1896 [arXiv:1111.6097] [INSPIRE].

[40] CMS collaboration, *Pileup mitigation at CMS in 13 TeV data*, 2020 *JINST* **15** P09018 [arXiv:2003.00503] [INSPIRE].

[41] CMS collaboration, *Jet energy scale and resolution in the CMS experiment in pp collisions at 8 TeV*, 2017 *JINST* **12** P02014 [arXiv:1607.03663] [INSPIRE].

[42] CMS collaboration, *Identification of heavy-flavour jets with the CMS detector in pp collisions at 13 TeV*, 2018 *JINST* **13** P05011 [arXiv:1712.07158] [INSPIRE].

[43] E. Bols et al., *Jet Flavour Classification Using DeepJet*, 2020 *JINST* **15** P12012 [arXiv:2008.10519] [INSPIRE].

[44] CMS collaboration, *Performance of the DeepJet b tagging algorithm using 41.9* fb^{-1} *of data from proton-proton collisions at 13 TeV with Phase-1 CMS detector*, CMS Detector Performance Note CMS-DP-2018-058 (2018).

[45] CMS collaboration, *Performance of reconstruction and identification of* τ *leptons decaying to hadrons and* ν_τ *in pp collisions at* $\sqrt{s} = 13$ *TeV*, 2018 *JINST* **13** P10005 [arXiv:1809.02816] [INSPIRE].

[46] CMS collaboration, *Identification of hadronic tau lepton decays using a deep neural network*, 2022 *JINST* **17** P07023 [arXiv:2201.08458] [INSPIRE].

[47] CMS collaboration, *Performance of missing transverse momentum reconstruction in proton-proton collisions at* $\sqrt{s} = 13$ *TeV using the CMS detector*, 2019 *JINST* **14** P07004 [arXiv:1903.06078] [INSPIRE].

JHEP05(2026)186

[48] CMS collaboration, *Precision luminosity measurement in proton-proton collisions at $\sqrt{s} = 13$ TeV in 2015 and 2016 at CMS*, *Eur. Phys. J. C* **81** (2021) 800 [arXiv:2104.01927] [INSPIRE].

[49] CMS collaboration, *CMS luminosity measurement for the 2017 data-taking period at $\sqrt{s} = 13$ TeV*, CMS-PAS-LUM-17-004 (2018) [INSPIRE].

[50] CMS collaboration, *CMS luminosity measurement for the 2018 data-taking period at $\sqrt{s} = 13$ TeV*, CMS-PAS-LUM-18-002 (2019) [INSPIRE].

[51] E. Bagnaschi, G. Degrassi, P. Slavich and A. Vicini, *Higgs production via gluon fusion in the POWHEG approach in the SM and in the MSSM*, *JHEP* **02** (2012) 088 [arXiv:1111.2854] [INSPIRE].

[52] G. Heinrich et al., *NLO predictions for Higgs boson pair production with full top quark mass dependence matched to parton showers*, *JHEP* **08** (2017) 088 [arXiv:1703.09252] [INSPIRE].

[53] G. Heinrich et al., *Probing the trilinear Higgs boson coupling in di-Higgs production at NLO QCD including parton shower effects*, *JHEP* **06** (2019) 066 [arXiv:1903.08137] [INSPIRE].

[54] S. Jones and S. Kuttimalai, *Parton Shower and NLO-Matching uncertainties in Higgs Boson Pair Production*, *JHEP* **02** (2018) 176 [arXiv:1711.03319] [INSPIRE].

[55] G. Heinrich, S.P. Jones, M. Kerner and L. Scyboz, *A non-linear EFT description of $gg \to HH$ at NLO interfaced to POWHEG*, *JHEP* **10** (2020) 021 [arXiv:2006.16877] [INSPIRE].

[56] P. Nason, *A new method for combining NLO QCD with shower Monte Carlo algorithms*, *JHEP* **11** (2004) 040 [hep-ph/0409146] [INSPIRE].

[57] S. Frixione, P. Nason and C. Oleari, *Matching NLO QCD computations with Parton Shower simulations: the POWHEG method*, *JHEP* **11** (2007) 070 [arXiv:0709.2092] [INSPIRE].

[58] S. Alioli, P. Nason, C. Oleari and E. Re, *A general framework for implementing NLO calculations in shower Monte Carlo programs: the POWHEG BOX*, *JHEP* **06** (2010) 043 [arXiv:1002.2581] [INSPIRE].

[59] D. de Florian et al., *Anomalous couplings in Higgs-boson pair production at approximate NNLO QCD*, *JHEP* **09** (2021) 161 [arXiv:2106.14050] [INSPIRE].

[60] A. Carvalho et al., *On the reinterpretation of non-resonant searches for Higgs boson pairs*, *JHEP* **02** (2021) 049 [arXiv:1710.08261] [INSPIRE].

[61] J. Alwall et al., *The automated computation of tree-level and next-to-leading order differential cross sections, and their matching to parton shower simulations*, *JHEP* **07** (2014) 079 [arXiv:1405.0301] [INSPIRE].

[62] SHERPA collaboration, *Event Generation with Sherpa 2.2*, *SciPost Phys.* **7** (2019) 034 [arXiv:1905.09127] [INSPIRE].

[63] J. Alwall et al., *Comparative study of various algorithms for the merging of parton showers and matrix elements in hadronic collisions*, *Eur. Phys. J. C* **53** (2008) 473 [arXiv:0706.2569] [INSPIRE].

[64] R. Frederix and S. Frixione, *Merging meets matching in MC@NLO*, *JHEP* **12** (2012) 061 [arXiv:1209.6215] [INSPIRE].

[65] CMS collaboration, *Event generator tunes obtained from underlying event and multiparton scattering measurements*, *Eur. Phys. J. C* **76** (2016) 155 [arXiv:1512.00815] [INSPIRE].

[66] CMS collaboration, *Extraction and validation of a new set of CMS PYTHIA8 tunes from underlying-event measurements*, *Eur. Phys. J. C* **80** (2020) 4 [arXiv:1903.12179] [INSPIRE].

JHEP05(2026)186

[67] NNPDF collaboration, *Parton distributions from high-precision collider data*, *Eur. Phys. J. C* **77** (2017) 663 [arXiv:1706.00428] [INSPIRE].

[68] GEANT4 collaboration, *GEANT4 — A Simulation Toolkit*, *Nucl. Instrum. Meth. A* **506** (2003) 250 [INSPIRE].

[69] P. Baldi et al., *Parameterized neural networks for high-energy physics*, *Eur. Phys. J. C* **76** (2016) 235 [arXiv:1601.07913] [INSPIRE].

[70] S. Choi and H. Oh, *Improved extrapolation methods of data-driven background estimations in high energy physics*, *Eur. Phys. J. C* **81** (2021) 643 [arXiv:1906.10831] [INSPIRE].

[71] CMS collaboration, *Performance of Electron Reconstruction and Selection with the CMS Detector in Proton-Proton Collisions at* $\sqrt{s} = 8$ *TeV*, 2015 *JINST* **10** P06005 [arXiv:1502.02701] [INSPIRE].

[72] T. Chen and C. Guestrin, *XGBoost: A Scalable Tree Boosting System*, arXiv:1603.02754 [DOI:10.1145/2939672.2939785] [INSPIRE].

[73] L. Bianchini, J. Conway, E.K. Friis and C. Veelken, *Reconstruction of the Higgs mass in* $H \to \tau\tau$ *Events by Dynamical Likelihood techniques*, *J. Phys. Conf. Ser.* **513** (2014) 022035 [INSPIRE].

[74] P.D. Dauncey, M. Kenzie, N. Wardle and G.J. Davies, *Handling uncertainties in background shapes: the discrete profiling method*, 2015 *JINST* **10** P04015 [arXiv:1408.6865] [INSPIRE].

[75] M.J. Oreglia, *A study of the reactions* $\psi' \to \gamma\gamma\psi$, Ph.D. Thesis, Stanford University, U.S.A. (1980).

[76] J.E. Gaiser, *Charmonium Spectroscopy From Radiative Decays of the* J/ψ *and* ψ', MSc Thesis, Stanford University, U.S.A. (1982).

[77] P. Virtanen et al., *SciPy 1.0: Fundamental Algorithms for Scientific Computing in Python*, *Nature Meth.* **17** (2020) 261 [arXiv:1907.10121] [INSPIRE].

[78] P. Alfeld, *A trivariate clough-tocher scheme for tetrahedral data*, *Comput. Aided Geom. Des.* **1** (1984) 169.

[79] R.A. Fisher, *On the Interpretation of* χ^2 *from Contingency Tables, and the Calculation of P*, *J. Roy. Statist. Soc.* **85** (1922) 87.

[80] CMS collaboration, *Search for narrow resonances in the b-tagged dijet mass spectrum in proton-proton collisions at* $\sqrt{s} = 13$ *TeV*, *Phys. Rev. D* **108** (2023) 012009 [arXiv:2205.01835] [INSPIRE].

[81] CMS collaboration, *Measurements of Higgs boson production cross sections and couplings in the diphoton decay channel at* $\sqrt{s} = 13$ *TeV*, *JHEP* **07** (2021) 027 [arXiv:2103.06956] [INSPIRE].

[82] J. Butterworth et al., *PDF4LHC recommendations for LHC Run II*, *J. Phys. G* **43** (2016) 023001 [arXiv:1510.03865] [INSPIRE].

[83] LHC Higgs Cross Section Working Group collaboration, *Handbook of LHC Higgs Cross Sections: 3. Higgs Properties*, arXiv:1307.1347 [DOI:10.5170/CERN-2013-004] [INSPIRE].

[84] CMS collaboration, *Measurement of the Inclusive W and Z Production Cross Sections in pp Collisions at* $\sqrt{s} = 7$ *TeV*, *JHEP* **10** (2011) 132 [arXiv:1107.4789] [INSPIRE].

[85] T. Junk, *Confidence level computation for combining searches with small statistics*, *Nucl. Instrum. Meth. A* **434** (1999) 435 [hep-ex/9902006] [INSPIRE].

[86] A.L. Read, *Presentation of search results: The* CL_s *technique*, *J. Phys. G* **28** (2002) 2693 [INSPIRE].

JHEP05(2026)186

[87] ATLAS et al. collaborations, *Procedure for the LHC Higgs boson search combination in Summer 2011*, CMS-NOTE-2011-005 (2011) [INSPIRE].

[88] G. Cowan, K. Cranmer, E. Gross and O. Vitells, *Asymptotic formulae for likelihood-based tests of new physics*, *Eur. Phys. J. C* **71** (2011) 1554 [*Erratum ibid.* **73** (2013) 2501] [arXiv:1007.1727] [INSPIRE].

[89] F. Maltoni, D. Pagani, A. Shivaji and X. Zhao, *Trilinear Higgs coupling determination via single-Higgs differential measurements at the LHC*, *Eur. Phys. J. C* **77** (2017) 887 [arXiv:1709.08649] [INSPIRE].

[90] A. Carvalho, *Gravity particles from Warped Extra Dimensions, predictions for LHC*, arXiv:1404.0102 [INSPIRE].

[91] U. Ellwanger and C. Hugonie, *Benchmark planes for Higgs-to-Higgs decays in the NMSSM*, *Eur. Phys. J. C* **82** (2022) 406 [arXiv:2203.05049] [INSPIRE].

[92] U. Ellwanger, J.F. Gunion and C. Hugonie, *NMHDECAY: A Fortran code for the Higgs masses, couplings and decay widths in the NMSSM*, *JHEP* **02** (2005) 066 [hep-ph/0406215] [INSPIRE].

[93] U. Ellwanger and C. Hugonie, *NMHDECAY 2.0: An updated program for sparticle masses, Higgs masses, couplings and decay widths in the NMSSM*, *Comput. Phys. Commun.* **175** (2006) 290 [hep-ph/0508022] [INSPIRE].

[94] G. Belanger, F. Boudjema, A. Pukhov and A. Semenov, *micrOMEGAs_3: A program for calculating dark matter observables*, *Comput. Phys. Commun.* **185** (2014) 960 [arXiv:1305.0237] [INSPIRE].

JHEP05(2026)186

The CMS collaboration

A. Hayrapetyan[1], A. Tumasyan[1,a], W. Adam[2], J.W. Andrejkovic[2], L. Benato[2], T. Bergauer[2], S. Chatterjee[2], K. Damanakis[2], M. Dragicevic[2], P.S. Hussain[2], M. Jeitler[2,b], N. Krammer[2], A. Li[2], D. Liko[2], I. Mikulec[2], J. Schieck[2,b], D. Schwarz[2], R. Schöfbeck[2,b], M. Sonawane[2], W. Waltenberger[2], C.-E. Wulz[2,b], T. Janssen[3], T. Van Laer[3], P. Van Mechelen[3], N. Breugelmans[4], J. D'Hondt[4], S. Dansana[4], A. De Moor[4], M. Delcourt[4], F. Heyen[4], S. Lowette[4], I. Makarenko[4], D. Müller[4], S. Tavernier[4], M. Tytgat[4,c], G.P. Van Onsem[4], S. Van Putte[4], D. Vannerom[4], B. Bilin[5], B. Clerbaux[5], A.K. Das[5], I. De Bruyn[5], G. De Lentdecker[5], H. Evard[5], L. Favart[5], P. Gianneios[5], J. Jaramillo[5], A. Khalilzadeh[5], F.A. Khan[5], K. Lee[5], A. Malara[5], M.A. Shahzad[5], L. Thomas[5], M. Vanden Bemden[5], C. Vander Velde[5], P. Vanlaer[5], M. De Coen[6], D. Dobur[6], G. Gokbulut[6], Y. Hong[6], J. Knolle[6], L. Lambrecht[6], D. Marckx[6], K. Mota Amarilo[6], K. Skovpen[6], N. Van Den Bossche[6], J. van der Linden[6], L. Wezenbeek[6], S. Bein[7], A. Benecke[7], A. Bethani[7], G. Bruno[7], C. Caputo[7], J. De Favereau De Jeneret[7], C. Delaere[7], I.S. Donertas[7], A. Giammanco[7], A.O. Guzel[7], Sa. Jain[7], V. Lemaitre[7], J. Lidrych[7], P. Mastrapasqua[7], T.T. Tran[7], S. Turkcapar[7], G.A. Alves[8], E. Coelho[8], G. Correia Silva[8], C. Hensel[8], T. Menezes De Oliveira[8], C. Mora Herrera[8,d], P. Rebello Teles[8], M. Soeiro[8], E.J. Tonelli Manganote[8,e], A. Vilela Pereira[8,d], W.L. Aldá Júnior[9], M. Barroso Ferreira Filho[9], H. Brandao Malbouisson[9], W. Carvalho[9], J. Chinellato[9,f], E.M. Da Costa[9], G.G. Da Silveira[9,g], D. De Jesus Damiao[9], S. Fonseca De Souza[9], R. Gomes De Souza[9], T. Laux Kuhn[9,g], M. Macedo[9], J. Martins[9], L. Mundim[9], H. Nogima[9], J.P. Pinheiro[9], A. Santoro[9], A. Sznajder[9], M. Thiel[9], C.A. Bernardes[10,g], L. Calligaris[10], E.M. Gregores[10], I. Maietto Silverio[10], P.G. Mercadante[10], S.F. Novaes[10], B. Orzari[10], Sandra S. Padula[10], T.R. Fernandez Perez Tomei[10], A. Aleksandrov[11], G. Antchev[11], R. Hadjiiska[11], P. Iaydjiev[11], M. Misheva[11], M. Shopova[11], G. Sultanov[11], A. Dimitrov[12], L. Litov[12], B. Pavlov[12], P. Petkov[12], A. Petrov[12], E. Shumka[12], S. Keshri[13], D. Laroze[13], S. Thakur[13], T. Cheng[14], T. Javaid[14], L. Yuan[14], Z. Hu[15], Z. Liang[15], J. Liu[15], G.M. Chen[16,h], H.S. Chen[16,h], M. Chen[16,h], F. Iemmi[16], C.H. Jiang[16], A. Kapoor[16,i], H. Liao[16], Z.-A. Liu[16,j], R. Sharma[16,k], J.N. Song[16,j], J. Tao[16], C. Wang[16,h], J. Wang[16], Z. Wang[16,h], H. Zhang[16], J. Zhao[16], A. Agapitos[17], Y. Ban[17], A. Carvalho Antunes De Oliveira[17], S. Deng[17], B. Guo[17], C. Jiang[17], A. Levin[17], C. Li[17], Q. Li[17], Y. Mao[17], S. Qian[17], S.J. Qian[17], X. Qin[17], X. Sun[17], D. Wang[17], H. Yang[17], L. Zhang[17], Y. Zhao[17], C. Zhou[17], S. Yang[18], Z. You[19], K. Jaffel[20], N. Lu[20], G. Bauer[21,l], B. Li[21,m], K. Yi[21,n], J. Zhang[21], Y. Li[22], Z. Lin[23], C. Lu[23], M. Xiao[23], C. Avila[24], D.A. Barbosa Trujillo[24], A. Cabrera[24], C. Florez[24], J. Fraga[24], J.A. Reyes Vega[24], C. Rendón[25], M. Rodriguez[25], A.A. Ruales Barbosa[25], J.D. Ruiz Alvarez[25], D. Giljanovic[26], N. Godinovic[26], D. Lelas[26], A. Sculac[26], M. Kovac[27], A. Petkovic[27], T. Sculac[27], P. Bargassa[28], V. Brigljevic[28], B.K. Chitroda[28], D. Ferencek[28], K. Jakovcic[28], A. Starodumov[28,o], T. Susa[28], A. Attikis[29], K. Christoforou[29], A. Hadjiagapiou[29], C. Leonidou[29], J. Mousa[29], C. Nicolaou[29], L. Paizanos[29], F. Ptochos[29], P.A. Razis[29], H. Rykaczewski[29], H. Saka[29], A. Stepennov[29], M. Finger[30], M. Finger Jr.[30], A. Kveton[30], E. Ayala[31], E. Carrera Jarrin[32],

JHEP05(2026)186

H. Abdalla[33,p], Y. Assran[33,q,r], B. El-mahdy[33], M.A. Mahmoud[34], M. Abdullah Al-Mashad[34], K. Ehataht[35], M. Kadastik[35], T. Lange[35], C. Nielsen[35], J. Pata[35], M. Raidal[35], L. Tani[35], C. Veelken[35], H. Kirschenmann[36], K. Osterberg[36], M. Voutilainen[36], S. Bharthuar[37], N. Bin Norjoharuddeen[37], E. Brücken[37], F. Garcia[37], P. Inkaew[37], K.T.S. Kallonen[37], T. Lampén[37], K. Lassila-Perini[37], S. Lehti[37], T. Lindén[37], M. Myllymäki[37], M.m. Rantanen[37], H. Siikonen[37], J. Tuominiemi[37], P. Luukka[38], H. Petrow[38], M. Besancon[39], F. Couderc[39], M. Dejardin[39], D. Denegri[39], J.L. Faure[39], F. Ferri[39], S. Ganjour[39], P. Gras[39], G. Hamel de Monchenault[39], M. Kumar[39], V. Lohezic[39], J. Malcles[39], F. Orlandi[39], L. Portales[39], A. Rosowsky[39], M.Ö. Sahin[39], A. Savoy-Navarro[39,s], P. Simkina[39], M. Titov[39], M. Tornago[39], F. Beaudette[40], G. Boldrini[40], P. Busson[40], A. Cappati[40], C. Charlot[40], M. Chiusi[40], T.D. Cuisset[40], F. Damas[40], O. Davignon[40], A. De Wit[40], I.T. Ehle[40], B.A. Fontana Santos Alves[40], S. Ghosh[40], A. Gilbert[40], R. Granier de Cassagnac[40], A. Hakimi[40], B. Harikrishnan[40], L. Kalipoliti[40], G. Liu[40], M. Nguyen[40], C. Ochando[40], R. Salerno[40], J.B. Sauvan[40], Y. Sirois[40], L. Urda Gómez[40], E. Vernazza[40], A. Zabi[40], A. Zghiche[40], J.-L. Agram[41,t], J. Andrea[41], D. Apparu[41], D. Bloch[41], J.-M. Brom[41], E.C. Chabert[41], C. Collard[41], S. Falke[41], U. Goerlach[41], R. Haeberle[41], A.-C. Le Bihan[41], M. Meena[41], O. Poncet[41], G. Saha[41], M.A. Sessini[41], P. Van Hove[41], P. Vaucelle[41], A. Di Florio[42], D. Amram[43], S. Beauceron[43], B. Blancon[43], G. Boudoul[43], N. Chanon[43], D. Contardo[43], P. Depasse[43], C. Dozen[43,u], H. El Mamouni[43], J. Fay[43], S. Gascon[43], M. Gouzevitch[43], C. Greenberg[43], G. Grenier[43], B. Ille[43], E. Jourd'huy[43], I.B. Laktineh[43], M. Lethuillier[43], L. Mirabito[43], S. Perries[43], A. Purohit[43], M. Vander Donckt[43], P. Verdier[43], J. Xiao[43], G. Adamov[44], I. Lomidze[44], Z. Tsamalaidze[44,v], V. Botta[45], S. Consuegra Rodríguez[45], L. Feld[45], K. Klein[45], M. Lipinski[45], D. Meuser[45], A. Pauls[45], D. Pérez Adán[45], N. Röwert[45], M. Teroerde[45], S. Diekmann[46], A. Dodonova[46], N. Eich[46], D. Eliseev[46], F. Engelke[46], J. Erdmann[46], M. Erdmann[46], P. Fackeldey[46], B. Fischer[46], T. Hebbeker[46], K. Hoepfner[46], F. Ivone[46], A. Jung[46], M.y. Lee[46], F. Mausolf[46], M. Merschmeyer[46], A. Meyer[46], S. Mukherjee[46], D. Noll[46], F. Nowotny[46], A. Pozdnyakov[46], Y. Rath[46], W. Redjeb[46], F. Rehm[46], H. Reithler[46], V. Sarkisovi[46], A. Schmidt[46], C. Seth[46], A. Sharma[46], J.L. Spah[46], A. Stein[46], F. Torres Da Silva De Araujo[46,w], S. Wiedenbeck[46], S. Zaleski[46], C. Dziwok[47], G. Flügge[47], T. Kress[47], A. Nowack[47], O. Pooth[47], A. Stahl[47], T. Ziemons[47], A. Zotz[47], H. Aarup Petersen[48], M. Aldaya Martin[48], J. Alimena[48], S. Amoroso[48], Y. An[48], J. Bach[48], S. Baxter[48], M. Bayatmakou[48], H. Becerril Gonzalez[48], O. Behnke[48], A. Belvedere[48], F. Blekman[48,x], K. Borras[48,y], A. Campbell[48], A. Cardini[48], C. Cheng[48], F. Colombina[48], G. Eckerlin[48], D. Eckstein[48], L.I. Estevez Banos[48], E. Gallo[48,x], A. Geiser[48], V. Guglielmi[48], M. Guthoff[48], A. Hinzmann[48], L. Jeppe[48], B. Kaech[48], M. Kasemann[48], C. Kleinwort[48], R. Kogler[48], M. Komm[48], D. Krücker[48], W. Lange[48], D. Leyva Pernia[48], K. Lipka[48,z], W. Lohmann[48,aa], F. Lorkowski[48], R. Mankel[48], I.-A. Melzer-Pellmann[48], M. Mendizabal Morentin[48], A.B. Meyer[48], G. Milella[48], K. Moral Figueroa[48], A. Mussgiller[48], L.P. Nair[48], J. Niedziela[48], A. Nürnberg[48], Y. Otarid[48], J. Park[48], E. Ranken[48], A. Raspereza[48], D. Rastorguev[48], L. Rygaard[48], J. Rübenach[48], A. Saggio[48], M. Scham[48,ab,ac], S. Schnake[48,y], C. Schwanenberger[48,x],

JHEP05(2026)186

P. Schütze[48], D. Selivanova[48], K. Sharko[48], M. Shchedrolosiev[48], D. Stafford[48], F. Vazzoler[48], A. Ventura Barroso[48], R. Walsh[48], D. Wang[48], Q. Wang[48], K. Wichmann[48], L. Wiens[48,y], C. Wissing[48], Y. Yang[48], A. Zimermmane Castro Santos[48], A. Albrecht[49], S. Albrecht[49], M. Antonello[49], S. Bollweg[49], M. Bonanomi[49], P. Connor[49], K. El Morabit[49], Y. Fischer[49], E. Garutti[49], A. Grohsjean[49], J. Haller[49], D. Hundhausen[49], H.R. Jabusch[49], G. Kasieczka[49], P. Keicher[49], R. Klanner[49], W. Korcari[49], T. Kramer[49], C.c. Kuo[49], V. Kutzner[49], F. Labe[49], J. Lange[49], A. Lobanov[49], C. Matthies[49], L. Moureaux[49], M. Mrowietz[49], A. Nigamova[49], Y. Nissan[49], A. Paasch[49], K.J. Pena Rodriguez[49], T. Quadfasel[49], B. Raciti[49], M. Rieger[49], D. Savoiu[49], J. Schindler[49], P. Schleper[49], M. Schröder[49], J. Schwandt[49], M. Sommerhalder[49], H. Stadie[49], G. Steinbrück[49], A. Tews[49], B. Wiederspan[49], M. Wolf[49], S. Brommer[50], E. Butz[50], T. Chwalek[50], A. Dierlamm[50], A. Droll[50], U. Elicabuk[50], N. Faltermann[50], M. Giffels[50], A. Gottmann[50], F. Hartmann[50,ad], R. Hofsaess[50], M. Horzela[50], U. Husemann[50], J. Kieseler[50], M. Klute[50], O. Lavoryk[50], J.M. Lawhorn[50], M. Link[50], A. Lintuluoto[50], S. Maier[50], S. Mitra[50], M. Mormile[50], Th. Müller[50], M. Neukum[50], M. Oh[50], E. Pfeffer[50], M. Presilla[50], G. Quast[50], K. Rabbertz[50], B. Regnery[50], N. Shadskiy[50], I. Shvetsov[50], H.J. Simonis[50], L. Sowa[50], L. Stockmeier[50], K. Tauqeer[50], M. Toms[50], B. Topko[50], N. Trevisani[50], R.F. Von Cube[50], M. Wassmer[50], S. Wieland[50], F. Wittig[50], R. Wolf[50], X. Zuo[50], G. Anagnostou[51], G. Daskalakis[51], A. Kyriakis[51], A. Papadopoulos[51,ad], A. Stakia[51], G. Melachroinos[52], Z. Painesis[52], I. Paraskevas[52], N. Saoulidou[52], K. Theofilatos[52], E. Tziaferi[52], K. Vellidis[52], I. Zisopoulos[52], G. Bakas[53], T. Chatzistavrou[53], G. Karapostoli[53], K. Kousouris[53], I. Papakrivopoulos[53], E. Siamarkou[53], G. Tsipolitis[53], A. Zacharopoulou[53], I. Bestintzanos[54], I. Evangelou[54], C. Foudas[54], C. Kamtsikis[54], P. Katsoulis[54], P. Kokkas[54], P.G. Kosmoglou Kioseoglou[54], N. Manthos[54], I. Papadopoulos[54], J. Strologas[54], C. Hajdu[55], D. Horvath[55,ae,af], K. Márton[55], A.J. Rádl[55,ag], F. Sikler[55], V. Veszpremi[55], M. Csanád[56], K. Farkas[56], A. Fehérkuti[56,ah], M.M.A. Gadallah[56,ai], Á. Kadlecsik[56], P. Major[56], G. Pásztor[56], G.I. Veres[56], L. Olah[57], B. Ujvari[57], G. Bencze[58], S. Czellar[58], J. Molnar[58], Z. Szillasi[58], T. Csorgo[59,ah], F. Nemes[59,ah], T. Novak[59], S. Bansal[60], S.B. Beri[60], V. Bhatnagar[60], G. Chaudhary[60], S. Chauhan[60], N. Dhingra[60,aj], A. Kaur[60], A. Kaur[60], H. Kaur[60], M. Kaur[60], S. Kumar[60], T. Sheokand[60], J.B. Singh[60], A. Singla[60], A. Ahmed[61], A. Bhardwaj[61], A. Chhetri[61], B.C. Choudhary[61], A. Kumar[61], A. Kumar[61], M. Naimuddin[61], S. Saumya[61], K. Ranjan[61], M.K. Saini[61], S. Baradia[62], S. Barman[62,ak], S. Bhattacharya[62], S. Das Gupta[62], S. Dutta[62], S. Dutta[62], S. Sarkar[62], M.M. Ameen[63], P.K. Behera[63], S.C. Behera[63], S. Chatterjee[63], G. Dash[63], P. Jana[63], P. Kalbhor[63], S. Kamble[63], J.R. Komaragiri[63,al], D. Kumar[63,al], T. Mishra[63], B. Parida[63,am], P.R. Pujahari[63], N.R. Saha[63], A. Sharma[63], A.K. Sikdar[63], R.K. Singh[63], P. Verma[63], S. Verma[63], A. Vijay[63], S. Dugad[64], G.B. Mohanty[64], M. Shelake[64], P. Suryadevara[64], A. Bala[65], S. Banerjee[65], R.M. Chatterjee[65], M. Guchait[65], Sh. Jain[65], A. Jaiswal[65], S. Kumar[65], G. Majumder[65], K. Mazumdar[65], S. Parolia[65], A. Thachayath[65], S. Bahinipati[66,an], C. Kar[66], D. Maity[66,ao], P. Mal[66], K. Naskar[66,ao], A. Nayak[66,ao], S. Nayak[66], K. Pal[66], P. Sadangi[66], S.K. Swain[66], S. Varghese[66,ao], D. Vats[66,ao], S. Acharya[67,ap], A. Alpana[67], S. Dube[67], B. Gomber[67,ap], P. Hazarika[67], B. Kansal[67], A. Laha[67], B. Sahu[67,ap], S. Sharma[67], K.Y. Vaish[67],

JHEP05(2026)186

H. Bakhshiansohi[68,aq], A. Jafari[68,ar], M. Zeinali[68,as], S. Bashiri[69], S. Chenarani[69,at], S.M. Etesami[69], Y. Hosseini[69], M. Khakzad[69], E. Khazaie[69], M. Mohammadi Najafabadi[69], S. Tizchang[69,au], M. Felcini[70], M. Grunewald[70], M. Abbrescia[71a,71b], A. Colaleo[71a,71b], D. Creanza[71a,71c], B. D'Anzi[71a,71b], N. De Filippis[71a,71c], M. De Palma[71a,71b], W. Elmetenawee[71a,71b,av], N. Ferrara[71a,71b], L. Fiore[71a], G. Iaselli[71a,71c], L. Longo[71a], M. Louka[71a,71b], G. Maggi[71a,71c], M. Maggi[71a], I. Margjeka[71a], V. Mastrapasqua[71a,71b], S. My[71a,71b], S. Nuzzo[71a,71b], A. Pellecchia[71a,71b], A. Pompili[71a,71b], G. Pugliese[71a,71c], R. Radogna[71a,71b], D. Ramos[71a], A. Ranieri[71a], L. Silvestris[71a], F.M. Simone[71a,71c], A. Stamerra[71a,71b], Ü. Sözbilir[71a], D. Troiano[71a,71b], R. Venditti[71a,71b], P. Verwilligen[71a], A. Zaza[71a,71b], G. Abbiendi[72a], C. Battilana[72a,72b], D. Bonacorsi[72a,72b], P. Capiluppi[72a,72b], A. Castro[72a,72b,†], F.R. Cavallo[72a], M. Cuffiani[72a,72b], G.M. Dallavalle[72a], T. Diotalevi[72a,72b], F. Fabbri[72a], A. Fanfani[72a,72b], D. Fasanella[72a], P. Giacomelli[72a], L. Giommi[72a,72b], C. Grandi[72a], L. Guiducci[72a,72b], S. Lo Meo[72a,aw], M. Lorusso[72a,72b], L. Lunerti[72a], S. Marcellini[72a], G. Masetti[72a], F.L. Navarria[72a,72b], G. Paggi[72a,72b], A. Perrotta[72a], F. Primavera[72a,72b], A.M. Rossi[72a,72b], S. Rossi Tisbeni[72a,72b], T. Rovelli[72a,72b], G.P. Siroli[72a,72b], S. Costa[73a,73b,ax], A. Di Mattia[73a], A. Lapertosa[73a], R. Potenza[73a,73b], A. Tricomi[73a,73b,ax], C. Tuve[73a,73b], P. Assiouras[74a], G. Barbagli[74a], G. Bardelli[74a,74b], B. Camaiani[74a,74b], A. Cassese[74a], R. Ceccarelli[74a], V. Ciulli[74a,74b], C. Civinini[74a], R. D'Alessandro[74a,74b], E. Focardi[74a,74b], T. Kello[74a], G. Latino[74a,74b], P. Lenzi[74a,74b], M. Lizzo[74a], M. Meschini[74a], S. Paoletti[74a], A. Papanastassiou[74a,74b], G. Sguazzoni[74a], L. Viliani[74a], L. Benussi[75], S. Bianco[75], S. Meola[75,ay], D. Piccolo[75], M. Alves Gallo Pereira[76a], F. Ferro[76a], E. Robutti[76a], S. Tosi[76a,76b], A. Benaglia[77a], F. Brivio[77a], F. Cetorelli[77a,77b], F. De Guio[77a,77b], M.E. Dinardo[77a,77b], P. Dini[77a], S. Gennai[77a], R. Gerosa[77a,77b], A. Ghezzi[77a,77b], P. Govoni[77a,77b], L. Guzzi[77a], M.T. Lucchini[77a,77b], M. Malberti[77a], S. Malvezzi[77a], A. Massironi[77a], D. Menasce[77a], L. Moroni[77a], M. Paganoni[77a,77b], S. Palluotto[77a,77b], D. Pedrini[77a], A. Perego[77a,77b], B.S. Pinolini[77a], G. Pizzati[77a,77b], S. Ragazzi[77a,77b], T. Tabarelli de Fatis[77a,77b], S. Buontempo[78a], A. Cagnotta[78a,78b], F. Carnevali[78a,78b], N. Cavallo[78a,78c], F. Fabozzi[78a,78c], A.O.M. Iorio[78a,78b], L. Lista[78a,78b,az], P. Paolucci[78a,ad], B. Rossi[78a], R. Ardino[79a], P. Azzi[79a], N. Bacchetta[79a,ba], A. Bergnoli[79a], D. Bisello[79a,79b], P. Bortignon[79a], G. Bortolato[79a,79b], A. Bragagnolo[79a,79b], A.C.M. Bulla[79a], R. Carlin[79a,79b], P. Checchia[79a], T. Dorigo[79a,bb], F. Gasparini[79a,79b], U. Gasparini[79a,79b], S. Giorgetti[79a], E. Lusiani[79a], M. Margoni[79a,79b], A.T. Meneguzzo[79a,79b], M. Migliorini[79a,79b], J. Pazzini[79a,79b], P. Ronchese[79a,79b], R. Rossin[79a,79b], F. Simonetto[79a,79b], M. Tosi[79a,79b], A. Triossi[79a,79b], M. Zanetti[79a,79b], P. Zotto[79a,79b], A. Zucchetta[79a,79b], G. Zumerle[79a,79b], A. Braghieri[80a], S. Calzaferri[80a], D. Fiorina[80a], P. Montagna[80a,80b], V. Re[80a], C. Riccardi[80a,80b], P. Salvini[80a], I. Vai[80a,80b], P. Vitulo[80a,80b], S. Ajmal[81a,81b], M.E. Ascioti[81a,81b], G.M. Bilei[81a], C. Carrivale[81a,81b], D. Ciangottini[81a,81b], L. Fanò[81a,81b], M. Magherini[81a,81b], V. Mariani[81a,81b], M. Menichelli[81a], F. Moscatelli[81a,bc], A. Rossi[81a,81b], A. Santocchia[81a,81b], D. Spiga[81a], T. Tedeschi[81a,81b], C. Aimè[82a], C.A. Alexe[82a,82c], P. Asenov[82a,82b], P. Azzurri[82a], G. Bagliesi[82a], R. Bhattacharya[82a], L. Bianchini[82a,82b], T. Boccali[82a], E. Bossini[82a], D. Bruschini[82a,82c], R. Castaldi[82a], M.A. Ciocci[82a,82b], M. Cipriani[82a,82b],

JHEP05(2026)186

V. D'Amante[82a,82d], R. Dell'Orso[82a], S. Donato[82a], A. Giassi[82a], F. Ligabue[82a,82c], A.C. Marini[82a,82b], D. Matos Figueiredo[82a], A. Messineo[82a,82b], S. Mishra[82a], V.K. Muraleedharan Nair Bindhu[82a,82b,ao], M. Musich[82a,82b], S. Nandan[82a], F. Palla[82a], A. Rizzi[82a,82b], G. Rolandi[82a,82c], S. Roy Chowdhury[82a], T. Sarkar[82a], A. Scribano[82a], P. Spagnolo[82a], R. Tenchini[82a], G. Tonelli[82a,82b], N. Turini[82a,82d], F. Vaselli[82a,82c], A. Venturi[82a], P.G. Verdini[82a], C. Baldenegro Barrera[83a,83b], P. Barria[83a], C. Basile[83a,83b], F. Cavallari[83a], L. Cunqueiro Mendez[83a,83b], D. Del Re[83a,83b], E. Di Marco[83a,83b], M. Diemoz[83a], F. Errico[83a,83b], R. Gargiulo[83a,83b], E. Longo[83a,83b], L. Martikainen[83a,83b], J. Mijuskovic[83a,83b], G. Organtini[83a,83b], F. Pandolfi[83a], R. Paramatti[83a,83b], C. Quaranta[83a,83b], S. Rahatlou[83a,83b], C. Rovelli[83a], F. Santanastasio[83a,83b], L. Soffi[83a], V. Vladimirov[83a,83b], N. Amapane[84a,84b], R. Arcidiacono[84a,84c], S. Argiro[84a,84b], M. Arneodo[84a,84c], N. Bartosik[84a], R. Bellan[84a,84b], A. Bellora[84a,84b], C. Biino[84a], C. Borca[84a,84b], N. Cartiglia[84a], M. Costa[84a,84b], R. Covarelli[84a,84b], N. Demaria[84a], L. Finco[84a], M. Grippo[84a,84b], B. Kiani[84a,84b], F. Legger[84a], F. Luongo[84a,84b], C. Mariotti[84a], L. Markovic[84a,84b], S. Maselli[84a], A. Mecca[84a,84b], L. Menzio[84a,84b], P. Meridiani[84a], E. Migliore[84a,84b], M. Monteno[84a], R. Mulargia[84a], M.M. Obertino[84a,84b], G. Ortona[84a], L. Pacher[84a,84b], N. Pastrone[84a], M. Pelliccioni[84a], M. Ruspa[84a,84c], F. Siviero[84a,84b], V. Sola[84a,84b], A. Solano[84a,84b], A. Staiano[84a], C. Tarricone[84a,84b], D. Trocino[84a], G. Umoret[84a,84b], R. White[84a,84b], J. Babbar[85a,85b], S. Belforte[85a], V. Candelise[85a,85b], M. Casarsa[85a], F. Cossutti[85a], K. De Leo[85a], G. Della Ricca[85a,85b], S. Dogra[86], J. Hong[86], B. Kim[86], J. Kim[86], D. Lee[86], H. Lee[86], S.W. Lee[86], C.S. Moon[86], Y.D. Oh[86], M.S. Ryu[86], S. Sekmen[86], B. Tae[86], Y.C. Yang[86], M.S. Kim[87], G. Bak[88], P. Gwak[88], H. Kim[88], D.H. Moon[88], E. Asilar[89], J. Choi[89,bd], D. Kim[89], T.J. Kim[89], J.A. Merlin[89], Y. Ryou[89], S. Choi[90], S. Han[90], B. Hong[90], K. Lee[90], K.S. Lee[90], S. Lee[90], J. Yoo[90], J. Goh[91], S. Yang[91], H. S. Kim[92], Y. Kim[92], S. Lee[92], J. Almond[93], J.H. Bhyun[93], J. Choi[93], J. Choi[93], W. Jun[93], J. Kim[93], Y.W. Kim[93], S. Ko[93], H. Kwon[93], H. Lee[93], J. Lee[93], J. Lee[93], B.H. Oh[93], S.B. Oh[93], H. Seo[93], U.K. Yang[93], I. Yoon[93], W. Jang[94], D.Y. Kang[94], Y. Kang[94], S. Kim[94], B. Ko[94], J.S.H. Lee[94], Y. Lee[94], I.C. Park[94], Y. Roh[94], I.J. Watson[94], S. Ha[95], K. Hwang[95], H.D. Yoo[95], M. Choi[96], M.R. Kim[96], H. Lee[96], Y. Lee[96], I. Yu[96], T. Beyrouthy[97], Y. Gharbia[97], F. Alazemi[98], K. Dreimanis[99], A. Gaile[99], C. Munoz Diaz[99], D. Osite[99], G. Pikurs[99], A. Potrebko[99], M. Seidel[99], D. Sidiropoulos Kontos[99], N.R. Strautnieks[100], M. Ambrozas[101], A. Juodagalvis[101], A. Rinkevicius[101], G. Tamulaitis[101], I. Yusuff[102,be], Z. Zolkapli[102], J.F. Benitez[103], A. Castaneda Hernandez[103], H.A. Encinas Acosta[103], L.G. Gallegos Maríñez[103], M. León Coello[103], J.A. Murillo Quijada[103], A. Sehrawat[103], L. Valencia Palomo[103], G. Ayala[104], H. Castilla-Valdez[104], H. Crotte Ledesma[104], E. De La Cruz-Burelo[104], I. Heredia-De La Cruz[104,bf], R. Lopez-Fernandez[104], J. Mejia Guisao[104], C.A. Mondragon Herrera[104], A. Sánchez Hernández[104], C. Oropeza Barrera[105], D.L. Ramirez Guadarrama[105], M. Ramírez García[105], I. Bautista[106], F.E. Neri Huerta[106], I. Pedraza[106], H.A. Salazar Ibarguen[106], C. Uribe Estrada[106], I. Bubanja[107], N. Raicevic[107], P.H. Butler[108], A. Ahmad[109], M.I. Asghar[109], A. Awais[109], M.I.M. Awan[109], H.R. Hoorani[109], W.A. Khan[109], V. Avati[110], L. Grzanka[110], M. Malawski[110], H. Bialkowska[111], M. Bluj[111], M. Górski[111], M. Kazana[111], M. Szleper[111],

JHEP05(2026)186

P. Zalewski[111], K. Bunkowski[112], K. Doroba[112], A. Kalinowski[112], M. Konecki[112], J. Krolikowski[112], A. Muhammad[112], P. Fokow[113], K. Pozniak[113], W. Zabolotny[113], M. Araujo[114], D. Bastos[114], C. Beirão Da Cruz E Silva[114], A. Boletti[114], M. Bozzo[114], T. Camporesi[114], G. Da Molin[114], P. Faccioli[114], M. Gallinaro[114], J. Hollar[114], N. Leonardo[114], G.B. Marozzo[114], A. Petrilli[114], M. Pisano[114], J. Seixas[114], J. Varela[114], J.W. Wulff[114], P. Adzic[115], P. Milenovic[115], D. Devetak[116], M. Dordevic[116], J. Milosevic[116], L. Nadderd[116], V. Rekovic[116], J. Alcaraz Maestre[117], J.A. Brochero Cifuentes[117], M. Cepeda[117], M. Cerrada[117], N. Colino[117], B. De La Cruz[117], A. Delgado Peris[117], A. Escalante Del Valle[117], Cristina F. Bedoya[117], D. Fernández Del Val[117], J.P. Fernández Ramos[117], J. Flix[117], M.C. Fouz[117], O. Gonzalez Lopez[117], S. Goy Lopez[117], J.M. Hernandez[117], M.I. Josa[117], J. Llorente Merino[117], Oliver M. Carretero[117], C. Martin Perez[117], E. Martin Viscasillas[117], D. Moran[117], C. M. Morcillo Perez[117], Á. Navarro Tobar[117], C. Perez Dengra[117], J. Puerta Pelayo[117], A. Pérez-Calero Yzquierdo[117], I. Redondo[117], J. Sastre[117], S. Sánchez Navas[117], J. Vazquez Escobar[117], J.F. de Trocóniz[118], B. Alvarez Gonzalez[119], J. Cuevas[119], J. Fernandez Menendez[119], S. Folgueras[119], I. Gonzalez Caballero[119], P. Leguina[119], E. Palencia Cortezon[119], J. Prado Pico[119], C. Ramón Álvarez[119], V. Rodríguez Bouza[119], A. Soto Rodríguez[119], A. Trapote[119], C. Vico Villalba[119], P. Vischia[119], S. Bhowmik[120], S. Blanco Fernández[120], I.J. Cabrillo[120], A. Calderon[120], J. Duarte Campderros[120], M. Fernandez[120], G. Gomez[120], C. Lasaosa García[120], R. Lopez Ruiz[120], C. Martinez Rivero[120], P. Martinez Ruiz del Arbol[120], F. Matorras[120], P. Matorras Cuevas[120], E. Navarrete Ramos[120], J. Piedra Gomez[120], L. Scodellaro[120], I. Vila[120], J.M. Vizan Garcia[120], D.D.C. Wickramarathna[121], B. Kailasapathy[121,bg], W.G.D. Dharmaratna[122,bh], K. Liyanage[122], N. Perera[122], D. Abbaneo[123], C. Amendola[123], E. Auffray[123], G. Auzinger[123], J. Baechler[123], D. Barney[123], A. Bermúdez Martínez[123], M. Bianco[123], A.A. Bin Anuar[123], A. Bocci[123], L. Borgonovi[123], C. Botta[123], E. Brondolin[123], C.E. Brown[123], C. Caillol[123], G. Cerminara[123], N. Chernyavskaya[123], D. d'Enterria[123], A. Dabrowski[123], A. David[123], A. De Roeck[123], M.M. Defranchis[123], M. Deile[123], M. Dobson[123], G. Franzoni[123], W. Funk[123], S. Giani[123], D. Gigi[123], K. Gill[123], F. Glege[123], J. Hegeman[123], J.K. Heikkilä[123], B. Huber[123], V. Innocente[123], T. James[123], P. Janot[123], O. Kaluzinska[123], O. Karacheban[123,aa], S. Laurila[123], P. Lecoq[123], E. Leutgeb[123], C. Lourenço[123], L. Malgeri[123], M. Mannelli[123], M. Matthewman[123], A. Mehta[123], F. Meijers[123], S. Mersi[123], E. Meschi[123], V. Milosevic[123], F. Monti[123], F. Moortgat[123], M. Mulders[123], I. Neutelings[123], S. Orfanelli[123], F. Pantaleo[123], G. Petrucciani[123], A. Pfeiffer[123], M. Pierini[123], H. Qu[123], D. Rabady[123], B. Ribeiro Lopes[123], F. Riti[123], M. Rovere[123], H. Sakulin[123], R. Salvatico[123], S. Sanchez Cruz[123], S. Scarfi[123], M. Selvaggi[123], A. Sharma[123], K. Shchelina[123], P. Silva[123], P. Sphicas[123,bi], A.G. Stahl Leiton[123], A. Steen[123], S. Summers[123], D. Treille[123], P. Tropea[123], D. Walter[123], J. Wanczyk[123,bj], J. Wang[123], S. Wuchterl[123], P. Zehetner[123], P. Zejdl[123], W.D. Zeuner[123], T. Bevilacqua[124,bk], L. Caminada[124,bk], A. Ebrahimi[124], W. Erdmann[124], R. Horisberger[124], Q. Ingram[124], H.C. Kaestli[124], D. Kotlinski[124], C. Lange[124], M. Missiroli[124,bk], L. Noehte[124,bk], T. Rohe[124], A. Samalan[124], T.K. Aarrestad[125], M. Backhaus[125], G. Bonomelli[125], A. Calandri[125],

JHEP05(2026)186

C. Cazzaniga[125], K. Datta[125], P. De Bryas Dexmiers D'archiac[125,bj], A. De Cosa[125], G. Dissertori[125], M. Dittmar[125], M. Donegà[125], F. Eble[125], M. Galli[125], K. Gedia[125], F. Glessgen[125], C. Grab[125], T.G. Harte[125], D. Hits[125], N. Härringer[125], W. Lustermann[125], A.-M. Lyon[125], R.A. Manzoni[125], M. Marchegiani[125], L. Marchese[125], A. Mascellani[125,bj], F. Nessi-Tedaldi[125], F. Pauss[125], V. Perovic[125], S. Pigazzini[125], B. Ristic[125], R. Seidita[125], J. Steggemann[125,bj], A. Tarabini[125], D. Valsecchi[125], R. Wallny[125], C. Amsler[126,bl], P. Bärtschi[126], M.F. Canelli[126], K. Cormier[126], M. Huwiler[126], W. Jin[126], A. Jofrehei[126], B. Kilminster[126], S. Leontsinis[126], S.P. Liechti[126], A. Macchiolo[126], P. Meiring[126], F. Meng[126], J. Motta[126], A. Reimers[126], P. Robmann[126], M. Senger[126], E. Shokr[126], F. Stäger[126], R. Tramontano[126], C. Adloff[127,bm], D. Bhowmik[127], C.M. Kuo[127], W. Lin[127], P.K. Rout[127], P.C. Tiwari[127,al], L. Ceard[128], K.F. Chen[128], Z.g. Chen[128], A. De Iorio[128], W.-S. Hou[128], T.h. Hsu[128], Y.w. Kao[128], S. Karmakar[128], G. Kole[128], Y.y. Li[128], R.-S. Lu[128], E. Paganis[128], X.f. Su[128], J. Thomas-Wilsker[128], L.s. Tsai[128], D. Tsionou[128], H.y. Wu[128], E. Yazgan[128], C. Asawatangtrakuldee[129], N. Srimanobhas[129], V. Wachirapusitanand[129], Y. Maghrbi[130], D. Agyel[131], F. Boran[131], F. Dolek[131], I. Dumanoglu[131,bn], E. Eskut[131], Y. Guler[131,bo], E. Gurpinar Guler[131,bo], C. Isik[131], O. Kara[131], A. Kayis Topaksu[131], Y. Komurcu[131], G. Onengut[131], K. Ozdemir[131,bp], A. Polatoz[131], B. Tali[131,bq], U.G. Tok[131], E. Uslan[131], I.S. Zorbakir[131], G. Sokmen[132], M. Yalvac[132,br], B. Akgun[133], I.O. Atakisi[133], E. Gülmez[133], M. Kaya[133,bs], O. Kaya[133,bt], S. Tekten[133,bu], A. Cakir[134], K. Cankocak[134,bn,bv], G.G. Dincer[134,bn], S. Sen[134,bw], O. Aydilek[135,bx], B. Hacisahinoglu[135], I. Hos[135,by], B. Kaynak[135], S. Ozkorucuklu[135], O. Potok[135], H. Sert[135], C. Simsek[135], C. Zorbilmez[135], S. Cerci[136], B. Isildak[136,bz], D. Sunar Cerci[136], T. Yetkin[136], A. Boyaryntsev[137], B. Grynyov[137], L. Levchuk[138], D. Anthony[139], J.J. Brooke[139], A. Bundock[139], F. Bury[139], E. Clement[139], D. Cussans[139], H. Flacher[139], M. Glowacki[139], J. Goldstein[139], H.F. Heath[139], M.-L. Holmberg[139], L. Kreczko[139], S. Paramesvaran[139], L. Robertshaw[139], V.J. Smith[139], K. Walkingshaw Pass[139], A.H. Ball[140], K.W. Bell[140], A. Belyaev[140,ca], C. Brew[140], R.M. Brown[140], D.J.A. Cockerill[140], C. Cooke[140], A. Elliot[140], K.V. Ellis[140], K. Harder[140], S. Harper[140], J. Linacre[140], K. Manolopoulos[140], D.M. Newbold[140], E. Olaiya[140], D. Petyt[140], T. Reis[140], A.R. Sahasransu[140], G. Salvi[140], T. Schuh[140], C.H. Shepherd-Themistocleous[140], I.R. Tomalin[140], K.C. Whalen[140], T. Williams[140], I. Andreou[141], R. Bainbridge[141], P. Bloch[141], O. Buchmuller[141], C.A. Carrillo Montoya[141], G.S. Chahal[141,cb], D. Colling[141], J.S. Dancu[141], I. Das[141], P. Dauncey[141], G. Davies[141], M. Della Negra[141], S. Fayer[141], G. Fedi[141], G. Hall[141], A. Howard[141], G. Iles[141], C.R. Knight[141], P. Krueper[141], J. Langford[141], K.H. Law[141], J. León Holgado[141], L. Lyons[141], A.-M. Magnan[141], B. Maier[141], S. Mallios[141], M. Mieskolainen[141], J. Nash[141,cc], M. Pesaresi[141], P.B. Pradeep[141], B.C. Radburn-Smith[141], A. Richards[141], A. Rose[141], K. Savva[141], C. Seez[141], R. Shukla[141], A. Tapper[141], K. Uchida[141], G.P. Uttley[141], T. Virdee[141,ad], M. Vojinovic[141], N. Wardle[141], D. Winterbottom[141], J.E. Cole[142], A. Khan[142], P. Kyberd[142], I.D. Reid[142], S. Abdullin[143], A. Brinkerhoff[143], E. Collins[143], M.R. Darwish[143], J. Dittmann[143], K. Hatakeyama[143], V. Hegde[143], J. Hiltbrand[143], B. McMaster[143], J. Samudio[143], S. Sawant[143], C. Sutantawibul[143], J. Wilson[143], R. Bartek[144], A. Dominguez[144], A.E. Simsek[144], S.S. Yu[144], B. Bam[145],

JHEP05(2026)186

A. Buchot Perraguin[145], R. Chudasama[145], S.I. Cooper[145], C. Crovella[145], S.V. Gleyzer[145], E. Pearson[145], C.U. Perez[145], P. Rumerio[145,cd], E. Usai[145], R. Yi[145], A. Akpinar[146], C. Cosby[146], G. De Castro[146], Z. Demiragli[146], C. Erice[146], C. Fangmeier[146], C. Fernandez Madrazo[146], E. Fontanesi[146], D. Gastler[146], F. Golf[146], S. Jeon[146], J. O'cain[146], I. Reed[146], J. Rohlf[146], K. Salyer[146], D. Sperka[146], D. Spitzbart[146], I. Suarez[146], A. Tsatsos[146], A.G. Zecchinelli[146], G. Barone[147], G. Benelli[147], D. Cutts[147], L. Gouskos[147], M. Hadley[147], U. Heintz[147], K.W. Ho[147], J.M. Hogan[147,ce], T. Kwon[147], G. Landsberg[147], K.T. Lau[147], J. Luo[147], S. Mondal[147], T. Russell[147], S. Sagir[147,cf], X. Shen[147], F. Simpson[147], M. Stamenkovic[147], N. Venkatasubramanian[147], S. Abbott[148], B. Barton[148], C. Brainerd[148], R. Breedon[148], H. Cai[148], M. Calderon De La Barca Sanchez[148], M. Chertok[148], M. Citron[148], J. Conway[148], P.T. Cox[148], R. Erbacher[148], F. Jensen[148], O. Kukral[148], G. Mocellin[148], M. Mulhearn[148], S. Ostrom[148], W. Wei[148], S. Yoo[148], F. Zhang[148], K. Adamidis[149], M. Bachtis[149], D. Campos[149], R. Cousins[149], A. Datta[149], G. Flores Avila[149], J. Hauser[149], M. Ignatenko[149], M.A. Iqbal[149], T. Lam[149], Y.f. Lo[149], E. Manca[149], A. Nunez Del Prado[149], D. Saltzberg[149], V. Valuev[149], R. Clare[150], J.W. Gary[150], G. Hanson[150], A. Aportela[151], A. Arora[151], J.G. Branson[151], S. Cittolin[151], S. Cooperstein[151], D. Diaz[151], J. Duarte[151], L. Giannini[151], Y. Gu[151], J. Guiang[151], R. Kansal[151], V. Krutelyov[151], R. Lee[151], J. Letts[151], M. Masciovecchio[151], F. Mokhtar[151], S. Mukherjee[151], M. Pieri[151], D. Primosch[151], M. Quinnan[151], V. Sharma[151], M. Tadel[151], E. Vourliotis[151], F. Würthwein[151], Y. Xiang[151], A. Yagil[151], A. Barzdukas[152], L. Brennan[152], C. Campagnari[152], K. Downham[152], C. Grieco[152], M.M. Hussain[152], J. Incandela[152], J. Kim[152], A.J. Li[152], P. Masterson[152], H. Mei[152], J. Richman[152], S.N. Santpur[152], U. Sarica[152], R. Schmitz[152], F. Setti[152], J. Sheplock[152], D. Stuart[152], T.Á. Vámi[152], X. Yan[152], D. Zhang[152], S. Bhattacharya[153], A. Bornheim[153], O. Cerri[153], A. Latorre[153], J. Mao[153], H.B. Newman[153], G. Reales Gutiérrez[153], M. Spiropulu[153], J.R. Vlimant[153], C. Wang[153], S. Xie[153], R.Y. Zhu[153], J. Alison[154], S. An[154], P. Bryant[154], M. Cremonesi[154], V. Dutta[154], T. Ferguson[154], T.A. Gómez Espinosa[154], A. Harilal[154], A. Kallil Tharayil[154], C. Liu[154], T. Mudholkar[154], S. Murthy[154], P. Palit[154], K. Park[154], M. Paulini[154], A. Roberts[154], A. Sanchez[154], W. Terrill[154], J.P. Cumalat[155], W.T. Ford[155], A. Hart[155], A. Hassani[155], G. Karathanasis[155], N. Manganelli[155], J. Pearkes[155], C. Savard[155], N. Schonbeck[155], K. Stenson[155], K.A. Ulmer[155], S.R. Wagner[155], N. Zipper[155], D. Zuolo[155], J. Alexander[156], S. Bright-Thonney[156], X. Chen[156], D.J. Cranshaw[156], J. Dickinson[156], J. Fan[156], X. Fan[156], S. Hogan[156], P. Kotamnives[156], J. Monroy[156], M. Oshiro[156], J.R. Patterson[156], M. Reid[156], A. Ryd[156], J. Thom[156], P. Wittich[156], R. Zou[156], M. Albrow[157], M. Alyari[157], O. Amram[157], G. Apollinari[157], A. Apresyan[157], L.A.T. Bauerdick[157], D. Berry[157], J. Berryhill[157], P.C. Bhat[157], K. Burkett[157], J.N. Butler[157], A. Canepa[157], G.B. Cerati[157], H.W.K. Cheung[157], F. Chlebana[157], G. Cummings[157], I. Dutta[157], V.D. Elvira[157], Y. Feng[157], J. Freeman[157], A. Gandrakota[157], Z. Gecse[157], L. Gray[157], D. Green[157], A. Grummer[157], S. Grünendahl[157], D. Guerrero[157], O. Gutsche[157], R.M. Harris[157], T.C. Herwig[157], J. Hirschauer[157], B. Jayatilaka[157], S. Jindariani[157], M. Johnson[157], U. Joshi[157], T. Klijnsma[157], B. Klima[157], K.H.M. Kwok[157], S. Lammel[157], C. Lee[157],

JHEP05(2026)186

D. Lincoln[157], R. Lipton[157], T. Liu[157], C. Madrid[157], K. Maeshima[157], D. Mason[157], P. McBride[157], P. Merkel[157], S. Mrenna[157], S. Nahn[157], J. Ngadiuba[157], D. Noonan[157], S. Norberg[157], V. Papadimitriou[157], N. Pastika[157], K. Pedro[157], C. Pena[157,cg], F. Ravera[157], A. Reinsvold Hall[157,ch], L. Ristori[157], M. Safdari[157], E. Sexton-Kennedy[157], N. Smith[157], A. Soha[157], L. Spiegel[157], S. Stoynev[157], J. Strait[157], L. Taylor[157], S. Tkaczyk[157], N.V. Tran[157], L. Uplegger[157], E.W. Vaandering[157], I. Zoi[157], C. Aruta[158], P. Avery[158], D. Bourilkov[158], P. Chang[158], V. Cherepanov[158], R.D. Field[158], C. Huh[158], E. Koenig[158], M. Kolosova[158], J. Konigsberg[158], A. Korytov[158], K. Matchev[158], N. Menendez[158], G. Mitselmakher[158], K. Mohrman[158], A. Muthirakalayil Madhu[158], N. Rawal[158], S. Rosenzweig[158], Y. Takahashi[158], J. Wang[158], T. Adams[159], A. Al Kadhim[159], A. Askew[159], S. Bower[159], R. Hashmi[159], R.S. Kim[159], S. Kim[159], T. Kolberg[159], G. Martinez[159], H. Prosper[159], P.R. Prova[159], M. Wulansatiti[159], R. Yohay[159], J. Zhang[159], B. Alsufyani[160], S. Butalla[160], S. Das[160], T. Elkafrawy[160,ci], M. Hohlmann[160], E. Yanes[160], M.R. Adams[161], A. Baty[161], C. Bennett[161], R. Cavanaugh[161], D. S. Lemos[161], R. Escobar Franco[161], O. Evdokimov[161], C.E. Gerber[161], M. Hawksworth[161], A. Hingrajiya[161], D.J. Hofman[161], J.h. Lee[161], A.H. Merrit[161], C. Mills[161], S. Nanda[161], G. Oh[161], B. Ozek[161], D. Pilipovic[161], R. Pradhan[161], E. Prifti[161], T. Roy[161], S. Rudrabhatla[161], N. Singh[161], M.B. Tonjes[161], N. Varelas[161], M.A. Wadud[161], Z. Ye[161], J. Yoo[161], M. Alhusseini[162], D. Blend[162], K. Dilsiz[162,cj], L. Emediato[162], G. Karaman[162], O.K. Köseyan[162], J.-P. Merlo[162], A. Mestvirishvili[162,ck], O. Neogi[162], H. Ogul[162,cl], Y. Onel[162], A. Penzo[162], C. Snyder[162], E. Tiras[162,cm], B. Blumenfeld[163], L. Corcodilos[163], J. Davis[163], A.V. Gritsan[163], L. Kang[163], S. Kyriacou[163], P. Maksimovic[163], M. Roguljic[163], J. Roskes[163], S. Sekhar[163], M. Swartz[163], A. Abreu[164], L.F. Alcerro Alcerro[164], J. Anguiano[164], S. Arteaga Escatel[164], P. Baringer[164], A. Bean[164], Z. Flowers[164], D. Grove[164], J. King[164], G. Krintiras[164], M. Lazarovits[164], C. Le Mahieu[164], J. Marquez[164], M. Murray[164], M. Nickel[164], M. Pitt[164], S. Popescu[164,cn], C. Rogan[164], C. Royon[164], S. Sanders[164], C. Smith[164], G. Wilson[164], B. Allmond[165], A. Ivanov[165], K. Kaadze[165], Y. Maravin[165], J. Natoli[165], R. Gujju Gurunadha[165], D. Roy[165], G. Sorrentino[165], A. Baden[166], A. Belloni[166], J. Bistany-riebman[166], Y.M. Chen[166], S.C. Eno[166], N.J. Hadley[166], S. Jabeen[166], R.G. Kellogg[166], T. Koeth[166], B. Kronheim[166], Y. Lai[166], S. Lascio[166], A.C. Mignerey[166], S. Nabili[166], C. Palmer[166], C. Papageorgakis[166], M.M. Paranjpe[166], E. Popova[166,co], A. Shevelev[166], L. Wang[166], J. Bendavid[167], I.A. Cali[167], P.c. Chou[167], M. D'Alfonso[167], J. Eysermans[167], C. Freer[167], G. Gomez-Ceballos[167], M. Goncharov[167], G. Grosso[167], P. Harris[167], D. Hoang[167], D. Kovalskyi[167], J. Krupa[167], L. Lavezzo[167], Y.-J. Lee[167], K. Long[167], C. Mcginn[167], A. Novak[167], M.I. Park[167], C. Paus[167], C. Reissel[167], C. Roland[167], G. Roland[167], S. Rothman[167], G.S.F. Stephans[167], Z. Wang[167], B. Wyslouch[167], T. J. Yang[167], B. Crossman[168], B.M. Joshi[168], C. Kapsiak[168], M. Krohn[168], D. Mahon[168], J. Mans[168], B. Marzocchi[168], M. Revering[168], R. Rusack[168], R. Saradhy[168], N. Strobbe[168], K. Bloom[169], D.R. Claes[169], G. Haza[169], J. Hossain[169], C. Joo[169], I. Kravchenko[169], A. Rohilla[169], J.E. Siado[169], W. Tabb[169], A. Vagnerini[169], A. Wightman[169], F. Yan[169], D. Yu[169], H. Bandyopadhyay[170], L. Hay[170], H.w. Hsia[170], I. Iashvili[170], A. Kalogeropoulos[170], A. Kharchilava[170], M. Morris[170], D. Nguyen[170],

JHEP05(2026)186

S. Rappoccio[170], H. Rejeb Sfar[170], A. Williams[170], P. Young[170], G. Alverson[171], E. Barberis[171], J. Bonilla[171], B. Bylsma[171], M. Campana[171], J. Dervan[171], Y. Haddad[171], Y. Han[171], I. Israr[171], A. Krishna[171], J. Li[171], M. Lu[171], R. Mccarthy[171], D.M. Morse[171], V. Nguyen[171], T. Orimoto[171], A. Parker[171], L. Skinnari[171], E. Tsai[171], D. Wood[171], J. Bueghly[172], S. Dittmer[172], K.A. Hahn[172], D. Li[172], Y. Liu[172], M. Mcginnis[172], Y. Miao[172], D.G. Monk[172], M.H. Schmitt[172], A. Taliercio[172], M. Velasco[172], G. Agarwal[173], R. Band[173], R. Bucci[173], S. Castells[173], A. Das[173], R. Goldouzian[173], M. Hildreth[173], K. Hurtado Anampa[173], T. Ivanov[173], C. Jessop[173], K. Lannon[173], J. Lawrence[173], N. Loukas[173], L. Lutton[173], J. Mariano[173], N. Marinelli[173], I. Mcalister[173], T. McCauley[173], C. Mcgrady[173], C. Moore[173], Y. Musienko[173,o], H. Nelson[173], M. Osherson[173], A. Piccinelli[173], R. Ruchti[173], A. Townsend[173], Y. Wan[173], M. Wayne[173], H. Yockey[173], M. Zarucki[173], L. Zygala[173], A. Basnet[174], M. Carrigan[174], L.S. Durkin[174], C. Hill[174], M. Joyce[174], M. Nunez Ornelas[174], K. Wei[174], D.A. Wenzl[174], B.L. Winer[174], B. R. Yates[174], H. Bouchamaoui[175], K. Coldham[175], P. Das[175], G. Dezoort[175], P. Elmer[175], A. Frankenthal[175], B. Greenberg[175], N. Haubrich[175], K. Kennedy[175], G. Kopp[175], S. Kwan[175], D. Lange[175], A. Loeliger[175], D. Marlow[175], I. Ojalvo[175], J. Olsen[175], D. Stickland[175], C. Tully[175], L.H. Vage[175], S. Malik[176], R. Sharma[176], A.S. Bakshi[177], S. Chandra[177], R. Chawla[177], A. Gu[177], L. Gutay[177], M. Jones[177], A.W. Jung[177], A. K. Virdi[177], A.M. Koshy[177], M. Liu[177], G. Negro[177], N. Neumeister[177], G. Paspalaki[177], S. Piperov[177], V. Scheurer[177], J.F. Schulte[177], M. Stojanovic[177], J. Thieman[177], F. Wang[177], A. Wildridge[177], W. Xie[177], Y. Yao[177], J. Dolen[178], N. Parashar[178], A. Pathak[178], D. Acosta[179], A. Agrawal[179], T. Carnahan[179], K.M. Ecklund[179], P.J. Fernández Manteca[179], S. Freed[179], P. Gardner[179], F.J.M. Geurts[179], I. Krommydas[179], W. Li[179], J. Lin[179], O. Miguel Colin[179], B.P. Padley[179], R. Redjimi[179], J. Rotter[179], E. Yigitbasi[179], Y. Zhang[179], A. Bodek[180], P. de Barbaro[180], R. Demina[180], J.L. Dulemba[180], A. Garcia-Bellido[180], O. Hindrichs[180], A. Khukhunaishvili[180], N. Parmar[180], P. Parygin[180,co], R. Taus[180], B. Chiarito[181], J.P. Chou[181], S.V. Clark[181], D. Gadkari[181], Y. Gershtein[181], E. Halkiadakis[181], C. Houghton[181], D. Jaroslawski[181], S. Konstantinou[181], I. Laflotte[181], A. Lath[181], R. Montalvo[181], K. Nash[181], M. Heindl[181], J. Reichert[181], P. Saha[181], S. Salur[181], S. Schnetzer[181], S. Somalwar[181], R. Stone[181], S.A. Thayil[181], S. Thomas[181], J. Vora[181], H. Wang[181], D. Ally[182], A.G. Delannoy[182], S. Fiorendi[182], S. Higginbotham[182], T. Holmes[182], A.R. Kanuganti[182], N. Karunarathna[182], L. Lee[182], E. Nibigira[182], S. Spanier[182], D. Aebi[183], M. Ahmad[183], T. Akhter[183], K. Androsov[183,bj], O. Bouhali[183,cp], R. Eusebi[183], J. Gilmore[183], T. Huang[183], T. Kamon[183,cq], H. Kim[183], S. Luo[183], R. Mueller[183], D. Overton[183], D. Rathjens[183], A. Safonov[183], N. Akchurin[184], J. Damgov[184], N. Gogate[184], A. Hussain[184], Y. Kazhykarim[184], K. Lamichhane[184], S.W. Lee[184], A. Mankel[184], T. Peltola[184], I. Volobouev[184], E. Appelt[185], Y. Chen[185], S. Greene[185], A. Gurrola[185], W. Johns[185], R. Kunnawalkam Elayavalli[185], A. Melo[185], F. Romeo[185], P. Sheldon[185], S. Tuo[185], J. Velkovska[185], J. Viinikainen[185], B. Cardwell[186], H. Chung[186], B. Cox[186], J. Hakala[186], R. Hirosky[186], A. Ledovskoy[186], C. Mantilla[186], C. Neu[186], S. Bhattacharya[187], P.E. Karchin[187], A. Aravind[188], S. Banerjee[188], K. Black[188], T. Bose[188], E. Chavez[188], S. Dasu[188], P. Everaerts[188],

JHEP05(2026)186

C. Galloni[188], H. He[188], M. Herndon[188], A. Herve[188], C.K. Koraka[188], A. Lanaro[188], R. Loveless[188], J. Madhusudanan Sreekala[188], A. Mallampalli[188], A. Mohammadi[188], S. Mondal[188], G. Parida[188], D. Pinna[188], L. Pétré[188], A. Savin[188], V. Shang[188], V. Sharma[188], W.H. Smith[188], D. Teague[188], H.F. Tsoi[188], W. Vetens[188], A. Warden[188], S. Afanasiev[189], V. Alexakhin[189], D. Budkouski[189], I. Golutvin[189,†], I. Gorbunov[189], V. Karjavine[189], V. Korenkov[189], A. Lanev[189], A. Malakhov[189], V. Matveev[189,o], V. Palichik[189], V. Perelygin[189], M. Savina[189], V. Shalaev[189], S. Shmatov[189], S. Shulha[189], V. Smirnov[189], O. Teryaev[189], N. Voytishin[189], B.S. Yuldashev[189,cr], A. Zarubin[189], I. Zhizhin[189], Yu. Andreev[190], V. Andreev[190], T. Aushev[190], M. Azarkin[190], A. Babaev[190], V. Blinov[190,o], E. Boos[190], V. Borshch[190], V. Bunichev[190], R. Chistov[190,o], M. Danilov[190,o], A. Dermenev[190], T. Dimova[190,o], D. Druzhkin[190], M. Dubinin[190,cg], L. Dudko[190], A. Ershov[190], G. Gavrilov[190], V. Gavrilov[190], S. Gninenko[190], V. Golovtcov[190], N. Golubev[190], Y. Ivanov[190], K. Ivanov[190], V. Kachanov[190], A. Karneyeu[190], V. Kim[190,o], M. Kirakosyan[190], D. Kirpichnikov[190], M. Kirsanov[190], V. Klyukhin[190], O. Kodolova[190,cs], A. Kozyrev[190,o], N. Krasnikov[190], P. Levchenko[190,ct], N. Lychkovskaya[190], V. Murzin[190], A. Nikitenko[190,cu,cv], S. Obraztsov[190], V. Oreshkin[190], M. Perfilov[190], S. Petrushanko[190], S. Polikarpov[190,o], V. Popov[190], O. Radchenko[190,o], V. Savrin[190], Y. Skovpen[190,o], S. Slabospitskii[190], D. Sosnov[190], V. Sulimov[190], A. Terkulov[190], I. Tlisova[190], A. Toropin[190], L. Uvarov[190], A. Uzunian[190], A. Vorobyev[190,†], G. Vorotnikov[190], A. Zhokin[190]

[1] *Yerevan Physics Institute, Yerevan, Armenia*
[2] *Institut für Hochenergiephysik, Vienna, Austria*
[3] *Universiteit Antwerpen, Antwerpen, Belgium*
[4] *Vrije Universiteit Brussel, Brussel, Belgium*
[5] *Université Libre de Bruxelles, Bruxelles, Belgium*
[6] *Ghent University, Ghent, Belgium*
[7] *Université Catholique de Louvain, Louvain-la-Neuve, Belgium*
[8] *Centro Brasileiro de Pesquisas Fisicas, Rio de Janeiro, Brazil*
[9] *Universidade do Estado do Rio de Janeiro, Rio de Janeiro, Brazil*
[10] *Universidade Estadual Paulista, Universidade Federal do ABC, São Paulo, Brazil*
[11] *Institute for Nuclear Research and Nuclear Energy, Bulgarian Academy of Sciences, Sofia, Bulgaria*
[12] *University of Sofia, Sofia, Bulgaria*
[13] *Instituto De Alta Investigación, Universidad de Tarapacá, Casilla 7 D, Arica, Chile*
[14] *Beihang University, Beijing, China*
[15] *Department of Physics, Tsinghua University, Beijing, China*
[16] *Institute of High Energy Physics, Beijing, China*
[17] *State Key Laboratory of Nuclear Physics and Technology, Peking University, Beijing, China*
[18] *State Key Laboratory of Nuclear Physics and Technology, Institute of Quantum Matter, South China Normal University, Guangzhou, China*
[19] *Sun Yat-Sen University, Guangzhou, China*
[20] *University of Science and Technology of China, Hefei, China*
[21] *Nanjing Normal University, Nanjing, China*
[22] *Institute of Modern Physics and Key Laboratory of Nuclear Physics and Ion-beam Application (MOE) – Fudan University, Shanghai, China*
[23] *Zhejiang University, Hangzhou, Zhejiang, China*
[24] *Universidad de Los Andes, Bogota, Colombia*
[25] *Universidad de Antioquia, Medellin, Colombia*

JHEP05(2026)186

[26] University of Split, Faculty of Electrical Engineering, Mechanical Engineering and Naval Architecture, Split, Croatia
[27] University of Split, Faculty of Science, Split, Croatia
[28] Institute Rudjer Boskovic, Zagreb, Croatia
[29] University of Cyprus, Nicosia, Cyprus
[30] Charles University, Prague, Czech Republic
[31] Escuela Politecnica Nacional, Quito, Ecuador
[32] Universidad San Francisco de Quito, Quito, Ecuador
[33] Academy of Scientific Research and Technology of the Arab Republic of Egypt, Egyptian Network of High Energy Physics, Cairo, Egypt
[34] Center for High Energy Physics (CHEP-FU), Fayoum University, El-Fayoum, Egypt
[35] National Institute of Chemical Physics and Biophysics, Tallinn, Estonia
[36] Department of Physics, University of Helsinki, Helsinki, Finland
[37] Helsinki Institute of Physics, Helsinki, Finland
[38] Lappeenranta-Lahti University of Technology, Lappeenranta, Finland
[39] IRFU, CEA, Université Paris-Saclay, Gif-sur-Yvette, France
[40] Laboratoire Leprince-Ringuet, CNRS/IN2P3, Ecole Polytechnique, Institut Polytechnique de Paris, Palaiseau, France
[41] Université de Strasbourg, CNRS, IPHC UMR 7178, Strasbourg, France
[42] Centre de Calcul de l'Institut National de Physique Nucleaire et de Physique des Particules, CNRS/IN2P3, Villeurbanne, France
[43] Institut de Physique des 2 Infinis de Lyon (IP2I), Villeurbanne, France
[44] Georgian Technical University, Tbilisi, Georgia
[45] RWTH Aachen University, I. Physikalisches Institut, Aachen, Germany
[46] RWTH Aachen University, III. Physikalisches Institut A, Aachen, Germany
[47] RWTH Aachen University, III. Physikalisches Institut B, Aachen, Germany
[48] Deutsches Elektronen-Synchrotron, Hamburg, Germany
[49] University of Hamburg, Hamburg, Germany
[50] Karlsruher Institut fuer Technologie, Karlsruhe, Germany
[51] Institute of Nuclear and Particle Physics (INPP), NCSR Demokritos, Aghia Paraskevi, Greece
[52] National and Kapodistrian University of Athens, Athens, Greece
[53] National Technical University of Athens, Athens, Greece
[54] University of Ioánnina, Ioánnina, Greece
[55] HUN-REN Wigner Research Centre for Physics, Budapest, Hungary
[56] MTA-ELTE Lendület CMS Particle and Nuclear Physics Group, Eötvös Loránd University, Budapest, Hungary
[57] Faculty of Informatics, University of Debrecen, Debrecen, Hungary
[58] HUN-REN ATOMKI – Institute of Nuclear Research, Debrecen, Hungary
[59] Karoly Robert Campus, MATE Institute of Technology, Gyongyos, Hungary
[60] Panjab University, Chandigarh, India
[61] University of Delhi, Delhi, India
[62] Saha Institute of Nuclear Physics, HBNI, Kolkata, India
[63] Indian Institute of Technology Madras, Madras, India
[64] Tata Institute of Fundamental Research-A, Mumbai, India
[65] Tata Institute of Fundamental Research-B, Mumbai, India
[66] National Institute of Science Education and Research, An OCC of Homi Bhabha National Institute, Bhubaneswar, Odisha, India
[67] Indian Institute of Science Education and Research (IISER), Pune, India
[68] Isfahan University of Technology, Isfahan, Iran
[69] Institute for Research in Fundamental Sciences (IPM), Tehran, Iran
[70] University College Dublin, Dublin, Ireland
[71a] INFN Sezione di Bari, Bari, Italy
[71b] Università di Bari, Bari, Italy

JHEP05(2026)186

[71c] *Politecnico di Bari, Bari, Italy*
[72a] *INFN Sezione di Bologna, Bologna, Italy*
[72b] *Università di Bologna, Bologna, Italy*
[73a] *INFN Sezione di Catania, Catania, Italy*
[73b] *Università di Catania, Catania, Italy*
[74a] *INFN Sezione di Firenze, Firenze, Italy*
[74b] *Università di Firenze, Firenze, Italy*
[75] *INFN Laboratori Nazionali di Frascati, Frascati, Italy*
[76a] *INFN Sezione di Genova, Genova, Italy*
[76b] *Università di Genova, Genova, Italy*
[77a] *INFN Sezione di Milano-Bicocca, Milano, Italy*
[77b] *Università di Milano-Bicocca, Milano, Italy*
[78a] *INFN Sezione di Napoli, Napoli, Italy*
[78b] *Università di Napoli 'Federico II', Napoli, Italy*
[78c] *Università della Basilicata, Potenza, Italy*
[78d] *Scuola Superiore Meridionale (SSM), Napoli, Italy*
[79a] *INFN Sezione di Padova, Padova, Italy*
[79b] *Università di Padova, Padova, Italy*
[79c] *Universita degli Studi di Cagliari, Cagliari, Italy*
[80a] *INFN Sezione di Pavia, Pavia, Italy*
[80b] *Università di Pavia, Pavia, Italy*
[81a] *INFN Sezione di Perugia, Perugia, Italy*
[81b] *Università di Perugia, Perugia, Italy*
[82a] *INFN Sezione di Pisa, Pisa, Italy*
[82b] *Università di Pisa, Pisa, Italy*
[82c] *Scuola Normale Superiore di Pisa, Pisa, Italy*
[82d] *Università di Siena, Siena, Italy*
[83a] *INFN Sezione di Roma, Roma, Italy*
[83b] *Sapienza Università di Roma, Roma, Italy*
[84a] *INFN Sezione di Torino, Torino, Italy*
[84b] *Università di Torino, Torino, Italy*
[84c] *Università del Piemonte Orientale, Novara, Italy*
[85a] *INFN Sezione di Trieste, Trieste, Italy*
[85b] *Università di Trieste, Trieste, Italy*
[86] *Kyungpook National University, Daegu, Korea*
[87] *Department of Mathematics and Physics – GWNU, Gangneung, Korea*
[88] *Chonnam National University, Institute for Universe and Elementary Particles, Kwangju, Korea*
[89] *Hanyang University, Seoul, Korea*
[90] *Korea University, Seoul, Korea*
[91] *Kyung Hee University, Department of Physics, Seoul, Korea*
[92] *Sejong University, Seoul, Korea*
[93] *Seoul National University, Seoul, Korea*
[94] *University of Seoul, Seoul, Korea*
[95] *Yonsei University, Department of Physics, Seoul, Korea*
[96] *Sungkyunkwan University, Suwon, Korea*
[97] *College of Engineering and Technology, American University of the Middle East (AUM), Dasman, Kuwait*
[98] *Kuwait University – College of Science – Department of Physics, Safat, Kuwait*
[99] *Riga Technical University, Riga, Latvia*
[100] *University of Latvia (LU), Riga, Latvia*
[101] *Vilnius University, Vilnius, Lithuania*
[102] *National Centre for Particle Physics, Universiti Malaya, Kuala Lumpur, Malaysia*
[103] *Universidad de Sonora (UNISON), Hermosillo, Mexico*
[104] *Centro de Investigacion y de Estudios Avanzados del IPN, Mexico City, Mexico*

JHEP05(2026)186

[105] Universidad Iberoamericana, Mexico City, Mexico
[106] Benemerita Universidad Autonoma de Puebla, Puebla, Mexico
[107] University of Montenegro, Podgorica, Montenegro
[108] University of Canterbury, Christchurch, New Zealand
[109] National Centre for Physics, Quaid-I-Azam University, Islamabad, Pakistan
[110] AGH University of Krakow, Krakow, Poland
[111] National Centre for Nuclear Research, Swierk, Poland
[112] Institute of Experimental Physics, Faculty of Physics, University of Warsaw, Warsaw, Poland
[113] Warsaw University of Technology, Warsaw, Poland
[114] Laboratório de Instrumentação e Física Experimental de Partículas, Lisboa, Portugal
[115] Faculty of Physics, University of Belgrade, Belgrade, Serbia
[116] VINCA Institute of Nuclear Sciences, University of Belgrade, Belgrade, Serbia
[117] Centro de Investigaciones Energéticas Medioambientales y Tecnológicas (CIEMAT), Madrid, Spain
[118] Universidad Autónoma de Madrid, Madrid, Spain
[119] Universidad de Oviedo, Instituto Universitario de Ciencias y Tecnologías Espaciales de Asturias (ICTEA), Oviedo, Spain
[120] Instituto de Física de Cantabria (IFCA), CSIC-Universidad de Cantabria, Santander, Spain
[121] University of Colombo, Colombo, Sri Lanka
[122] University of Ruhuna, Department of Physics, Matara, Sri Lanka
[123] CERN, European Organization for Nuclear Research, Geneva, Switzerland
[124] PSI Center for Neutron and Muon Sciences, Villigen, Switzerland
[125] ETH Zurich – Institute for Particle Physics and Astrophysics (IPA), Zurich, Switzerland
[126] Universität Zürich, Zurich, Switzerland
[127] National Central University, Chung-Li, Taiwan
[128] National Taiwan University (NTU), Taipei, Taiwan
[129] High Energy Physics Research Unit, Department of Physics, Faculty of Science, Chulalongkorn University, Bangkok, Thailand
[130] Tunis El Manar University, Tunis, Tunisia
[131] Çukurova University, Physics Department, Science and Art Faculty, Adana, Turkey
[132] Middle East Technical University, Physics Department, Ankara, Turkey
[133] Bogazici University, Istanbul, Turkey
[134] Istanbul Technical University, Istanbul, Turkey
[135] Istanbul University, Istanbul, Turkey
[136] Yildiz Technical University, Istanbul, Turkey
[137] Institute for Scintillation Materials of National Academy of Science of Ukraine, Kharkiv, Ukraine
[138] National Science Centre, Kharkiv Institute of Physics and Technology, Kharkiv, Ukraine
[139] University of Bristol, Bristol, U.K.
[140] Rutherford Appleton Laboratory, Didcot, U.K.
[141] Imperial College, London, U.K.
[142] Brunel University, Uxbridge, U.K.
[143] Baylor University, Waco, Texas, U.S.A.
[144] Catholic University of America, Washington, DC, U.S.A.
[145] The University of Alabama, Tuscaloosa, Alabama, U.S.A.
[146] Boston University, Boston, Massachusetts, U.S.A.
[147] Brown University, Providence, Rhode Island, U.S.A.
[148] University of California, Davis, Davis, California, U.S.A.
[149] University of California, Los Angeles, California, U.S.A.
[150] University of California, Riverside, Riverside, California, U.S.A.
[151] University of California, San Diego, La Jolla, California, U.S.A.
[152] University of California, Santa Barbara – Department of Physics, Santa Barbara, California, U.S.A.
[153] California Institute of Technology, Pasadena, California, U.S.A.
[154] Carnegie Mellon University, Pittsburgh, Pennsylvania, U.S.A.
[155] University of Colorado Boulder, Boulder, Colorado, U.S.A.

JHEP05(2026)186

[156] Cornell University, Ithaca, New York, U.S.A.
[157] Fermi National Accelerator Laboratory, Batavia, Illinois, U.S.A.
[158] University of Florida, Gainesville, Florida, U.S.A.
[159] Florida State University, Tallahassee, Florida, U.S.A.
[160] Florida Institute of Technology, Melbourne, Florida, U.S.A.
[161] University of Illinois Chicago, Chicago, Illinois, U.S.A.
[162] The University of Iowa, Iowa City, Iowa, U.S.A.
[163] Johns Hopkins University, Baltimore, Maryland, U.S.A.
[164] The University of Kansas, Lawrence, Kansas, U.S.A.
[165] Kansas State University, Manhattan, Kansas, U.S.A.
[166] University of Maryland, College Park, Maryland, U.S.A.
[167] Massachusetts Institute of Technology, Cambridge, Massachusetts, U.S.A.
[168] University of Minnesota, Minneapolis, Minnesota, U.S.A.
[169] University of Nebraska-Lincoln, Lincoln, Nebraska, U.S.A.
[170] State University of New York at Buffalo, Buffalo, New York, U.S.A.
[171] Northeastern University, Boston, Massachusetts, U.S.A.
[172] Northwestern University, Evanston, Illinois, U.S.A.
[173] University of Notre Dame, Notre Dame, Indiana, U.S.A.
[174] The Ohio State University, Columbus, Ohio, U.S.A.
[175] Princeton University, Princeton, New Jersey, U.S.A.
[176] University of Puerto Rico, Mayaguez, Puerto Rico, U.S.A.
[177] Purdue University, West Lafayette, Indiana, U.S.A.
[178] Purdue University Northwest, Hammond, Indiana, U.S.A.
[179] Rice University, Houston, Texas, U.S.A.
[180] University of Rochester, Rochester, New York, U.S.A.
[181] Rutgers, The State University of New Jersey, Piscataway, New Jersey, U.S.A.
[182] University of Tennessee, Knoxville, Tennessee, U.S.A.
[183] Texas A&M University, College Station, Texas, U.S.A.
[184] Texas Tech University, Lubbock, Texas, U.S.A.
[185] Vanderbilt University, Nashville, Tennessee, U.S.A.
[186] University of Virginia, Charlottesville, Virginia, U.S.A.
[187] Wayne State University, Detroit, Michigan, U.S.A.
[188] University of Wisconsin – Madison, Madison, Wisconsin, U.S.A.
[189] An institute or international laboratory covered by a cooperation agreement with CERN
[190] An institute formerly covered by a cooperation agreement with CERN

[a] Also at Yerevan State University, Yerevan, Armenia
[b] Also at TU Wien, Vienna, Austria
[c] Also at Ghent University, Ghent, Belgium
[d] Also at Universidade do Estado do Rio de Janeiro, Rio de Janeiro, Brazil
[e] Also at FACAMP – Faculdades de Campinas, Sao Paulo, Brazil
[f] Also at Universidade Estadual de Campinas, Campinas, Brazil
[g] Also at Federal University of Rio Grande do Sul, Porto Alegre, Brazil
[h] Also at University of Chinese Academy of Sciences, Beijing, China
[i] Also at China Center of Advanced Science and Technology, Beijing, China
[j] Also at University of Chinese Academy of Sciences, Beijing, China
[k] Also at China Spallation Neutron Source, Guangdong, China
[l] Now at Henan Normal University, Xinxiang, China
[m] Also at University of Shanghai for Science and Technology, Shanghai, China
[n] Now at The University of Iowa, Iowa City, Iowa, U.S.A.
[o] Also at Another institute formerly covered by a cooperation agreement with CERN
[p] Also at Cairo University, Cairo, Egypt
[q] Also at Suez University, Suez, Egypt

JHEP05(2026)186

[r] Now at British University in Egypt, Cairo, Egypt
[s] Also at Purdue University, West Lafayette, Indiana, U.S.A.
[t] Also at Université de Haute Alsace, Mulhouse, France
[u] Also at Istinye University, Istanbul, Turkey
[v] Also at Another institute or international laboratory covered by a cooperation agreement with CERN
[w] Also at The University of the State of Amazonas, Manaus, Brazil
[x] Also at University of Hamburg, Hamburg, Germany
[y] Also at RWTH Aachen University, III. Physikalisches Institut A, Aachen, Germany
[z] Also at Bergische University Wuppertal (BUW), Wuppertal, Germany
[aa] Also at Brandenburg University of Technology, Cottbus, Germany
[ab] Also at Forschungszentrum Jülich, Juelich, Germany
[ac] Now at RWTH Aachen University, III. Physikalisches Institut A, Aachen, Germany
[ad] Also at CERN, European Organization for Nuclear Research, Geneva, Switzerland
[ae] Also at HUN-REN ATOMKI – Institute of Nuclear Research, Debrecen, Hungary
[af] Now at Universitatea Babes-Bolyai – Facultatea de Fizica, Cluj-Napoca, Romania
[ag] Also at MTA-ELTE Lendület CMS Particle and Nuclear Physics Group, Eötvös Loránd University, Budapest, Hungary
[ah] Also at HUN-REN Wigner Research Centre for Physics, Budapest, Hungary
[ai] Also at Physics Department, Faculty of Science, Assiut University, Assiut, Egypt
[aj] Also at Punjab Agricultural University, Ludhiana, India
[ak] Also at University of Visva-Bharati, Santiniketan, India
[al] Also at Indian Institute of Science (IISc), Bangalore, India
[am] Also at Amity University Uttar Pradesh, Noida, India
[an] Also at IIT Bhubaneswar, Bhubaneswar, India
[ao] Also at Institute of Physics, Bhubaneswar, India
[ap] Also at University of Hyderabad, Hyderabad, India
[aq] Also at Deutsches Elektronen-Synchrotron, Hamburg, Germany
[ar] Also at Isfahan University of Technology, Isfahan, Iran
[as] Also at Sharif University of Technology, Tehran, Iran
[at] Also at Department of Physics, University of Science and Technology of Mazandaran, Behshahr, Iran
[au] Also at Department of Physics, Faculty of Science, Arak University, ARAK, Iran
[av] Also at Helwan University, Cairo, Egypt
[aw] Also at Italian National Agency for New Technologies, Energy and Sustainable Economic Development, Bologna, Italy
[ax] Also at Centro Siciliano di Fisica Nucleare e di Struttura Della Materia, Catania, Italy
[ay] Also at Università degli Studi Guglielmo Marconi, Roma, Italy
[az] Also at Scuola Superiore Meridionale, Università di Napoli 'Federico II', Napoli, Italy
[ba] Also at Fermi National Accelerator Laboratory, Batavia, Illinois, U.S.A.
[bb] Also at Lulea University of Technology, Lulea, Sweden
[bc] Also at Consiglio Nazionale delle Ricerche – Istituto Officina dei Materiali, Perugia, Italy
[bd] Also at Institut de Physique des 2 Infinis de Lyon (IP2I), Villeurbanne, France
[be] Also at Department of Applied Physics, Faculty of Science and Technology, Universiti Kebangsaan Malaysia, Bangi, Malaysia
[bf] Also at Consejo Nacional de Ciencia y Tecnología, Mexico City, Mexico
[bg] Also at Trincomalee Campus, Eastern University, Sri Lanka, Nilaveli, Sri Lanka
[bh] Also at Saegis Campus, Nugegoda, Sri Lanka
[bi] Also at National and Kapodistrian University of Athens, Athens, Greece
[bj] Also at Ecole Polytechnique Fédérale Lausanne, Lausanne, Switzerland
[bk] Also at Universität Zürich, Zurich, Switzerland
[bl] Also at Stefan Meyer Institute for Subatomic Physics, Vienna, Austria
[bm] Also at Laboratoire d'Annecy-le-Vieux de Physique des Particules, IN2P3-CNRS, Annecy-le-Vieux, France
[bn] Also at Near East University, Research Center of Experimental Health Science, Mersin, Turkey
[bo] Also at Konya Technical University, Konya, Turkey

JHEP05(2026)186

[bp] Also at Izmir Bakircay University, Izmir, Turkey
[bq] Also at Adiyaman University, Adiyaman, Turkey
[br] Also at Bozok Universitetesi Rektörlügü, Yozgat, Turkey
[bs] Also at Marmara University, Istanbul, Turkey
[bt] Also at Milli Savunma University, Istanbul, Turkey
[bu] Also at Kafkas University, Kars, Turkey
[bv] Now at Istanbul Okan University, Istanbul, Turkey
[bw] Also at Hacettepe University, Ankara, Turkey
[bx] Also at Erzincan Binali Yildirim University, Erzincan, Turkey
[by] Also at Istanbul University – Cerrahpasa, Faculty of Engineering, Istanbul, Turkey
[bz] Also at Yildiz Technical University, Istanbul, Turkey
[ca] Also at School of Physics and Astronomy, University of Southampton, Southampton, U.K.
[cb] Also at IPPP Durham University, Durham, U.K.
[cc] Also at Monash University, Faculty of Science, Clayton, Australia
[cd] Also at Università di Torino, Torino, Italy
[ce] Also at Bethel University, St. Paul, Minnesota, U.S.A.
[cf] Also at Karamanoğlu Mehmetbey University, Karaman, Turkey
[cg] Also at California Institute of Technology, Pasadena, California, U.S.A.
[ch] Also at United States Naval Academy, Annapolis, Maryland, U.S.A.
[ci] Also at Ain Shams University, Cairo, Egypt
[cj] Also at Bingol University, Bingol, Turkey
[ck] Also at Georgian Technical University, Tbilisi, Georgia
[cl] Also at Sinop University, Sinop, Turkey
[cm] Also at Erciyes University, Kayseri, Turkey
[cn] Also at Horia Hulubei National Institute of Physics and Nuclear Engineering (IFIN-HH), Bucharest, Romania
[co] Now at Another institute formerly covered by a cooperation agreement with CERN
[cp] Also at Texas A&M University at Qatar, Doha, Qatar
[cq] Also at Kyungpook National University, Daegu, Korea
[cr] Also at Institute of Nuclear Physics of the Uzbekistan Academy of Sciences, Tashkent, Uzbekistan
[cs] Also at Yerevan Physics Institute, Yerevan, Armenia
[ct] Also at Northeastern University, Boston, Massachusetts, U.S.A.
[cu] Also at Imperial College, London, U.K.
[cv] Now at Yerevan Physics Institute, Yerevan, Armenia
[†] Deceased

JHEP05(2026)186